QUANTUM CHEMICAL STUDIES OF RING CURRENTS OF AROMATIC MOLECULES

A thesis submitted for the degree of *Doctor Philosophiae*

Markus Rauhalahti

University of Helsinki

Department of Chemistry

Helsinki, Finland

To be presented for public examination with the permission of the Faculty of Science of the University of Helsinki in Auditorium A129, Chemicum, A. I. Virtasen aukio 1, Helsinki on 25th November 2022 at 13 o'clock

Helsinki, 2022

Doctoral Programme in Chemistry and Molecular Sciences

Supervised by
 Prof. Dage Sundholm
 University of Helsinki

 Doc. Mikael P. Johansson
 University of Helsinki

Reviewed by
 Prof. Antti Karttunen
 Aalto University

 Prof. Henrik Ottosson
 Uppsala University

Opponent
 Prof. Renana Gershoni-Poranne
 Technion - Israel Institute of Technology

Custos
 Prof. Dage Sundholm
 University of Helsinki

The Faculty of Science uses the Ouriginal system (plagiarism recognition)
to examine all doctoral dissertations

Abstract

Aromaticity - the delocalization of electrons along a closed atomic circuit - has its manifestations in the energetic, structural, electronic, and spectroscopic properties of molecules and in how they react with each other. This phenomenon is central in chemistry, and the history of chemists using the concept as an "intuition pump" to understand and design new molecules goes back to the 1800s when Kekulé first time came up with the snake-eating-its-tail model of benzene.

Those days predate the discovery of the electron and quantum mechanics, and the concept has evolved since. While the physics of chemistry is understood, the utility of intuitive concepts still remains. Science as of today is still a human business, and to most of us chemists the fluctuations of the fermionic field, or their computational representation as tensors, don't give much food for thought.

In this Ph.D. thesis, I present my research in which quantum chemical methods were used to study different types of aromatic compounds. The focus is on assessing their aromaticity by probing the ring currents of molecules - the net flow of electrons around when it's placed in a magnetic field. Calculation of this magnetically induced current density and the bond currents yield an accurate measure for electron delocalization.

The studied systems present different types of aromaticities and aromatic molecules: through-bond aromaticity in the substituent ring of benzene derivatives, the intricacies of current pathways in naphtalene-fused porphyrinoids and in copper coordination complexes, and the magnetic-field orientation dependence of aromaticity in gaudiene, a spherical aromatic, but not spherically aromatic compound. The presented results disprove old conclusions for some compounds and enrich the understanding of others.

Yleistajuinen tiivistelmä

Kemiassa aromaattisuuden käsite ei tyypillisesti viittaa tuoksuihin, vaikka sen juuret ulottuvatkin näiden eriskummallisten molekyylien aromiin. Kemistit kutsuvat aromaattisuudeksi ilmiötä, jossa molekyylin elektronit eivät tyydy kohtaloonsa kahden atomiytimen välimaastossa, vaan leviävät yli atomikehikon muodostaen suljetun virtapiirin.

Tuon syklisen delokalisaation myötä aromaattisilla molekyyleillä on erityisiä ominaisuuksia. Vastaavasti kuten elektroniikan virtapiirissä hieman vääränlainen resistori voi saada aikaan ennalta arvaamattoman oikosulun, myös atomitasolla nämä näennäisen pienet muutokset voivat kytkeä aromaattisuuden pois päältä ja muuttaa molekyylin ominaisuuksia suuresti - kokonaisuus on enemmän kuin osiensa summa.

Aromaattisia molekyylejä on kaikkialla, arkkityyppinä niistä on kuusikulmion muotoinen bentseeni. Evoluutio on valjastanut nämä aromaattiset molekyylit osaksi olevaisuuttamme: geeniperimämme on kirjoitettu DNA:n vakailla aromaattisilla emäspareilla. Solujemme toiminta pyörii aromaattisuutensa keinoin elektroneja välittävillä koentsyymeillä, ja aromaattisuudella on mitä keskeisin rooli porfyriinimolekyylien kyvyssä niin sitoa happea kuljettavat rauta-atomit verisoluissamme kuin vastaanottaa auringon säteilemä energia kasvien viherhiukkasissa.

Luonto on löytänyt aromaattisille molekyyleille paljon käyttöä, ja näistä prosesseista kummunneet kemistit jatkavat sen työtä. Aromaattisuuden käsite on tärkeä väline tässä työkalupakissa. Toinen tärkeä työkalu on kvanttifysiikka - sen avulla olemme noin sadan vuoden ajan kyenneet kunnolla ymmärtämään molekyylejä, sekä sittemmin tietokoneiden kehittymisen myötä onnistuneet laskemaan niiden ominaisuuksia tarkasti.

Väitöstutkimuksessani sovelsin laskennallisen kvanttikemian menetelmiä aromaattisuuden määrittämiseksi. Väitöskirja rakentuu neljän tieteellisen julkaisun ympärille, joissa tarkastelemme erilaisten molekyylien aromaattisuutta laskemalla rengasvirtoja - ulkoisen magneettikentän aiheuttamaa elektronien virtausta atomiydinten muodosta-

man virtapiirin ympäri.

Tulosten avulla kykenimme ymmärtämään tiettyjen molekyylien aromaattisuutta paremmin sekä kumoamaan joitakin väärinkäsityksiä. Tehdyn perustutkimuksen löydökset todentavat rengasvirtojen antavan tarkan ja fysikaalisesti perustellun kuvan aromaattisuudesta - erityisesti jos sitä vertaa 1800-luvun hajunvaraiseen toimintaan - ja rengasvirtojen olevan tärkeä menetelmä aromaattisuuden ymmärtämisessä.

Acknowledgements

This thesis collates my work on the topic of aromaticity, done during my formative years spent at the Computational Quantum Chemistry group, earlier known as Laboratory for the Instruction in Swedish, where in 2014 I started my path as a researcher as a second-year student. This path with its many branches has spanned quite large territories. I wish to thank Prof. Dage Sundholm and Dr. Mikael Johansson for providing me with support, interesting projects, and most importantly, an environment to pursue and grow my curiosity about molecules.

I want to express my gratitude to Dr. Stefan Taubert for his mentorship and for teaching me the tricks of the trade back in 2014, and Dr. Alvaro Muñoz-Castro in Santiago and Prof. Robert Paton in Colorado for being great hosts during my longer visits. My Ph.D. was on hiatus starting from the COVID pandemic. During this time, I got embedded in a new world of data-related problems in analytical chemistry, and want to thank the team at Sensmet for the experience. The door back to the computational study of (much larger) molecules opened a year ago. I'm deeply grateful to Dr. Vivek Sharma for offering me a postdoctoral position in his biophysics group, and for his understanding of my process of wrapping up this thesis on the side. The research in this thesis was done in the company of great coworkers: Maria, Lukas, Susi, Pauli, Eelis, Matias, Iiris, Atif, Sergio, Elias, Moses, and many others - thank you!

I owe gratitude to all the close ones I've shared this path with. Ludmila, thank you for being you, and for enduring my bungholery during writing this thesis. Tapio and Ilmari - you know very well the role of your friendship, support, and importantly being low in agreeableness, in me getting to where I am. Aleksi, Boris, and Bart - thank you for good nerding company. Hanna and Annalise - thank you for understanding me. I'm grateful to JP and AK for the insights, to Bobo and Sencha for being the good dogs they were and are, and to all my friends that have had an important part in this process - Robin, Anssi, Nikke, Joel, Lauri, David, Levi, Elva, Sara, Joel, Tiia, Laura, Vladimir, and all the ones not listed here - you rule! Last but not least, I thank my family for their support and care, and for pushing me forward. I wouldn't be here without you.

This thesis is dedicated to my late grandfather Matti, to Eelis, who tragically passed away at the end of his Ph.D. studies in our group, and to Levi and Armelle, to whom I wish strength in their battle against their illnesses.

Contents

Publications

Publications included in the thesis and the author's contributions

I. **Rauhalahti, M.**; Muñoz-Castro, A.; Sundholm, D. "Magnetic Response Properties of Gaudiene–a Cavernous and Aromatic Carbocage." *Phys. Chem. Chem. Phys.* **2016**, 18 (28), 18880–18886.

- MR did the calculations of structures and ring currents, took part in the other calculations, and wrote the manuscript with AMC and DS.

II. **Rauhalahti, M.**; Taubert, S.; Sundholm, D.; Liégeois, V. "Calculations of Current Densities for Neutral and Doubly Charged Persubstituted Benzenes Using Effective Core Potentials." *Phys. Chem. Chem. Phys.* **2017**, 19 (10), 7124–7131.

- MR did most of the calculations and visualizations and wrote the manuscript with ST, DS, and VL.

III. Molina, V.; **Rauhalahti, M.**; Hurtado, J.; Fliegl, H.; Sundholm, D.; Muñoz-Castro, A. "Aromaticity Introduced by Antiferromagnetic Ligand Mediated Metal–metal Interactions. Insights from the Induced Magnetic Response in $[Cu_6(dmPz)_6(OH)_6]$." *Inorg. Chem. Front.* **2017**, 4 (6), 986–993.

- MR did the ring current calculations and took part in writing the manuscript

IV. **Rauhalahti, M.**; Sundholm, D.; Johansson, M. P. "Magnetically Induced Ring Currents in Naphthalene-Fused Heteroporphyrinoids." *Phys. Chem. Chem. Phys.* **2021**, 23 (31), 16629–16634.

- MR came up with the idea of the project and formulated its scope, performed most of the calculations, and wrote the initial draft of the paper.

Other publications

V. **Rauhalahti, M.** ; Muñoz-Castro, A. "Interaction in Multilayer Clusters: A Theoretical Survey of $[Sn@Cu_{12}@Sn_{20}]^{12-}$, a Three-Layer Matryoshka-like Intermetalloid." *RSC Adv.* **2015**, 5 (24), 18782–18787.

VI. **Rauhalahti, M.** ; Muñoz-Castro, A.; Sundholm, D. "Thiolate-Protected Golden Fullerenes. A 32-ve Core Involving a Hollow Au_{32} Cage." *RSC Adv.* **2016**, 6 (26), 21332–21336.

VII. Sundholm, D.; **Rauhalahti, M.** ; Özcan, N.; Mera-Adasme, R.; Kussmann, J.; Luenser, A.; Ochsenfeld, C. "Nuclear Magnetic Shieldings of Stacked Aromatic and Antiaromatic Molecules." *J. Chem. Theory Comput.* **2017**, 13 (5), 1952–1962.

VIII. Johansson, M. P.; Niederegger, L.; **Rauhalahti, M.**; Hess, C. R.; Kaila, V. R. I. "Dispersion Forces Drive Water Oxidation in Molecular Ruthenium Catalysts." *RSC Adv.* **2020**, 11 (1), 425–432.

List of Figures

List of Tables

List of Abbreviations

AACID . Anisotropy of the Asymmetric Magnetically Induced Current Density

ACID . . Anisotropy of Induced Current Density

AE . . . All-electron, refers to not using an effective core potential

ARE . . Adiabatic resonance energy

ASE . . . Aromatic stabilization energy

AdNDP . Adaptive Natural Density Partitioning

BLW . . Block-localized wave function

CC . . . Coupled cluster

CDST . . Current density susceptibility tensor

CI . . . . Configuration interaction

CPP . . . Cycloparaphenylene

CSGT . . Continuous Set of Gauge Transformations

CTOCD . Continuous Transformation Origin of the Current Density

CTOCD-DZ Diamagneti-zero Continuous Transformation Origin of the Current Density

DI . . . . Delocalization index

DZ . . . Double-ζ, refers to basis set

ECP . . . Effective core potential

EDA . . Energy decomposition analysis

EDDB . . Electron density of delocalized bonds

ELF . . . Electron localization function

FR . . . Fully relativistic

GGA . . Generalized Gradient Approximation

GIAO . . Gauge-including atomic orbital

GIMIC . Gauge-including Magnetically Induced Current Method

GTO . . Gaussian-type orbital

HF . . . Hartree-Fock

HOMA . Harmonic oscillator model of aromaticity

HOMO . Highest occupied molecular orbital

KS-DFT Kohn-Sham density functional theory

LCAO . . Linear combination of atomic orbitals

LDA . . . Local Density Approximation

LUMO . Lowest unoccupied molecular orbital

MCI . . . Multi-center index

MP . . . Møller-Plesset

NBO . . Natural bond orbital

NICS . . Nuclear-independent chemical shift

NMR . . Nuclear magnetic resonance

NR . . . Non-relativistic

QR . . . Quasi-relativistic

QTAIM . Quantum Theory of Atoms in Molecules

RCS . . . Ring current strength

RE . . . Resonance energy

RHF . . . Restricted Hartree-Fock

ROHF . . Restricted open-shell Hartree-Fock

SCF . . . Self-consistent field

SD . . . . Slater determinant

STO . . . Slater-type orbital

SZ . . . . Single-ζ

TZ . . . . Triple-ζ

UHF . . Unrestricted Hartree-Fock

VB . . . Valence bond

VRE   . .   Vertical resonance energy

XC   . . .   Exchange-correlation

Chapter 1

Introduction

Aromatic molecules, or more precisely, their aromatic states, are ones in which electrons are delocalized in a closed two- or three-dimensional circuit. This phenomenon has many manifestations in the energetic, structural, spectroscopic, and magnetic response properties of molecules, making it a central topic in chemistry. In this thesis, the latter one, ring currents induced by a magnetic field, are studied with the computer as a laboratory.

In Chapter 2, I present the quantum chemical methods that allow us to take these entities of the physical world to objects that we can calculate the properties, and overview the theory and methods for calculating magnetically induced ring currents. Chapter 3 first discusses the utility of chemical concepts and the history of aromaticity and then presents the physicochemical manifestations and the various computational metrics developed for assessing the aromaticity of molecules. The Chapter ends with a section presenting an overview of the chemical space of aromatic compounds, highlighting the richness, complexity, and possibilities of these special molecules.

In Chapter 4, I present the results of Articles I-IV, in which we used ring current calculations to study four distinct classes of aromatic compounds. These calculations act as a microscope to the through-space aromaticity and its switching of double aromatic benzenes. They allow us to understand the intricacies and correct misunderstandings of the aromaticity of naphtalene-fused porphyrinoids. They are used to enrich the understanding aromaticity of organometallic $[Cu_6(dmPz)_6(OH)_6]$, and to elucidate the aromaticity of the spherical gaudiene molecule.

The thesis ends in Chapter 5, in which I discuss the results in the context of the

computational assessment of aromaticity. I also give future directions, presenting iden-
tified bottlenecks and ways to overcome them. Overcoming these would make the
automated analysis of aromatic compounds possible, a task needed in the upcoming
era of computational molecular discovery.

Chapter 2

Theory and methods

2.1   Schrödinger equation

Molecules consist of atomic nuclei and electrons, and their interactions and dynamics
are described by quantum mechanics.

In quantum mechanics, the state of the system is represented by a wave function ψ,
an element of the Hilbert space. We use state vector formalism, in which a wave function
is written as ket-vector $\psi = |\psi\rangle$, its complex conjugate as a bra-vector $\psi^* = \langle\psi|$, and
the inner product as $\langle\psi|\psi\rangle$.

Physical quantities are represented by Hermitian operators $\mathbf{\Omega}$. Upon measurement
of the quantity, the state of the system is changed to some of its eigenstates $|\omega\rangle$, and
the observed quantity is the corresponding eigenvalue with a probability of $|\langle\omega|\psi\rangle|^2$.
The position and momentum of a particle are represented by the operators $\mathbf{x}$ and $\mathbf{p}$,
which do not commute:

$$[\mathbf{x}, \mathbf{p}] = \mathbf{x}\mathbf{p} - \mathbf{p}\mathbf{x} = i\hbar. \tag{2.1}$$

Noncommuting operators, i.e., those with $[\mathbf{a}, \mathbf{b}] \neq 0$, have different eigenstates and
can not be determined simultaneously. Heisenberg's uncertainty relation relates the
variances of momentum and position: they are inversely proportional to each other:

$$\Delta\mathbf{x}\Delta\mathbf{p} \geq \hbar/2. \tag{2.2}$$

Undisturbed by external influences, the time evolution of a state is described by the
Schrödinger equation:

$$i\hbar \frac{\mathrm{d} \left| \psi(r,t) \right\rangle}{\mathrm{d}t} = \mathbf{H}(t) \left| \psi(r,t) \right\rangle \tag{2.3}$$

Here, $\mathbf{H}$ is the Hamiltonian operator, or briefly Hamiltonian, which represents the total energy of the system. It is obtained from its classical analog by replacing position and momentum variables with the corresponding operators and requiring that their commutation relation is fulfilled [1]. When the Hamiltonian operator is independent of time, we obtain the time-independent Schrödinger equation. The eigenstates of time-independent Hamiltonian are called stationary states, and their time evolution is explained by a phase-factor [1]:

$$\mathbf{H}(\mathbf{r},t) = \mathbf{T}(\mathbf{r}) + \mathbf{V}(\mathbf{r},t) \tag{2.4}$$

$$\mathbf{V}(\mathbf{r},t) = \mathbf{V}(\mathbf{r}) \to \mathbf{H} \left| \Psi \right\rangle = E \left| \Psi \right\rangle \tag{2.5}$$

$$\left| \Psi(t) \right\rangle = e^{-iEt} \left| \Psi(t_0) \right\rangle \tag{2.6}$$

2.2 Electronic problem

We are interested in solving the electronic problem – obtaining the stationary states for a molecule by solving the time-dependent Schrödinger equation. For this, we need to specify our Hamiltonian and the form of the wave function.

The molecular Hamiltonian consists of kinetic and potential energy terms, $\mathbf{T}$ and $\mathbf{V}$, that describe the interactions of atomic nuclei and electrons, referred with the n and e subscripts:

$$\mathbf{H}_{mol} = \mathbf{T}_n + \mathbf{T}_e + \mathbf{V}_{ne} + \mathbf{V}_{ee} + \mathbf{V}_{nn}, \tag{2.7}$$

Two approximations are made to the Hamiltonian. In the Born-Oppenheimer approximation, the nuclear motion is ignored, and in the adiabatic approximation, the wave function is constrained to one electronic state. The nuclear kinetic energy term is thus ignored, and the positions of the nuclei enter the equation only as parameters. This results in the molecular electronic Hamiltonian $\mathbf{H}_{el}$, expressed here in atomic units[1] and using the one- and two electron operators $\mathbf{h}_i$ and $\mathbf{g}_{ij}$:

---

[1]$\hbar = e = a_0 = m_e = 1$

$$\mathbf{H}_{el} = \mathbf{T}_e + \mathbf{V}_{ne} + \mathbf{V}_{ee} + \mathbf{V}_{nn} \tag{2.8}$$

$$= \sum_i^{N_{\text{elec}}} \mathbf{h}_i + \sum_{i<j}^{N_{\text{elec}}} \mathbf{g}_{ij} + \mathbf{V}_{\text{nn}} \tag{2.9}$$

$$\mathbf{h}_i = -\frac{1}{2}\nabla_i^2 - \sum_K \frac{Z_A}{|\mathbf{R}_A - \mathbf{r}_i|} \tag{2.10}$$

$$\mathbf{g}_{ij} = \frac{1}{|r_i - r_j|}. \tag{2.11}$$

Here, the lower-case indices refer to electrons and capital indices to atomic nuclei. We use this to solve the Schrödinger equation to obtain the electronic wave function $|\Psi_{el}\rangle$:

$$\mathbf{H}_{el} |\Psi_{el}\rangle = E_{el} |\Psi_{el}\rangle \tag{2.12}$$

The molecular electronic wave function is built from one-electron functions called molecular orbitals $\phi(x)$. Electrons are defined by their position, and as fermions, by their spin angular momentum $s = \frac{1}{2}$, which can have z-component values $m_s = \pm\frac{1}{2}$. These are included by multiplying the spatial orbitals by spin functions σ, giving spin orbitals $\phi_{i\sigma} = \phi_i(\mathbf{r})\sigma$ with $\sigma = \alpha$ corresponding to $m_s = \frac{1}{2}$ and $\sigma = \beta$ to $m_s = -\frac{1}{2}$.

Both the spatial orbitals and spin functions orthonormal functions:

$$\langle \phi_i | \phi_j \rangle = \delta_{ij} \tag{2.13}$$

$$\langle \alpha | \alpha \rangle = \langle \beta | \beta \rangle = 1 \tag{2.14}$$

$$\langle \alpha | \beta \rangle = \langle \beta | \alpha \rangle = 0. \tag{2.15}$$

We will continue the presentation of theory and methods dealing mostly with the closed-shell case, in which the spin is disregarded and orbitals are taken to be doubly occupied. The starting point for constructing a wave function for molecules is the Hartree product of MOs:

$$\Theta(1,\ldots,n) = \phi_1(1)\cdots\phi_N(N) \tag{2.16}$$

Electrons are fermions, and the electronic wave function is antisymmetric: when the electron coordinates are interchanged, the wave function changes its sign. This

property is obtained by operating on Hartree product with antisymmetrizer operator $\mathbf{A}$, or equivalently, by writing it as a Slater determinant [2]:

$$\Phi_{\text{SD}} = \mathbf{A}\Theta \tag{2.17}$$

$$= \frac{1}{\sqrt{N!}} \begin{vmatrix} \phi_1(1) & \phi_2(1) & \cdots & \phi_N(1) \\ \phi_1(2) & \phi_2(2) & \cdots & \phi_N(2) \\ \vdots & \vdots & \ddots & \vdots \\ \phi_1(N) & \phi_2(N) & \cdots & \phi_N(N) \end{vmatrix} \tag{2.18}$$

$$\mathbf{A} = \frac{1}{\sqrt{N!}} \sum_{p=0}^{N-1} (-1)^p \mathbf{P} = \frac{1}{\sqrt{N!}} \left[\mathbf{1} - \sum_{ij} \mathbf{P}_{ij} + \sum_{ijk} \mathbf{P}_{ijk} - \cdots \right]. \tag{2.19}$$

2.3 Hartree-Fock method

The variational principle states that the ground state energy E_0 of the system is minimized by its true wave function Ψ_0, giving a computational recipe for calculating the wave function of the system. The method for finding such a Slater determinant is known as Hartree-Fock (HF) method. It is an iterative mean-field method, transforming the n-body problem into a two-body problem, in which an electron interacts with a frozen set of other electrons.

The energy of a Slater determinant can be derived by writing it as an antisymmetrized Hartree product, and calculating the expectation values of the electronic Hamiltonian:

$$E_{\text{SD}} = \langle \mathbf{A}\Theta | H_{\text{el}} | \mathbf{A}\Theta \rangle \tag{2.20}$$

Due to the orthogonality of MOs, only the first and second terms in the expansion of the antisymmetrizer remain, giving the following terms [2]:

$$\mathbf{V}_{nn} : V_{nn} \tag{2.21}$$

$$\mathbf{h}_1 : \langle \Theta | \mathbf{h}_1 | \Theta \rangle = \langle \phi_1(1) | \mathbf{h}_1 | \phi_1(1) \rangle = h_1 \tag{2.22}$$

$$\mathbf{g}_{12} : \begin{cases} \langle \Theta | \mathbf{g}_{12} | \Theta \rangle = \langle \phi_1(1)\phi_2(2) | \mathbf{g}_{12} | \phi_1(1)\phi_2(2) \rangle = J_{12} \\ \langle \Theta | \mathbf{g}_{12} | \mathbf{P}_{12}\Theta \rangle = \langle \phi_1(1)\phi_2(2) | \mathbf{g}_{12} | \phi_2(1)\phi_1(2) \rangle = K_{12} \end{cases} \tag{2.23}$$

The equation for energy becomes the following, which can be written with Coulomb and exchange operators $\mathbf{J}$ and $\mathbf{K}$ [2]:

$$E = \sum_{i=1}^{N_{\text{elec}}} h_i + \frac{1}{2} \sum_{i=1}^{N_{\text{elec}}} \sum_{j=1}^{N_{\text{elec}}} (J_{ij} - K_{ij}) + V_{\text{nn}} \tag{2.24}$$

$$= \sum_{i}^{N_{\text{elec}}} \langle \phi_i \, |\mathbf{h}_i| \, \phi_i \rangle + \frac{1}{2} \sum_{ij}^{N_{\text{elec}}} (\langle \phi_j \, |\mathbf{J}_i| \, \phi_j \rangle - \langle \phi_j \, |\mathbf{K}_i| \, \phi_j \rangle) + V_{\text{nn}} \tag{2.25}$$

$$\mathbf{J}_i \, |\phi_j(2)\rangle = \langle \phi_i(1) \, |\mathbf{g}_{12}| \, \phi_i(1) \rangle \, |\phi_j(2)\rangle \tag{2.26}$$

$$\mathbf{K}_i \, |\phi_j(2)\rangle = \langle \phi_i(1) \, |\mathbf{g}_{12}| \, \phi_j(1) \rangle \, |\phi_i(2)\rangle \tag{2.27}$$

The set of MOs that minimize the energy can be calculated with the method of Lagrange multipliers. In it, a set of multipliers λ_{ij} are found that make the variation of the Lagrangian δL equal zero under the constraint of orbital orthonormality [2]:

$$L = E - \sum_{ij}^{N_{\text{elec}}} \lambda_{ij} (\langle \phi_i \mid \phi_j \rangle - \delta_{ij}) \tag{2.28}$$

$$\delta L = \delta E - \sum_{ij}^{N_{\text{elec}}} \lambda_{ij} (\langle \delta \phi_i \mid \phi_j \rangle - \langle \phi_i \mid \delta \phi_j \rangle) = 0 \tag{2.29}$$

Inserting the energy expression 2.24 and doing calculus gives the Hartree-Fock equations, where $\mathbf{F}_i$ is the Fock operator [2]:

$$\mathbf{F}_i \phi_i = \sum_{j}^{N_{\text{elec}}} \lambda_{ij} \phi_j \tag{2.30}$$

$$\mathbf{F}_i = \mathbf{h}_i + \sum_{j}^{N_{\text{elec}}} (\mathbf{J}_j - \mathbf{K}_j) \tag{2.31}$$

The Slater determinant is invariant upon unitary transformations, and the Lagrange multipliers λ_{ij} can be diagonalized. These new resulting MOs ϕ_i' are called canonical MOs, and the eigenvalue equation is called canonical HF equation, with eigenvalue ϵ_i being the energy of the canonical MO [2]:

$$\mathbf{F}_i \phi_i' = \epsilon_i \phi_i' \tag{2.32}$$

In further discussions, MOs are assumed to be canonical, and the prime is dropped. The MO energies are matrix elements of the Fock operator, $\epsilon_i = \langle \phi_i | \mathbf{F}_i | \phi_i \rangle$. They have a physical meaning in being connected to ionization potentials and electron affinities via Koopman's theorem [3].

These equations are commonly solved by Roothaan-Hall's method. The MOs ϕ_i are written as linear-combination of atomic orbitals (LCAO), expanding them as a linear combination of M_{basis} atom centered basis functions χ_α:

$$\phi_i = \sum_{\alpha}^{M_{\text{basis}}} c_{\alpha i} \chi_\alpha. \tag{2.33}$$

These basis functions are typically Gaussian or Slater-type functions, and the basis sets built from them to represent the molecule's wave function are discussed more in Section 2.4. The Roothaan-Hall equations are obtained by inserting the expanded MOs into the HF equation 2.32:

$$\mathbf{FC} = \mathbf{SC}\epsilon. \tag{2.34}$$

. Here, $\mathbf{S}$ is the overlap matrix and $\mathbf{F}$ is the Fock matrix [2], both defined within the AO basis as:

$$S_{\alpha\beta} = \langle \chi_\alpha | \chi_\beta \rangle \tag{2.35}$$

$$F_{\alpha\beta} = \langle \chi_\alpha | \mathbf{h} | \chi_\beta \rangle + \sum_{\gamma\delta}^{M_{\text{basis}}} D_{\gamma\delta} \left(\langle \chi_\alpha \chi_\gamma | \mathbf{g} | \chi_\beta \chi_\delta \rangle - \langle \chi_\alpha \chi_\gamma | \mathbf{g} | \chi_\delta \chi_\beta \rangle \right) \tag{2.36}$$

$$= h_{\alpha\beta} + \sum_{\gamma\delta} G_{\alpha\beta\gamma\delta} D_{\gamma\delta}. \tag{2.37}$$

Here, $h_{\alpha\beta}$ is a matrix containing the one-electron integrals, $G_{\alpha\beta\gamma\delta}$ is the four-dimensional tensor containing two-electron integrals, contracted using the density matrix $D_{\gamma\delta}$ [2]:

$$\langle \chi_\alpha | \mathbf{h} | \chi_\beta \rangle = \int \chi_\alpha(1) \left(-\frac{1}{2}\nabla^2 \right) \chi_\beta(1)\mathrm{d}\mathbf{r}_1 \tag{2.38}$$

$$+ \sum_a^{N_{\text{nuclei}}} \int \chi_\alpha(1) \left(\frac{Z_a}{|\mathbf{R}_a - \mathbf{r}_1|} \right) \chi_\beta(1)\mathrm{d}\mathbf{r}_1 \tag{2.39}$$

$$\langle \chi_\alpha \chi_\gamma | \mathbf{g} | \chi_\beta \chi_\delta \rangle = \int \chi_\alpha(1)\chi_\gamma(2) \left(\frac{1}{|\mathbf{r}_1 - \mathbf{r}_2|} \right) \chi_\beta(1)\chi_\delta(2)\mathrm{d}\mathbf{r}_1\mathrm{d}\mathbf{r}_2 \tag{2.40}$$

$$D_{\gamma\delta} = \sum_j^{\text{occ.MO}} c_{\gamma j}c_{\delta_j}. \tag{2.41}$$

The self-consistent field (SCF) procedure for solving the HF equations in the Roothaan-Hall formalism starts by forming an initial guess of the density matrix. Then, the Fock matrix elements are calculated, the matrix is diagonalized, and a new density matrix is formed. If the change of energy or the density matrix is below some threshold, the calculation is converged, if not, the procedure is repeated.

The derivation here ignored the spin of the electrons, and the method is known as the restricted Hartree-Fock (RHF) method. In it, the α and β are paired to the same spatial orbitals. Lifting this restriction leads to the unrestricted Hartree-Fock method (UHF), in which the α and β electrons have their own spatial orbitals. In the restricted open-shell Hartree-Fock method (ROHF), doubly occupied orbitals are restricted to be spatially the same.

2.4 Basis sets

The atomic orbitals χ are commonly built from Gaussian (GTO) or Slater-type orbitals (STO), which are products of a spherical harmonic function $Y_{l,m}(\theta, \varphi)$ and a distance-dependent exponential term. STOs decay as $e^{-\zeta r}$ from the atom center, similarly to hydrogen-like molecules, whereas GTOs decay as a $e^{-\zeta r^2}$:

$$\text{STO}: \chi_{\zeta,n,l,m}(r, \theta, \varphi) = NY_{l,m}(\theta, \varphi)r^{n-1}\mathrm{e}^{-\zeta r} \tag{2.42}$$

$$\text{GTO}: \chi_{\zeta,n,l,m}(r, \theta, \varphi) = NY_{l,m}(\theta, \varphi)r^{2n-2-l}\mathrm{e}^{-\zeta r^2}. \tag{2.43}$$

Here, n, l, and m are the principal, angular, and magnetic quantum numbers. The spread of the orbital is controlled by the ζ parameter - a larger value leads to a tighter function, smaller to a more diffuse one.

STOs describe the wave function more accurately, capturing the cusp of the electron density at the atom center, and being more accurate at the tails. Integrals with GTOs are, however, easier to compute, and they are more commonly used, although more functions are needed to obtain the STO-like behavior.

A minimal basis set contains only one basis function for each occupied orbital, called a single-ζ basis set (SZ). Variational flexibility is obtained by adding more basis functions with the same angular momentum l. Doubling this leads to a double-ζ (DZ), tripling to triple-ζ basis sets (TZ), and so on. The basis functions are typically added to valence orbitals, as they are relevant for most of the chemical phenomena. These are called the split-valence basis sets.

Commonly higher angular momentum functions - polarization functions - are added to increase the flexibility - p type functions for s orbitals, d for p orbitals, and so on. Additionally, diffuse functions, ones with small ζ value, are used to better describe states that have electrons further away from the nucleus, such as anions or polarizable systems.

As chemistry often happens at the level of valence electrons, a common strategy is to replace the core electrons with a pseudopotential, known as effective core potential (ECP). ECPs differ by the number of electrons they replace, and to which reference where they were fit to. In addition to lowering the computational cost by lowering the amounts of electrons to consider, the use of ECPs can also include scalar relativistic effects.

The balance of accuracy and efficiency enters the choice of the size of the basis set. One typically calculates the property of interest with varying sizes of basis set to see where the results start to converge. One commonly used trick is complete basis set extrapolation, in which nZ level energy is calculated using $(n-2)Z$ and $(n-1)Z$ level energies [4]. One effect arising from the use of a finite basis set is the basis set superposition error, in which an atom uses the basis functions of other atoms to artificially lower its energy. This can be treated to some extent with counterpoise correction in the case of intermolecular interaction energies.

2.5 Treating electron correlation

The mean-field approximation for solving the many-body problem of electron-electron interactions in the HF method is surprisingly accurate, being able to capture around 99% of the total energy of the system. The chemical phenomena happen at the valence level, and the energetic difference between these options is very small relative to the total energies. Different electron correlation methods bridge this gap between the true and mean-field representations.

The electron correlation can be split into dynamic and static correlation. The dynamic correlation arises from the mean-field treatment of electron-electron interactions, whereas the static correlation arises from the inability of a single Slater determinant (SD) to describe the ground state of the system. Electron correlation can be described by a many-electron wave function built of SDs corresponding to different electron configurations. Three common approaches to dealing with dynamic electron correlation are configuration interaction, coupled cluster, and Møller-Plesset perturbation methods.

2.5.1 Configuration interaction

In Configuration interaction (CI), the many-electron wave function is built as a linear combination of HF and excited state SDs:

$$\Psi = a_0 \Phi_{\text{HF}} + \sum_{\text{S}} a_{\text{S}} \Phi_{\text{S}} + \sum_{\text{D}} a_{\text{D}} \Phi_{\text{D}} + \dots \qquad (2.44)$$

Here, the singles term $\sum_{\text{S}} a_{\text{S}} \Phi_{\text{S}}$ contains all the states generated by moving one electron from an occupied to the unoccupied orbital of the HF solution Φ_{HF}. Equivalently, the term D contains all the double excited states. In Full CI all N-fold excitations are considered for an N electron system, giving an exact wave function with the given basis set. Due to the combinatorial scaling arising from the different ways to distribute N electrons to K orbitals, the CI expansion is truncated. Including single and double excitations leads to CISD method, and so on. The expansion coefficients of states are calculated with a variational method, with many matrix elements being zero.

Truncated CI methods are not size-extensive: the correlation energy does not scale correctly with the amount of particles [5]. It is also not size-consistent, meaning that the

energies of two non-interacting systems do not equal the energies of individual systems [6].

2.5.2 Coupled cluster

Coupled cluster (CC) method is based on generating excitations through the exponentiated excitation operator [7]. The excitation operator $\mathbf{T}$ is a sum of n'th order excitation operators $\mathbf{T}_n$:

$$\mathbf{T} = \sum_i^{N_{\text{elec}}} \mathbf{T}_n = \mathbf{T}_S + \mathbf{T}_D + \dots \tag{2.45}$$

Here, the operator $\mathbf{T}_S$ generates singly excited states when applied to a reference wave function, giving the single's term in CI. The CC wave function is calculated by operating on the reference wave function with the exponentiated excitation operator expanded as a Taylor series [2]:

$$\Psi_{\text{CC}} = e^{\mathbf{T}} \Phi_{\text{HF}} \tag{2.46}$$

$$e^{\mathbf{T}} = \sum_{k=0} \frac{1}{k!} \mathbf{T}^k \tag{2.47}$$

$$= \mathbf{1} + \mathbf{T}_S + \left(\mathbf{T}_D + \frac{1}{2}\mathbf{T}_D^2 \right) + \left(\mathbf{T}_T + \mathbf{T}_D\mathbf{T}_S + \frac{1}{6}\mathbf{T}_S^3 \right) + \dots \tag{2.48}$$

Similarly to CI, an exact result is obtained when all terms are included, but the expansion is truncated at some level to make the calculation viable. The "gold standard" in quantum chemical calculations is CCSD(T), in which the series is expanded to single and double excitations, and the triple excitations are included as a perturbation.

2.5.3 Perturbation theory

In the perturbation theory approach, the true Hamiltonian $\mathbf{H}$ is written as a sum of an unperturbed Hamiltonian $\mathbf{H}_0$ and a perturbed Hamiltonian, assumed to be small in comparison to the unperturbed Hamiltonian $\mathbf{H}'$ [2]:

$$\mathbf{H} = \mathbf{H}_0 + \lambda\mathbf{H}', \tag{2.49}$$

where the λ controls the strength of the perturbation. Using the perturbed Hamiltonian, we get the Schrödinger equation:

$$\mathbf{H}\Psi = W\Psi. \tag{2.50}$$

The energy W and the wave function Ψ as a power series with respect to the perturbation parameter λ:

$$(\mathbf{H} + \lambda\mathbf{H}')\left(\sum_i \lambda^i \Psi_i\right) = \left(\sum_i \lambda^i W_i\right)\left(\sum_i \lambda^i \Psi_i\right) \tag{2.51}$$

Here, the term $i = 0$ is the non-perturbed case Ψ_0 with energy $W_0 = E_0$, and the higher order terms are the 1st, 2nd, ... order corrections. The higher order wave functions are defined to be orthonormal to the Ψ_0. These terms are grouped, collecting together terms with the same power of λ:

$$\lambda^n : \mathbf{H}_0\Psi_n + \mathbf{H}'\Psi_{n-1} = \sum_{i=0}^{n} W_i\Psi_{n-i}. \tag{2.52}$$

From this, it follows that the nth order energy can be calculated using $(n-1)$th order wave function:

$$W_n = \langle\Psi_0\,|\mathbf{H}'|\,\Psi_{n-1}\rangle \tag{2.53}$$

In Møller-Plesset (MP) perturbation theory [8], the unperturbed Hamiltonian $\mathbf{H}_0$ is the sum of operators, and the perturbation term is the difference between the true electron-electron repulsion and the average one obtained by HF, $\langle\mathbf{V}_{\text{ee}}\rangle$:

$$\mathbf{H}_0 = \sum_{i=1}^{N_{\text{elec}}} \mathbf{F}_i = \sum_{i=1}^{N_{\text{elec}}} \mathbf{h}_i + 2\langle\mathbf{V}_{\text{ee}}\rangle \tag{2.54}$$

$$\mathbf{H}' = \mathbf{H} - \mathbf{H}_0 = \mathbf{V}_{\text{ee}} - 2\langle\mathbf{V}_{\text{ee}}\rangle, \tag{2.55}$$

where the factor of two is due to the double counting of the V_{ee} term in Fock operators.

The n'th order perturbation is denoted as MPn. The MP0 energy is the sum of MO energies, MP1 is equal to the HF energy, and the MP2 energy is [2]:

$$E(\mathrm{MP2}) = \sum_{i<j}^{\mathrm{occ}} \sum_{a<b}^{\mathrm{vir}} \frac{\left(\langle \phi_i \phi_j \mid \phi_a \phi_b \rangle - \langle \phi_i \phi_j \mid \phi_b \phi_a \rangle \right)^2}{\varepsilon_i + \varepsilon_j - \varepsilon_a - \varepsilon_b}, \tag{2.56}$$

where the indices i and j refer to occupied MOs, a and b to unoccupied ones, and ϵ is MO energy.

MP is not a variational method - instead of asymptotic convergence to an exact result by including higher-order terms, the results oscillate around the true energy. Most commonly, the MP2 is used, which captures around 80-90% of the correlation energy [2].

2.6 Density functional theory

The combination of Hartree-Fock method with electron correlation methods allows the accurate determination of energy and molecular properties. However, they become computationally expensive due to the scaling that the methods have, and in their most accurate form are typically used for small compounds or ones with high symmetry.

The workhorse in computational quantum chemistry and materials science is the Kohn-Sham formulation of density functional theory (KS-DFT). It is a mean-field method that uses the same computational machinery as the HF method, but it is able to include some effects arising from the electron correlation. This is done with some clever tricks. The method has its shortcomings, but when used properly, it allows one to solve some real problems and deal with large and complex molecules.

2.6.1 Hohenberg-Kohn theorems

The basis of DFT is formed by Hohenberg-Kohn theorems [9], written originally for ground-state systems. The first theorem states that the external potential is, within the addition of a constant, a unique functional of the electron density. In the absence of external fields, the external potential is the potential of the nuclei. From this follows that the Hamiltonian operator, and thus the ground state of the system, is a unique functional of the electron density. This can be intuitively understood from electron density maps: the cusps and heights of electron density give the location and the

charge of the nuclei, and the integral of electron density gives the number of electrons of the system.

The second theorem states that the energy of a system is minimized by true electron density. This allows one to use the variational method to obtain the true electron density of the system.

In DFT, the molecular energy is written as a functional of the electron density

$$E[\rho] = T_e[\rho] + V_{ee}[\rho] + V_{ne}[\rho]. \tag{2.57}$$

Here, the nuclear-electron potential energy $V_{ne}[\rho]$, that defines the external potential, is system-specific. It can be calculated exactly from the Coulomb interaction between the electron density and the nuclear charges. The electron kinetic energy and electron-electron potential energy, $T_e[\rho] + V_{ee}[\rho]$, are universal terms and not dependent of the system, and they are grouped to universal functional $F[\rho]$:

$$E[\rho] = V_{ne}[\rho] + F[\rho] \tag{2.58}$$

The electron-electron potential energy can be split into two terms, the exactly calculable classical Coulomb part $J[\rho]$, and nonclassical part $E_{ncl}[\rho]$, which captures the effect of exchange and Coulomb correlation, and fixes the nonphysical interaction energy of the electron with itself.

The early versions of DFT did not use orbitals: they worked directly on electron density. These so-called orbital-free methods reduce the dimensionality of optimizing the wave function from 4N to 4 dimensions. The early methods had shortcomings: the kinetic energy part has wrong asymptotic behavior, and the models did not reproduce chemical bonding [2].

2.6.2 Kohn-Sham density functional theory

DFT is made usable in chemistry by Kohn-Sham DFT (KS-DFT) [10]. It introduces MOs of a hypothetical non-interacting reference system with the same density as the interacting electrons in order to ease the calculation of kinetic energy.

Similarly, as in splitting the electron-electron potential energy to Coulombic and nonclassical parts, this way the true kinetic energy can be split to one calculated using

orbitals $T_S[\rho]$, and the correction term $T_C[\rho]$. The exact kinetic energy is calculated with the KS orbitals ϕ_i as:

$$T_S = \sum_{i=1}^{N_{\text{elec}}} \left\langle \phi_i \left| -\frac{1}{2}\nabla^2 \right| \phi_i \right\rangle \tag{2.59}$$

The universal functional can then be divided into exactly calculable parts, and the unknown terms are grouped into the exchange-correlation (XC) functional $E_{\text{XC}}[\rho]$:

$$F[\rho] = T_S[\rho] + J[\rho] + E_{\text{XC}}[\rho] \tag{2.60}$$

$$E_{\text{XC}}[\rho] = (T[\rho] - T_S[\rho]) - (V_e e[\rho] - (J[\rho])) \tag{2.61}$$

$$= T_C[\rho] + E_{\text{ncl}}[\rho]. \tag{2.62}$$

The exact form of the XC-functional E_{XC} is not known. The next subsection describes different approximations developed, which perform reasonably well.

As in the HF method, the energy and the KS wave function are solved by determining the set of orthogonal orbitals that minimize the energy. Lagrangian optimization scheme gives analogous eigenvalue equations with one-electron operator $\mathbf{h}_{KS}$ in place of the Fock operator given previously in Equation 2.31 [2]:

$$\mathbf{h}_{KS}\phi_i = \epsilon_i \phi_i \tag{2.63}$$

$$\mathbf{h}_{\text{KS}} = \frac{1}{2}\nabla^2 + \mathbf{v}_{\text{eff}} \tag{2.64}$$

$$\mathbf{v}_{\text{eff}}(\mathbf{r}) = \mathbf{V}_{\text{ne}}(\mathbf{r}) + \int \frac{\rho(\mathbf{r}')}{|\mathbf{r} - \mathbf{r}'|}d\mathbf{r}' + \mathbf{V}_{\text{xc}}(\mathbf{r}) \tag{2.65}$$

$$\tag{2.66}$$

The effective potential consists of nuclear-electron, electron-electron, and XC-potentials, where XC-potential is functional derivative of XC-energy with respect to the electron density [2]:

$$\mathbf{V}_{\text{xc}}(\mathbf{r}) = \frac{\delta E_{\text{xc}}[\rho]}{\delta \rho(\mathbf{r})} = \varepsilon_{\text{xc}}[\rho(\mathbf{r})] + \int \rho(\mathbf{r}') \frac{\delta \varepsilon_{\text{xc}}(\mathbf{r}')}{\delta \rho(\mathbf{r})}d\mathbf{r}' \tag{2.67}$$

By expanding the KS orbitals as basis functions, one obtains Roothaan-Hall equations for DFT. The calculation of nuclear-electron interactions and Coulomb repulsion is done similarly as in HF method, but numerical integration is needed for calculating integrals in the XC-potential. The choice of a proper numerical integration grid is important [11], with some XC-functionals being more sensitive than others [12].

2.6.3 Exchange-correlation functionals

The search for more performant XC-functionals (denoted simply as functionals from now on) is guided by the physical and mathematical properties of an exact functional. Functionals are often grouped in a hierarchy known as Jacob's ladder [13]. However, unlike in wave function methods, there is in general no systematic way to obtain a better functional.

The XC-functional is commonly split to exchange and correlation functionals E_X and E_C, and the XC-functional be built of parts from different families [2]:

$$E_{XC}[\rho] = E_X[\rho] + E_C[\rho]. \tag{2.68}$$

On the first rung of this Jacob's ladder is the Local Density Approximation (LDA), in which the electron density is treated locally and as a homogeneous electron gas. It underestimates the correlation energy and overestimates the exchange energy. Next in the rank is the Generalized Gradient Approximation (GGA), where the exchange and correlation energies depend on the first derivative of the density. The inclusion of the second-order derivatives of electron density leads to meta-GGA functionals.

One fundamental issue of KS-DFT is the self-interaction error (SIE), the nonphysical interaction of an electron with itself. In HF, this is canceled by the exchange operator, but in DFT, the canceling is the responsibility of the approximate density functional. As a consequence, the electron density is too localized [14, 15]. Correction schemes exist [16], but commonly this is alleviated by the use of hybrid functionals.

Global hybrid functionals mix a fraction of HF exchange E_X^{HF}, calculated using the KS orbitals, to the exchange functional. In range-separated hybrid functionals, the exchange functional is split into short- and long-range parts, and different functionals are used for them. As SIE manifests commonly as incorrect asymptotic behavior of the XC-potential, a common way is to use a DFT exchange functional for the short-range,

and mix a fraction of HF exchange to the exchange functional used for the long-range parts.

In the final rung of Jacob's ladder are the double hybrid methods, which include the virtual KS orbitals to the correlation functional, commonly in the form of MP2-like perturbational treatment.

The approximate functionals are poor in describing dispersion interactions. The most popular way to overcome this is through the dispersion correction scheme of Grimme, in which a correction term consisting of pairwise semi-empirical potentials is added [17, 18].

A large collection of different functionals exist - in the libxc library, over 400 functionals are implemented [19]. Functionals have different performances in different application areas, and selecting the right one is a sort of art form itself. A recent perspective article by the group of Grimme collected the hidden knowledge of applying DFT to molecules [20]. Large benchmark studies have been done for different applications [21, 22]. Commonly, the choice is guided by intuition and knowledge of what usually works. This intuition can be wrong, and it is advisable to test the performance of different functionals for the task at hand.

2.7 Ring current calculations

An external magnetic field interacts with the electrons of a molecule by inducing a current. These magnetically induced currents are useful as a measure for aromaticity, as discussed in Section 3.4, and in understanding the nuclear magnetic shielding (NMR) and magnetizability measurements of molecules. By including the magnetic field in the quantum chemical description, the magnetically induced current density of a molecule can be calculated and processed to yield a quantitative measure for aromaticity.

2.7.1 Hamiltonian in an external magnetic field

The molecular electronic Hamiltonian in Equation 2.7 does not include the effects of external electromagnetic fields. The external magnetic field $\mathbf{B}$ is introduced to quantum chemical calculations in the form of the magnetic vector potential $\mathbf{A}$:

$$\mathbf{B} = \nabla \times \mathbf{A}. \tag{2.69}$$

This form leads to ambiguity known as gauge freedom. The gradient of any differentiable function with a vanishing curl $f(\mathbf{r})$ can be added to the magnetic vector potential without changing the magnetic field, as $\nabla \times \nabla f(\mathbf{r}) = 0$. The vector potential can be chosen arbitrarily, and typically one that fulfills the Coulomb gauge condition $\nabla \cdot \mathbf{A} = 0$ is used [23]. The magnetic vector potential for a uniform external magnetic field is [24]:

$$\mathbf{A}(\mathbf{r}) = \frac{1}{2}\mathbf{B} \times \mathbf{r_O}, \tag{2.70}$$

where the $\mathbf{r_O} = \mathbf{r} - \mathbf{O}$ is the distance vector between the evaluation point to the gauge origin $\mathbf{O}$. The gauge origin can be set freely by choosing the gauge to be $f\mathbf{r} = \frac{1}{2}(\mathbf{B} \times \mathbf{d} \cdot \mathbf{r})$, which displaces the gauge origin by a vector $\mathbf{d}$ while leaving the underlying magnetic field unchanged. The change of gauge origin is called gauge-transformation.

The effect of an external magnetic field is included in Hamiltonian by replacing the momentum operator $\mathbf{p}$ with a kinetic momentum operator π:

$$\mathbf{p} \to \pi = -i\hbar\nabla + e\mathbf{A}. \tag{2.71}$$

This leads to a Hamiltonian consisting of three terms: the original field-free Hamiltonian $\mathbf{H}^{(0)}$, the paramagnetic term $\mathbf{H}^{(1)}$ with a first-order dependency of the magnetic vector potential, and the diamagnetic term $\mathbf{H}^{(2)}$ with a second-order dependency:

$$\mathbf{H} = \mathbf{H}^{(0)} + \mathbf{H}^{(1)}_{\text{para}}(\mathbf{A}) + \mathbf{H}^{(2)}_{\text{dia}}\left(A^2\right) \tag{2.72}$$

The paramagnetic term describes the interaction of the magnetic field and the electron's angular and spin angular momentum. Based on the momenta, the paramagnetic term can either increase or decrease the total energy. The diamagnetic term always leads to an increase in energy. Using the form of the magnetic vector potential in Eq. 2.70, the terms are:

$$\mathbf{H}^{(1)} = \mathbf{H}_A^{(1)} + \mathbf{H}_S^{(1)} \tag{2.73}$$

$$= \frac{1}{2}\mathbf{B} \cdot \mathbf{L_O} + \mathbf{B} \cdot \mathbf{S} \tag{2.74}$$

$$\mathbf{H}^{(2)} = \frac{1}{8}\left(B^2 r^2 - (\mathbf{B} \cdot \mathbf{r})^2\right). \tag{2.75}$$

The $\mathbf{L_O}$ is the angular momentum operator that depends on the gauge origin:

$$\mathbf{L_O} = \mathbf{r_O} \times \mathbf{p}. \tag{2.76}$$

Gauge transformation is equivalent to a unitary transformation of the Hamiltonian, and does not change the total energy. The wave function, however, obtains a phase factor [25]:

$$\mathbf{H}(\mathbf{A}') = e^{-if}\mathbf{H}(\mathbf{A})e^{if} \tag{2.77}$$

$$\psi(\mathbf{A}') = e^{-if}\psi(\mathbf{A}) \tag{2.78}$$

While the solutions of the Schrödinger equation are gauge invariant, the same does not hold for quantum chemical calculations done with a finite basis set. A common way to mitigate this is the use of gauge-including atomic orbitals (GIAO) [26–28]. In this approach, the basis functions are modified by multiplying them by an exponential prefactor containing the magnetic vector potential $A_K^{\mathbf{B}}$ with the gauge origin at the atomic nucleus [24]:

$$\chi_K\left(\mathbf{r}, \mathbf{A}_K^{\mathbf{B}}\right) = \exp\left(-i\mathbf{r} \cdot \mathbf{A}_K^{\mathbf{B}}(\mathbf{r})\right)\chi_K(\mathbf{r}) \tag{2.79}$$

$$\mathbf{A}_K^{\mathbf{B}} = \frac{1}{2}\mathbf{B} \times (\mathbf{R}_K - \mathbf{O}) \tag{2.80}$$

While GIAOs remove the explicit reference to the gauge origin in molecular integrals related to the calculation of magnetic properties, they do not lead to gauge invariance. The properties however do have a rapid basis set convergence [23].

Another approach is the one presented in the continuous set of gauge transformations (CSGT) [29] and the continuous transformation of the origin of the current density (CTOCD) methods [30, 31]. In these, the gauge origin is set to the evaluation points of the property, $\mathbf{O} = \mathbf{r}$.

2.7.2 Magnetically induced current density

The conservation of probability density $\rho = |\Psi|^2$ can be written as a continuity equation:

$$\frac{\partial \rho}{\partial t} = -\nabla \cdot \mathbf{j}, \tag{2.81}$$

where $\mathbf{j}$ is the probability current density:

$$\mathbf{j}(\mathbf{r}) = -\frac{1}{2} \left(\Psi \mathbf{p} \Psi^* + \Psi^* \mathbf{p} \Psi \right) \tag{2.82}$$

In typical conditions, interactions between the electrons and the external magnetic field are much weaker than the electrostatic interactions within a molecule. Assuming that the magnetic field is uniform and infinitely weak, the response of the wave function to it can be treated with perturbation theory and represented by a series [24]:

$$\Psi_0 = \Psi_0^{(0)} + \Psi_0^{(1)} + \dots. \tag{2.83}$$

The first-order magnetically perturbed wave function $\Psi_0^{(1)}$ is obtained from the unperturbed wave function Ψ_0 using the angular momentum operator $\hat{\mathbf{L}}_{\mathbf{O}}$ from Eq. 2.76 as the perturbation [24]:

$$\Psi_0^{(1)} = \Psi_0^{\hat{\mathbf{L}}_{\mathbf{O}}} \cdot \mathbf{B} \tag{2.84}$$

$$= \frac{1}{2} \sum_{j \neq 0} \left| \Psi_j^{(0)} \right\rangle \frac{\left\langle \Psi_j^{(0)} | \hat{\mathbf{L}}_{\mathbf{O}} \cdot \mathbf{B} | \Psi_0^{(0)} \right\rangle}{E_j^{(0)} - E_0^{(0)}} \tag{2.85}$$

where the sum is over the excited states j. The numerator of the weight term is the transition moment between ground and excited states $\Psi_0^{(0)}$ and $\Psi_j^{(0)}$, and the denominator is their energy difference energy. Inserting this first-order magnetically perturbed wave function into the definition of probability current density in Eq. 2.82 gives equations for the corresponding first-order magnetically induced current density, $\mathbf{J}^{\mathbf{B}}$. This is commonly split into diamagnetic and paramagnetic terms [24]:

$$\mathbf{J^B} = \mathbf{J^B_{dia}} + \mathbf{J^B_{para}} \tag{2.86}$$

$$\mathbf{J^B_{dia}} = -\frac{1}{2}\mathbf{B} \times \mathbf{r_O}\left(\Psi_0^{(0)}\right)^2 \tag{2.87}$$

$$\mathbf{J^B_{para}} = -i\sum_{I \neq 0}\left(\Psi_I^{(1)}\nabla\Psi_0^{(0)} + \Psi_0^{(0)}\nabla\Psi_I^{(1)}\right) \tag{2.88}$$

The diamagnetic term $\mathbf{J^B_{dia}}$ corresponds to the classical Larmor current density. The paramagnetic term has current density components arising from the mixing of excited and ground states.

2.7.3 Calculation of the current densities and strengths of molecules

Current densities are typically calculated using perturbation theory. Similarly as in the previous subsection, the magnetic field is assumed to be infinitely weak and uniform. Expanding the current density as a series with respect to the magnetic field $\mathbf{B}$ [24, 32]:

$$\mathbf{J^B}(\mathbf{r}) = \mathbf{j_0}(\mathbf{r}) + \sum_{\beta \in \{x,y,z\}}\left.\frac{\partial\mathbf{J^B}(\mathbf{r})}{\partial B_\beta}\right|_{B_\beta=0}B_\beta + \cdots \tag{2.89}$$

The zeroth order term vanishes for closed-shell molecules, and the second term is the current density susceptibility tensor (CDST) [24]:

$$\mathcal{J}_\alpha^{B_\beta}(\mathbf{r}) = \left.\frac{\partial J_\alpha^{B}(\mathbf{r})}{\partial B_\beta}\right|_{B_\beta=0}, \text{ where } \alpha, \beta \in x, y, z.. \tag{2.90}$$

CDST is a second-rank tensor, describing the linear change in the magnitude of the current density with respect to the change of the external magnetic field. Contracting CDST with a magnetic field gives current density susceptibilities with units $nA\,T^{-1}\,m^{-2}$. Integration of current density susceptibility for a given domain gives current susceptibility with units of $nA\,T^{-1}$. In further sections, we will denote current susceptibilities and current density susceptibilities as current and current densities for brevity.

In the research presented in this thesis, we used the gauge-including magnetically induced current method (GIMIC) for the calculation of current densities [33]. As the

name implies, GIMIC uses GIAOs to deal with the gauge origin problem. The gauge dependency arising from the use of a finite basis set leads to the loss of charge conservation. As earlier discussed, the use of GIAOs lead to fast basis set convergence. The theory behind GIMIC and its various applications have been reviewed earlier [24, 34, 35].

To calculate the CDST, GIMIC requires the unperturbed and first-order magnetically perturbed density matrices, and is thus agnostic to the level of theory. The current implementation[2] supports the calculation of current density for both open- and closed-shell systems [36], with basis sets containing ECPs [37], and has interfaces to several quantum chemistry software.

The equation that GIMIC uses for the calculation CDST is derived by equating the analytical derivative and Biot-Savart expressions of nuclear magnetic shielding tensor $\sigma_{\alpha\beta}^I$. The analytical derivative expression is obtained by differentiating the total energy with respect to nuclear magnetic momenta and magnetic field [38]:

$$\sigma_{\alpha\beta}^I = \left.\frac{\partial^2 E}{\partial m_\alpha^I \partial B_\beta}\right|_{\substack{\mathbf{B}=0 \\ \mathbf{m}_I=0}} = \sum_{\mu\nu} D_{\mu\nu} \frac{\partial^2 h_{\mu\nu}}{\partial m_\alpha^I \partial B_\beta} + \sum_{\mu\nu} \frac{\partial D_{\mu\nu}}{\partial B_\beta} \frac{\partial h_{\mu\nu}}{\partial m_\alpha^I}. \tag{2.91}$$

Here $h_{\mu\nu}$ is the matrix containing one-electron integrals in atomic orbital basis, $D_{\mu\nu}$ is the density matrix, and the derivatives are given with respect to magnetic fields B_β and nuclear magnetic momenta m_α^I.

The equation for the Biot-Savart expression is [32]:

$$\sigma_{\alpha\beta}^I = -\epsilon_{\alpha\delta\gamma} \int \frac{(r_\delta - R_{I\delta})}{|\mathbf{r} - \mathbf{R}_I|^3} \mathcal{J}_\gamma^{B_\beta} d\mathbf{r} \tag{2.92}$$

where $\epsilon_{\alpha\delta\gamma}$ is the Levi-Civita tensor. Combining these leads to the final form of equations used in GIMIC to calculate the CDST [33]:

$$\mathcal{J}_\gamma^{B_\tau}(\mathbf{r}) = \sum_{\mu\nu} D_{\mu\nu} \frac{\partial \chi_\mu^*(\mathbf{r})}{\partial B_\tau} \chi_\nu(\mathbf{r}) + \sum_{\mu\nu} D_{\mu\nu} \chi_\mu^*(\mathbf{r}) \frac{\partial \tilde{h}}{\partial m_\alpha^I} \frac{\partial \chi_\nu(\mathbf{r})}{\partial B_\tau} \tag{2.93}$$

$$+ \sum_{\mu\nu} \frac{\partial D_{\mu\nu}}{\partial B_\tau} \chi_\mu^*(\mathbf{r}) \frac{\partial \tilde{h}}{\partial m_\alpha^I} \chi_\nu(\mathbf{r}) - \epsilon_{v\tau\delta} \left[\sum_{\mu\nu} D_{\mu\nu} \chi_\mu^*(\mathbf{r}) \frac{\partial^2 \tilde{h}}{\partial m_\alpha^I \partial B_\delta} \chi_\nu(\mathbf{r}) \right]. \tag{2.94}$$

---

[2]`https://github.com/qmcurrents/gimic`

Here, χ_ν are the GIAOs, and the operators $\partial \tilde{h} / \partial m_\alpha^I$ and $\partial^2 \tilde{h} / \partial m_\alpha^I \partial B_\delta$ are:

$$\left. \frac{\partial \tilde{h}}{\partial \mathbf{m}_I} \right|_{\substack{\mathbf{m}=0 \\ \mathbf{m}_I=0}} = (\mathbf{r} - \mathbf{R}_I) \times \mathbf{p} \qquad (2.95)$$

$$\left. \frac{\partial^2 \tilde{h}}{\partial \mathbf{m}_I \partial \mathbf{B}} \right|_{\substack{\mathbf{B}=0 \\ \mathbf{m}_I=0}} = \frac{1}{2} \left[(\mathbf{r} - \mathbf{R}_O) \cdot (\mathbf{r} - \mathbf{R}_I) \, \mathbf{1} - (\mathbf{r} - \mathbf{R}_O) \, (\mathbf{r} - \mathbf{R}_I) \right], \qquad (2.96)$$

where $\mathbf{R_I}$ are the nuclear coordinates and $\mathbf{R}_O$ is the gauge origin, both of which cancel, latter due to the use of GIAOs. These equations are implemented in GIMIC in a slightly less daunting tensorial form [33]:

$$\mathcal{J}_\alpha^B = \mathbf{v}^T \mathbf{P}_\beta \mathbf{d}_\alpha - \mathbf{b}_\beta^T \mathbf{D} \mathbf{d}_\alpha + \mathbf{v}^T \mathbf{D} \mathbf{q}_{\alpha\beta} - \epsilon_{\alpha\beta\gamma} \frac{1}{2} \left(\mathbf{v}^T \mathbf{D} \mathbf{v} \right) \mathbf{r}_\gamma. \qquad (2.97)$$

Here $\mathbf{v}$ is a vector containing basis-function values at each grid point $\mathbf{r}$, $\mathbf{D}$ is the AO density matrix, $\mathbf{P}_\alpha$ is the magnetically perturbed AO density matrix, and $\mathbf{b}_\alpha, \mathbf{d}_\alpha$, and $\mathbf{q}_{\alpha\beta}$ are the following derivatives of the basis functions:

$$\mathbf{b}_\alpha = \frac{\partial \mathbf{v}}{\partial \mathbf{B}_\alpha} \; ; \; \mathbf{d}_\alpha = \frac{\partial \mathbf{v}}{\partial \mathbf{r}_\alpha} \; ; \; \mathbf{q}_{\alpha\beta} = \frac{\partial^2 \mathbf{v}}{\partial \mathbf{r}_\alpha \mathbf{B}_\beta} \; , \; \text{where } \alpha, \beta = x, y, z \qquad (2.98)$$

GIMIC contracts the CDST tensor with a defined magnetic field to give current densities. The induced current depends on the orientation of the magnetic field. To study the ring current, the magnetic field is oriented parallel to the norm axis of the ring, i.e., the molecule is oriented in xy-plane and the magnetic field is pointed in the z-direction. The choice of the magnetic field is more ambiguous for non-planar systems, and it is important to have consistency in comparing different systems.

For calculating a bond current I_{AB} between atoms A and B, the $\mathbf{J^B}(\mathbf{r})$ is contracted by the norm vector $\mathbf{n}$ of the integration domain $\mathcal{S}$:

$$I = \int_{\mathcal{S}} \sum_{\beta \in x,y,z} \frac{B_\beta}{|\mathbf{B}|} \mathcal{J}^{B_\beta}(\mathbf{r}) \cdot \mathbf{n} \mathrm{d}s. \qquad (2.99)$$

The domain is chosen so that it contains all the current contributions between the two atoms. GIMIC implements a numerical integration procedure using two-dimensional Gaussian quadrature, and allows the manual definition of an integration

domain [33]. In the manual procedure of GIMIC, two atoms are given, the order of which defines the direction of the normal **n**, along with a distance defining the location on this vector, typically a mid-point of the bond. Additionally, a third point is given for defining the orientation of the rectangular domain and the distances that define its height and width.

Such a manual process is error-prone, and ensuring the validity requires painstaking analysis to ensure that only the relevant current contributions are captured. Automated procedures have recently been implemented. In AIMAll program, the integration domain is the intersection of two atomic surfaces as defined by QTAIM framework [39]. Irons et al. used a circular grid placed on bond cross-sections, with the radius defined based on the atomic radii of the bonding atoms [40]. In SYSMOIC program, the integration domain is defined as an area within the contour of certain cutoff of the current density at a plane bisecting the bond [41]. The latter approach is the most sensible, as the QTAIM approach uses electron density, not current density in the determination, and the use of a circular grid ignores the tails of current density distributions.

Chapter 3

Aromaticity

3.1 The fuzziness of aromaticity

Chemical models have existed long before quantum mechanics [42]. The roots of aromaticity date back to Faraday's discovery of benzene in 1825 [43]. This class of carbon compounds was found, in addition to their aroma, to have special reactivity and thermodynamic stability. The structure of benzene was a matter of debate. In 1865, Kekulé came up with the structure of benzene with alternating double and single bonds [44]. He later came up with the model of the two equivalent structures existing in resonance [45], the legend being that it came to his dream as an image of a snake eating its tail.
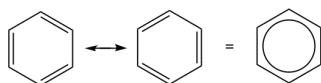
Figure 3.1: Two resonance structures of benzene

Upon the discovery of electrons and finally, with the advent of quantum mechanics, better models appeared. Much of chemical intuition is rooted in Lewis structures, in which two nuclei are bonded by sharing electron pairs to obtain an octet. Benzene has two equivalent resonance structures, indicating delocalization, the incapability of describing the bonds with a set of two-center two-electron bonds. Pauling formulated chemical bonding with hybrid orbitals in the valence bond (VB) framework, in which the resonance of localized structures describes aromaticity [46]. In MO theory, Hückel came up with the $4n + 2$ rule for aromaticity with an effective Hamiltonian describing

the π framework [47–49].

With quantum chemical methods, the properties of molecules can be calculated, often with high accuracy. However, a large part of chemistry is rooted in intuitive concepts, many of which predate the discovery of the electron, that lack a clear physical basis [50], and are "fuzzy". Aromaticity is one of the most intensely debated ones, but others are as common for the chemist, starting from the chemical bond, to atomic charges, strain, conjugation, and others. These concepts are a tool for intuition, an explanatory mechanism, and a heuristic for making sense of protons and electrons. Using these concepts, chemists can explain observations, predict outcomes, and perhaps, most importantly, design new molecules and materials. This has led to various methods and debates on how to extract them from the calculated wave function [50, 51]

The fuzzy nature of aromaticity has the confusing manifestation of a vast number of different types of aromaticities, rules, and measures. The definition adopted in this thesis follows that of Schleyer et al. [52]: *"Aromaticity is a manifestation of electron delocalization in closed circuits, either in two or in three dimensions. This results in energy lowering, often quite substantial, and various unusual chemical and physical properties. These include a tendency toward bond-length equalization, unusual reactivity, and characteristic spectroscopic features. Since aromaticity is related to induced ring currents, magnetic properties are particularly important for its detection and evaluation."*

The list of different aromaticities described in the literature is vast, Grunenberg listing the following types [51]: σ, π, δ, ϕ, Y, double, anti, homo, pseudo, Hückel, Möbius, Craig–Möbius, Hückel-Möbiusquasi, 3D, metal, multiple, conflicting, Shannon, hetero, super, bishomo, bicyclo, homo-anti, bishomoanti, spiro, trishomo, antihomo, chelato, cruci, dihydro, heteroanti, heterohomo, homohetero, hydro, hyper, hyperconjugative, mono, monohomo, non, pro, disk, quasianti, sila, pre. As the quantification of aromaticity is done using measures connected to its different physicochemical manifestations, dozens of methods exist. Some of these are covered in Sections 3.3 and 3.4, and a more extensive, yet still non-exhaustive list is given by Solà [53]: ASE, RE, ISE, AI, HOMA, Julg index, Jug index, Bird index, PDI, FLU, FLUπ, MCI, I_{ring}, I_{NG}, I_{NG}, I_{NB}, EDDB, AV1245, ELF$_\pi$, ATI, θ, PLR, η, ρ, RCP, Λ, ACID, ARCS, NICS, NICS$_{zz}$, NICS$_\pi$, NICS-XY-scan. These methods have their advantages and shortcomings and can give conflicting results.

The search for the Holy Grail of aromaticity measures is a long and still ongoing one, and brings to mind the comic by Munroe shown in Figure 3.2:
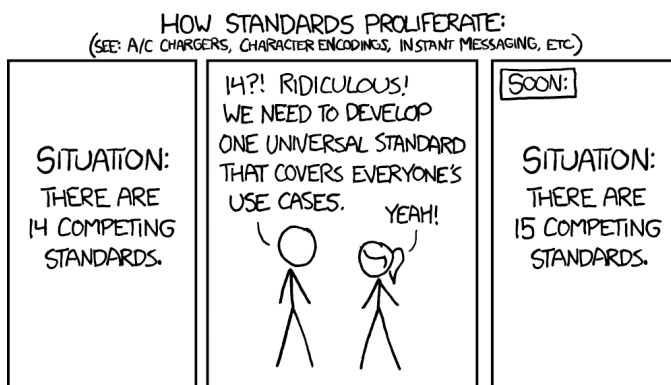
Figure 3.2: "Standards", a comic by Randall Munroe, published with CC BY-NC 2.5 license, `https://xkcd.com/927/`

3.2   Aromaticity rules

Why is one molecule aromatic and one not? Several rules exist to answer this question for molecules with different dimensions, topologies, and electronic states, as recently reviewed by Solà [54, 55].

The seminal rule for aromaticity was formulated by Hückel for planar monocycles in 1931, leading to the $4n + 2$ rule carrying his name [47–49]. It is based on the energy levels of π orbitals, calculated using a simplified MO theory approach for D_{nh} symmetric systems. The lowest energy MO is non-degenerate, and the latter ones are doubly degenerate. Each MO takes in two electrons, and when there are $4n + 2$ electrons, the electron shells are filled. When there are $4n$ electrons, there is a half-filled degenerate MO, and the system has a tendency to undergo a Jahn-Teller distortion - lowering its energy by undergoing a distortion that breaks the degeneracy. The $4n + 2$ rule can also be understood from the eigenfunctions of a Hamiltonian for a particle on a ring [56]. The eigenfunctions for a particle on a sphere Hamiltonian lead to Hirsch's rule: a system being spherically aromatic if there are $2(n + 1)^2$ delocalized electrons surrounding a roughly spherical nuclear scaffold [57].

In the case of planar open-shell molecules, the rules are changed. Baird's rule states that those molecules antiaromatic in their singlet ground state become aromatic in their lowest-lying triplet state, and aromatic compounds become antiaromatic [58]. This was generalized by Soncini and Fowler by noting that molecules with $4n + 2$ electrons are aromatic and $4n$ electrons are antiaromatic in the lowest-lying electronic state with even spin, and this is reversed when the spin is odd [59]. This was further generalized by both Mandado et al. and Valiev et al. by noting that systems with an odd number of α- and β electrons in the conjugation pathway are aromatic, and those with even number are antiaromatic [60, 61]. The Hirsch's rule was extended to open-shell systems by Poater and Solà, leading to a rule stating that spherical compounds with $2n^2 + 2n + 1$ electrons and a multiplicity of $S = n + \frac{1}{2}$ are aromatic [62].

Another change occurs when the topology of the conjugation circuit changes to a Möbius-like state. Heilbronner found the molecules with one twist are aromatic when they have $4n$ electrons, and antiaromatic with $4n+2$ electrons [63]. This was generalized by Rappaport and Rzepa [64] using the topological concept of linking number L_K, which represents the number of times that each curve winds around the other in an annulene [54]: those with an even L_K follow Hückel's $4n + 2$ rule, which is then inverted for those with $4n$ electrons. This holds for even-spin systems and is again inverted for those with odd-spin. The rules for planar systems were condensed to a cube by Ottosson [65] and extended by Solà to include Soncini-Fowler rule and different linking numbers [54]:
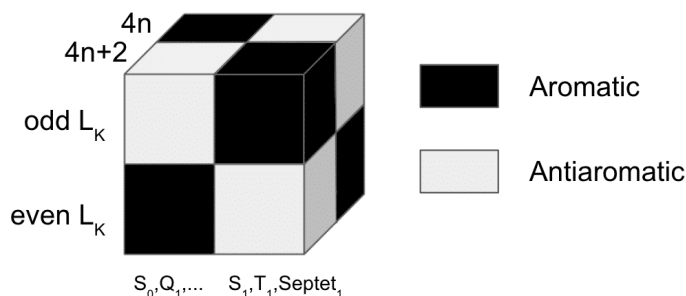

Figure 3.3: Ottoson's cube, adapted from Reference [54]

The aromaticity of polycyclic compounds is more complicated. While the spherical compounds described with Hirsch's rule are built from several cycles, the rules work under the assumption of the jellium model, where the nuclear scaffold can be treated

as an isotropic positively charged sphere. The delocalization circuits in polycyclic compounds in general are much more complex, arising from an intricate interplay between local and global aromaticities. One way to make sense of it is Clar's π-sextet rule [66, 67], which describes the dominant resonance structure of a polycyclic carbon molecule being the one with the maximum amount of drawn benzene rings, as shown for phenanthrene in Figure 3.4a. The rule was extended by Glidewell and Lloyd to non-benzenoid systems in stating that the preferred structure is the one in which the structures form the smallest $4n + 2$ groups and avoid forming the smallest $4n$ groups [55, 68], as shown in Figure 3.4b for bicyclodeca[6.2.0]pentaene.

(a)   **(b)**
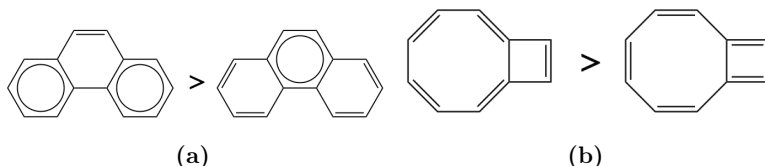
Figure 3.4: (a) Preferred Clar structure of phenanthrene and of (b) bicyclodeca[6.2.0]pentaene as predicted by Glidewell-Lloyd rule.

The ability of these simple rules to make predictions is a beautiful example of using theory to find simple and powerful models that aid chemists in their task of designing and understanding molecules. They are not without their shortcomings and fail in many cases as discussed by Solà in his review [55]. As the chemical space of possible aromatic compounds with varying aromaticities is vast, and these rules are a guide for molecular designers, the development and unification of these rules is an important line of development.

3.3 Physicochemical manifestations and quantification of aromaticity

The aromaticity of a molecule is evaluated by focusing on its physicochemical manifestations. Aromatic compounds have distinctive energetic stabilization, reactivity, and magnetic, optical, and structural properties. The delocalization can also be evaluated by wave function analysis. These different categories are called aromaticity criteria - in

this thesis, we study aromaticity based on magnetic criteria of aromaticity.

As listed in Section 3.1, many metrics exist for each criterion. It is common for them to have their shortcomings, and a knowledge of their form and applicability is needed to choose the proper one. Even if the most physically sound method is chosen, the results for aromaticity as per different criteria can give contradictory results. This is often termed the multidimensionality of aromaticity [53, 69–71]. The use of this description is criticized, with critics calling for better scrutiny for selecting methods [70, 72].

Here, we present an overview of various physicochemical manifestations of aromaticity along with some of their quantification methods.

3.3.1 Energetic stabilization

Energetic stabilization owing to aromaticity, or destabilization due to antiaromaticity, is one of the most important properties of aromatic compounds. This effect is somewhat tricky to calculate, and many of the other criteria are commonly used as a proxy measure for it.

The original measure for the stabilizing effect of aromaticity is resonance energy (RE), which quantifies the energy difference of a delocalized molecule to its hypothetical localized resonance structure [73]. Two types of REs exist: the vertical resonance energy (VRE), in which the delocalized and localized states have the same geometry, and the adiabatic resonance energy (ARE), in which the localized version has a bond-length alternating structure. One method to calculate this is the block-localized wave function (BLW) approach [74], which for benzene gives a VRE of $91.6 \, \text{kcal} \, \text{mol}^{-1}$ and ARE of $57.5 \, \text{kcal} \, \text{mol}^{-1}$ [75], the difference being distortion energy.

Resonance energies are measures of the total stabilization of the aromatic system compared to the hypothetical localized system. Often a more interesting quantity is the energetic stabilization of aromatic compounds with reference to a conjugated, but non-aromatic reference system [73]. This is known as the aromatic stabilization energy (ASE). The choice of the reference system is challenging: there are multiple causes for energy differences, and it may be challenging to select one in which only difference arises from aromaticity [76].

One way to calculate ASE is via isodesmic or homodesmotic reactions. Isodesmic reactions retain the same number of single and double bonds, homodesmotic reactions

retain the same number of bonds in each hybridization state, as shown below:

$$\text{Isodesmic: } 3H_2C{=}CH_2 + 3H_3C{-}CH_3 \longrightarrow C_6H_6 + 6CH_4 \tag{3.1}$$

$$\text{Homodesmotic: } 3H_2C{=}CH{-}CH{=}CH_2 \longrightarrow C_6H_6 + 3H_2C{=}CH_2 \tag{3.2}$$
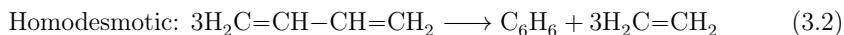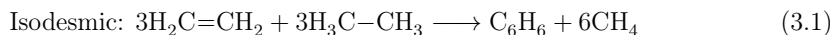
which lead to ASEs of $-67\,\text{kcal\,mol}^{-1}$ and $-23\,\text{kcal\,mol}^{-1}$, respectively [77], showing the importance of the correct choice of a reference system.

The effect of other stereoelectronic effects on the energy can be made smaller by computing isomerization stabilization energies. In it, the energy difference between the aromatic compound with an added methyl group and one with the methyl hydrogen transferred to the sp^2 carbon of an aromatic ring is calculated, as shown in Figure 3.5.
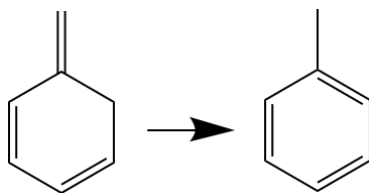
Figure 3.5: Reference system for calculating the isomerization stabilization energy of benzene

A clever way to dissect the different energetic interactions is the energy decomposition analysis (EDA) [78, 79]. In it, the interaction energies are divided into electrostatic, Pauli repulsion, and orbital interaction contributions. The orbital interaction contributions can be further divided into different symmetry components:

$$\Delta E_{\text{int}} = \Delta V_{\text{elstat}} + \Delta E_{\text{Pauli}} + \Delta E_{\text{orb}} \tag{3.3}$$

$$\Delta E_{\text{orb}} = \Delta E_\sigma + \Delta E_\pi + \Delta E_\delta \ldots \tag{3.4}$$

The ΔE_π component is a direct measure of the stabilization due of π-conjugation in a molecule. It does not require a reference molecule for its calculation [80]. For a π aromatic molecule, the ASE based on EDA can be calculated by comparing the ΔE_π value of the cyclic system to an acyclic reference structure.

3.3.2   Structural criteria

Geometric indices for aromaticity quantify the equalization of bond lengths in aromatic compounds [81]. Julg index A [82] calculates the variances of bond lengths along the circuit, while the harmonic oscillator model of aromaticity (HOMA) [83, 84] index compares the mean square errors of bond lengths compared to a reference bond length d_{ref}, which for hydrocarbons is the bond length of benzene 1.338 Å:

$$A = 1 - \frac{a}{n} \sum_{i=1}^{n} \left(1 - d_i/\bar{d}\right)^2 \tag{3.5}$$

$$\text{HOMA} = 1 - \frac{b}{n} \sum_{i=1}^{n} \left(d_i - d_{\text{ref}}\right)^2. \tag{3.6}$$

Here, the constants a and b are chosen to give zero to antiaromatic and one to aromatic reference systems, dependent on the studied molecules - different values are used for carbon and heterocyclic systems, for instance. Other forms of geometric measures have been developed, reviewed by Krygowski et al. [81], with an example of the harmonic oscillator stabilization energy (HOSE) that connects the mean squared errors in a slightly more complicatedly parametrized way to infer canonical pathways and resonance energies [85].

The Julg index has a deficiency in recognizing any systems with no bond-length alternation, such as cyclohexane. The geometric indices are formulated to reach a maximum for benzene, unable to differentiate between molecules with a stronger delocalization as indicated by magnetic measures.

Interestingly, the bond length equalization in aromatic molecules is driven by the σ electrons, while π electrons are distortive [86]. Pierrefixe and Bickelhaupt performed EDA analysis along the distortion pathway from delocalized to distorted structures. The propensity of π electrons to distort the structure is much higher in antiaromatic systems than in aromatic systems, while localizing tendency as the electrostatic and σ electrons is similar [87–89]. A similar effect holds for aromatic main-group molecules [90].

3.3.3   Electron delocalization methods

Quantum chemical methods give access to the wave function, in its computational representation of MOs and density matrices, and the corresponding electron density. As an

alternative to aromaticity descriptors based on calculated or experimentally determined molecular properties, one can work on the fundamental ψ and ρ directly [91].

Many of these electron delocalization methods are built on XC-density $\gamma_{\mathrm{XC}}(\mathbf{r}_1, \mathbf{r}_2)$. It gives a measure of spatial exclusion of one electron due to another, and is defined as the difference between uncorrelated densities and the true pair density of electrons [91]:

$$\gamma_{\mathrm{XC}}(\mathbf{r}_1, \mathbf{r}_2) = \gamma(\mathbf{r}_1 \mathbf{r}_2) - \rho(\mathbf{r}_1)\rho(\mathbf{r}_2). \tag{3.7}$$

Delocalization index (DI) $\delta(A, B)$ quantifies the delocalization for a pair of atoms A and B [92]. It is calculated as an integral of XC-density over their atomic basins, 3D region of an atom in a molecule, that is commonly done within the quantum theory of atoms in molecules (QTAIM) framework [93]. DI is defined as:

$$\delta(A, B) = -2 \int_B \int_A \gamma_{XC}(\mathbf{r}_1, \mathbf{r}_2)\,\mathrm{d}\mathbf{r}_1\mathrm{d}\mathbf{r}_2. \tag{3.8}$$

Which is in practice calculated by summing over the overlap matrix elements of the atomic basins. The comparison of these pairwise DIs to those of a reference system, similarly as in the structure-based aromaticity descriptors in the previous section, gives descriptors such as aromatic the fluctuation index [94]. DI can also be defined for multiple atoms. The ring delocalization index I_{ring} is built of DIs of neighboring atoms [95, 96], and its extension multicenter delocalization index (MCI) [97] calculates the permutations over all atoms in the conjugation pathway, which can capture through-space effects with the penalty of increased computational cost. These multicenter extensions are dependent on the number of ring atoms, requiring normalization to compare rings of different sizes [98].

Electron localization function (ELF) is a scalar real-space function, showing large values in regions where electrons are localized [99]. Topology analysis of the ELF field allows one to classify bonds and understand delocalization [100, 101]. One way to quantify bond strength is the bifurcation value, an isosurface value at which the ELF is no longer continuous between atoms. The total ELF value however is not able to quantify aromaticity. ELF function can be split to σ and π contributions[102], and the bifurcation value of ELF_π is related to aromaticity of π aromatic systems [103, 104].

Electron density of delocalized bonds (EDDB) is a recent method for measuring delocalization [105, 106]. It is based on an electron density decomposition scheme,

which partitions the electron density of a molecule to the densities localized at atoms, between atom pairs, and between multiple atoms. The latter quantity, EDDB($\mathbf{r}$) can be visualized to show the aromatic parts of molecules, and its electron occupation can be calculated to find the number of electrons involved. The EDDB for a peptide is shown in Figure 3.6 [106], showing the delocalized electron density of aromatic rings, and also in carboxylic acids.
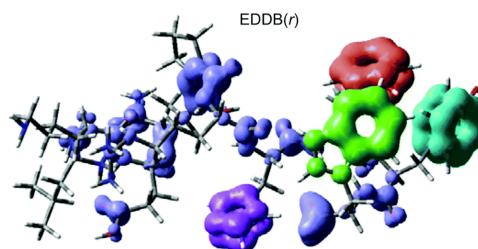
Figure 3.6: EDDB($\mathbf{r}$) function for an peptide. Taken from [106], published with CC-BY license.

Adaptive Natural Density Partitioning (AdNDP) is a method to identify N-center 2-electron bonds. It is based on natural bond orbitals (NBO), a method that transforms the delocalized wave function obtained to more interpretable, 2c-2e Lewis-like hybrid orbitals [107]. AdNDP extends it to delocalized bonding through an iterative algorithm described in [108]. It is a powerful qualitative tool for understanding delocalized chemical bonding, and has been applied to a wide variety of aromatic systems [109, 110]. AdNDP for benzene with the 2c-2e σ and the delocalized 6c-2e and 4c-2e π bonding patterns is shown in Figure 3.7.

Some work has been done on assessing aromaticity using only the electron density, a quantity that can also be obtained experimentally. Different measures of electron density at the ring-critical points, as defined in QTAIM, correlate with other aromaticity indices [93, 111, 112]. Similar correlations were found also for the information-theoretic Shannon entropy [113, 114], which has a beautiful and simple form:

$$S_S[\rho] = - \int \rho(\mathbf{r}) \ln \rho(\mathbf{r}) d\mathbf{r} \tag{3.9}$$
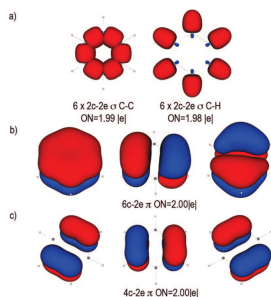
Figure 3.7: AdNDP for benzene, showing (a) 2c-2e σ, and the delocalized (b) 6c-2e and (c) 4c-2e π bonding patterns. Reprinted with permission from Reference [109]. Copyright 2022 American Chemical Society.

3.3.4 Spectroscopic methods

The electronic structure of aromatic compounds results in characteristic spectral fingerprints. In photoelectron spectroscopy, aromatic compounds have high electron detachment energies, while antiaromatic molecules have low ones. In UV spectra of aromatic compounds, the excitations occurring at frontier orbitals happen at higher energies, giving unique spectral fingerprints. These spectral fingerprints can be useful for qualitative assessment of aromaticity, especially in the case of aromaticity switching [115, 116]. Infrared spectroscopy can be used to obtain bond stretching force constants, which were found to be good measures for π delocalization for both aromatic and antiaromatic compounds [117].

3.3.5 Reactivity

In addition to the energetic stability due to aromaticity, aromatic compounds have distinctive reactivities. Aromaticity and antiaromaticity of transition states are also important in predicting reaction outcomes, for example in pericyclic reactions [118–121].

One tendency of aromatic compounds is to react by substitution reaction, in which the aromatic π system is retained, rather than by addition reactions, in which it would be lost [122]. Mucsi et al. developed a scale for aromaticity using both experimental and calculated enthalpies of hydrogenation [123]. They studied a set of monocyclic

compounds in which one of the double bonds of an aromatic compound is hydrogenated by cis addition. This hydrogenation enthalpy is compared to a hydrogen enthalpy of a non-aromatic reference compound. The more aromatic the compound, the harder it was to perform an addition reaction. A linear fit is done, giving benzene a value of 100% and cyclobutadiene a value of -100%. This measure was found to correlate well with NICS values, and in further study by Kumar and co-workers also with ring current strength and aromatic stabilization energies [124].

3.4 Magnetic criteria of aromaticity

3.4.1 Ring currents

An external magnetic field interacts with electrons by inducing currents. In aromatic molecules, a perpendicular magnetic field induces a net current around the conjugation pathway. This net current is called the ring current. In aromatic compounds, the ring current is diatropic, meaning that it circulates in the classical direction, i.e., clockwise when looking toward the negative direction of a magnetic field. Antiaromatic molecules have a paratropic ring current that circulates in the opposite counter-clockwise direction.

The magnetically induced current density of benzene is shown in Figure 3.8. On left, the current density is visualized in the molecular plane. Depending on the print quality of the thesis, the image shows the local circulations at the chemical bonds. On right, the current density is visualized $1\ a_0$[1] above the molecular plane, emphasizing the ring current of the π electrons.

The current density of a molecule is a vector field. It can be analyzed qualitatively by visualizations, a common way being to draw arrows with a length corresponding to the magnitude at the given point. Another way is to calculate the modulus of the current density, $|\mathbf{J}(\mathbf{r})|$, a scalar function which can be visualized as an isosurface.

For quantification, the current density is integrated at bonds in the conjugation pathway, giving the strength and the direction of the ring current. At the B3LYP/def2-TZVP level of theory, benzene has a diatropic ring current of 11.8 nA/T and cyclobutadiene has a paratropic ring current of -19.9 nA/T [125].

---

[1] $1\ a_0 = 0.529$ Å (10^{-10} m)

(a)   (b)
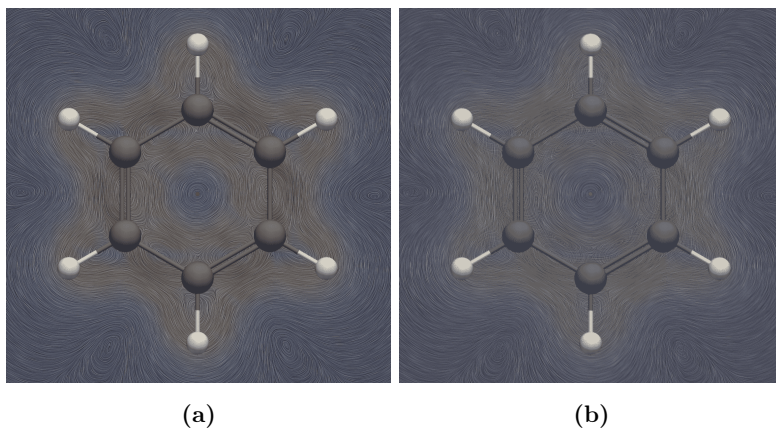
Figure 3.8: Current density of benzene at (a) the molecular plane and (b) 1 a_0 above.

In CTOCD-DZ, a formulation of CTOCD in which the gauge origin is chosen in a way that the diamagnetic contribution is annihilated, the current density can be dissected to orbital contributions [30, 31, 126]. This makes it possible to divide the ring current to σ and π contributions [127]. The π, σ, and total contributions of benzene's ring current are shown in Figure 3.9. At the HF/6-311+G(3df) level, the total ring current is 12.8 nA/T, of which 91.4% originate from the π electrons and 8.6% from the σ electrons.

Another result from the CTOCD-DZ formulation are the selection rules for diatropic and paratropic ring currents [128, 129]. The diatropic response is determined by translational and paratropic response by rotational transition matrix elements between the ground and excited states, $|\phi_a\rangle$ and $|\phi_j\rangle$ [24]:

$$\text{Diatropic}: \frac{\langle \phi_j \,|\mathbf{p}|\, \phi_a \rangle}{\varepsilon_j - \varepsilon_a} \tag{3.10}$$

$$\text{Paratropic}: \frac{\left\langle \phi_j \,\middle|\hat{\mathbf{l}}_{\mathbf{O}}\middle|\, \phi_a \right\rangle}{\varepsilon_j - \varepsilon_a} \tag{3.11}$$
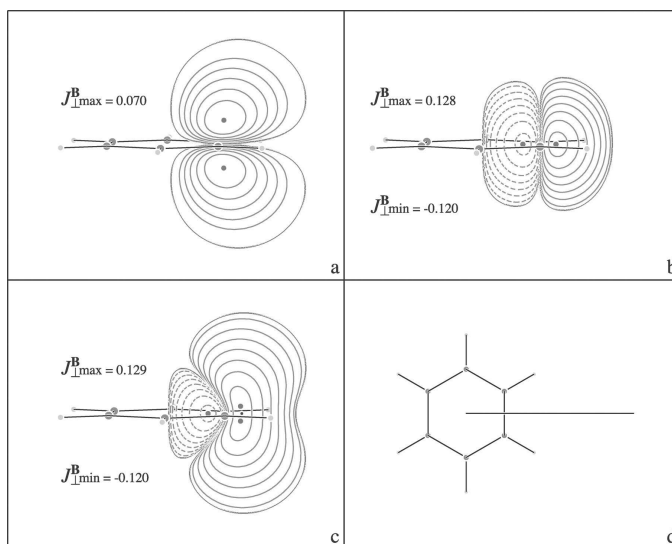
Figure 3.9: π, σ and total contributions of benzene's ring current. Reprinted with permission from Reference [127]. Copyright 2022 American Chemical Society.

In the language of group theory, diatropic currents for planar molecules in XY plane arise from excitations in which the product of representations of initial orbital $\Gamma(\phi_a)$, final orbital $\Gamma(\phi_j)$ and the in-plane translational operator $\Gamma(T_x, T_y)$ contains the totally symmetric component Γ_0. For paratropic the selection rule the translational operator is changed with in-plane rotation operator $\Gamma(R_z)$ [130]:

$$\text{Diatropic}: \Gamma(\phi_a) \times \Gamma(\phi_j) \times \Gamma(T_x, T_y) \supset \Gamma_0 \tag{3.12}$$

$$\text{Paratropic}: \Gamma(\phi_a) \times \Gamma(\phi_j) \times \Gamma(R_z) \supset \Gamma_0 \tag{3.13}$$

The strength of this response is modulated by the energy difference of unoccupied and occupied orbital in the denominator of the transition matrix elements. The largest contributors for ring currents are thus the frontier MOs, especially the HOMO-LUMO transitions. For planar annulenes, this selection rule gives an even simpler rule for qualitative determination of aromaticity: if the HOMO and LUMO differ by one angular node, the ring current is diatropic, and if by none, the ring current is paratropic [129].

The magnetically induced current density is dependent on the orientation of the magnetic field. For ring current calculations of planar molecules, the choice is unambiguous, as the magnetic field is oriented perpendicular to the molecular plane. Two

approaches to overcome this have been reported in the literature, one based on decompositions of the current density susceptibility tensor, and another on the vorticity of the current density.

The current density susceptibility tensor $\mathcal{J}_\alpha^{B_\beta}(\mathbf{r})$ can be decomposed to antisymmetric and symmetric components, $\mathbf{T} = \mathbf{S} + \mathbf{A}$. Using this decomposition, one can derive the anisotropy of induced current density (ACID) method [131] by calculating the standard deviation of eigenvalues s_i of the symmetric part $\mathbf{S}$:

$$\mathrm{ACID} = \sqrt{\sum_i (s_i - \bar{s})^2} \tag{3.14}$$

ACID is a scalar function, which can be visualized as densities showing the regions of delocalization. To obtain information on the direction of the current, the current density is overlaid as arrow plots. However, in a study by Fliegl and co-workers [132], the quantification of the ACID through integration did not yield consistent values. The obtained integrals were dependent on the location of the integration plane, and the quantitative picture is not always related to the qualitative one given by the visualization. Another quantity is the Anisotropy of the Asymmetric magnetically Induced Current Density (AACID) [133], calculated from the eigenvalues of the total current density susceptibility tensor:

$$\mathrm{AACID} = \sqrt{\frac{1}{3} \sum_i (t_i - \bar{t})^2}. \tag{3.15}$$

Integrated AACID on a plane bisecting a ring bond was shown to have a good agreement with Hückel delocalization energies by Monaco and Zanasi [134].

Another orientation-independent method derive from the vorticity tensor $\mathcal{V}_\alpha^{B_\delta}$. Vorticity tensor is the derivative of the curl of current susceptibility tensor with respect to magnetic field [135, 136]:

$$\mathcal{V}_\alpha^{B_\delta} = \frac{\partial(\nabla \times \mathbf{J^B})}{\partial B_\delta} = \varepsilon_{\alpha\beta\gamma} \nabla_\beta \mathcal{J}_\gamma^{B_\delta}. \tag{3.16}$$

where the Latin letters denote Cartesian directions. Scalar functions from its trace [137, 138] or the asymmetric component [139], are independent of the orientation of the magnetic field, and can be used to visualize the delocalization of electrons. The trace of the tensor also carries information on the tropicity of the current.

3.4.2 Magnetic shielding

The induced currents give rise to a secondary magnetic field $\mathbf{B}_{\text{loc}}$, as depicted in Figure 3.10a. The relation of the secondary magnetic field to the current is given by Biot-Savart's law:

$$\mathbf{B}_{\text{loc}} = \frac{\mu_0}{4\pi} \int \frac{\mathbf{r} \times \mathbf{J}^B(\mathbf{r})}{r^3}\ \mathrm{d}\mathbf{r}. \tag{3.17}$$

The induced magnetic field can either weaken or strengthen the applied field, called the shielding or deshielding effect, respectively. In aromatic compounds, the diatropic ring current induces a magnetic field that shields the inner part of the ring and deshields the outer part, and the paratropic ring currents have the opposite effect.

The induced magnetic field of benzene is shown in Figure 3.10b [140]. The shielding region is shown in blue, and it has a cylindrical shape, extending below and above the benzene ring, while the deshielding region, shown in red, is a hoop at the ring periphery.

(a)   (b)
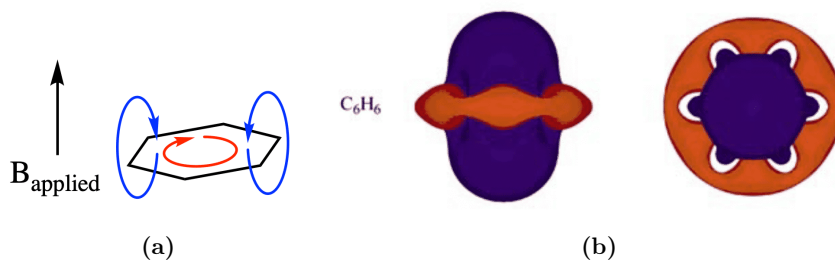
Figure 3.10: (a) Schematic illustration of the secondary magnetic field induced by a magnetically induced ring current, and (b) induced magnetic field of benzene. Blue indicates shielding and red deshielding regions. Reprinted with permission from Reference [140]. Copyright 2022 Wiley

The induced magnetic field is related to the applied magnetic field $\mathbf{B}_{\text{ext}}$ through the shielding tensor σ:

$$\mathbf{B}_{\text{loc}} = -\sigma \mathbf{B}_{\text{ext}} \tag{3.18}$$

This effect can be observed experimentally through nuclear magnetic resonance (NMR) spectroscopy, wherein the liquid phase the average of the diagonal components

of the shielding tensor is obtained in the form of chemical shift δ, given by the resonance frequencies of the nuclei relative to that of a standard:

$$\delta = \frac{\nu_{\text{mol}} - \nu_{\text{ref}}}{\nu_{\text{ref}}}. \tag{3.19}$$

This can be calculated reasonably accurately for most systems using quantum chemical methods [141] as the difference between shielding constants of reference and nuclei of the molecule:

$$\delta = \sigma_{\text{ref}} - \sigma_{\text{mol}} \tag{3.20}$$

The equations for calculating the tensor elements were given previously in Equations 2.91 and 2.92. The Biot-Savart expression describes the relation between the current density susceptibility tensor and the shielding tensor elements:

$$\sigma_{\alpha\beta}^I = -\epsilon_{\alpha\delta\gamma} \int \frac{(r_\delta - R_{I\delta})}{|\mathbf{r} - \mathbf{R}_I|^3} \mathcal{J}_\gamma^B d\mathbf{r}. \tag{3.21}$$

The integrand is called the magnetic shielding density. Its calculation was recently implemented in the GIMIC program [142, 143], and it can be visualized to show spatial origins of the shielding and deshielding contributions to the shielding constants of a nucleus. The regions with shielding (blue) and deshielding (red) spatial contributions of σ_{zz} for the lower-right proton of benzene are shown at the molecular plane in Figure 3.11a and one $1a_0$ above the molecular plane in Figure 3.11b.

The most commonly used computational method in the determination of the ring current is the nuclear-independent chemical shift (NICS) method [144]. In it, the shielding tensor $\sigma_{\alpha\beta}$ is calculated at different points, typically at the center or above of the ring, and the negative of some of its tensor components are used to deduce the sign and the tropicity of the ring current. Commonly, either the isotropic or the zz component is used, denoted as:

$$\text{NICS}(n)_{\text{iso}} = -\frac{1}{3}(\sigma_{xx} + \sigma_{yy} + \sigma_{zz}) \tag{3.22}$$

$$\text{NICS}(n)_{zz} = -\sigma_{zz} \tag{3.23}$$

$$. \tag{3.24}$$

(a)   **(b)**
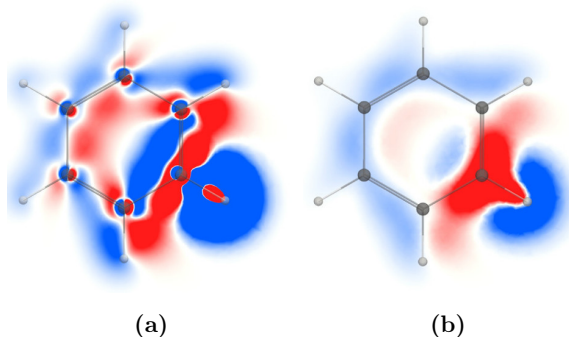
Figure 3.11: zz component of magnetic shielding density of benzene's lower-right proton, shown (a) on the molecular plane and (b) $1a_0$ above. Red regions show deshielding and blue regions the shielding contributions. Figures taken from [142], published with CC-BY license.

Here, the n is the height of the evaluation point from the ring center, given in Å. Large negative NICS values indicate an aromatic diatropic ring current, while large positive values indicate an antiaromatic paratropic ring current. The values calculated at the level of the molecular plane contain significant contributions from σ electrons, and the evaluation is commonly done 1Å above the molecular plane to limit this effect [145]. Furthermore, the isotropic contribution was found to contain contributions from many origins, and the σ_{zz} component for molecules aligned to xy plane was recommended for evaluating the π delocalization [146, 147]. The chemical shielding tensor can be dissected to orbital contributions, either via localized MOs [148] or with canonical MOs [149], allowing the dissection of NICS to σ and π contributions.

As NICS is sensitive to several effects, it can lead to spurious results. This is especially relevant in molecules with transition metals, where multiple examples exist of NICS giving qualitatively incorrect results of their aromaticity [150–156]. The reason for the discrepancies is the sensitivity of NICS to the strong local circulations.

The evaluation of NICS is not limited to single points. It can be calculated on a 3D grid to yield chemical-shielding isosurfaces [140, 157], evaluated as a 1D scan normal to the main symmetry axis of the ring yielding NICS-scan [158, 159], or in the perpendicular axes parallel to molecular plane yielding NICS-XY-scan [160].

Several schemes exist to calculate ring currents from NICS values by using Biot-

Savart's law [161–165]. However, these schemes can be problematic for molecules with more complex current patterns. Van Damme and co-workers studied the mapping between NICS values and current density, and concluded that the current density can not be reverse-engineered from NICS values [166]. In recent work, Paenurk and Gershoni-Poranne developed NICS2BC method for mapping NICS values to the bond currents of polycyclic aromatic hydrocarbons [167]. The bond currents obtained with their additive scheme based on Biot-Savart's law led to a nearly perfect correlation with the ones obtained by CSGT method.

3.4.3 Magnetizability

Magnetization is the process in which a magnetic moment is induced in a material due to an applied magnetic field. Their relationship is captured in the magnetic susceptibility tensor $\chi_{\alpha\beta}$

$$M_\alpha = B_\beta \chi_{\alpha\beta}, \text{where} \alpha, \beta \in x, y, z \tag{3.25}$$

$$\tag{3.26}$$

Diamagnetic molecules have negative magnetic susceptibilities, the induced magnetic moment opposes the magnetic field and the molecules are repelled by a magnet, opposite to paramagnetic molecules with a positive magnetic susceptibility. The magnetic susceptibility tensor is related to the current susceptibility tensor via [24]:

$$\chi_{\alpha\beta} = \frac{1}{2} \sum_{\delta\gamma} \varepsilon_{\alpha\delta\gamma} \int r_\delta \mathcal{J}_\gamma^{B_\beta}(\mathbf{r}) d\mathbf{r} \tag{3.27}$$

Analogously to the case of magnetic shielding density, the integrand above can be visualized to obtain the spatial contributions for magnetizability [168].

Ring currents manifest in the out-of-plane component of the magnetic susceptibility tensor, which can be assessed by the anisotropy of the magnetic susceptibility $\Delta\chi$ [32, 169]:

$$\Delta\chi = \chi_{zz}^{\mathrm{m}} - \frac{1}{2} \left\{ \chi_{xx}^{\mathrm{m}} + \chi_{yy}^{\mathrm{m}} \right\}. \tag{3.28}$$

Similar to NICS, the magnetic susceptibility is also affected by other phenomena aside ring currents [170]. As the other magnetic descriptors are easier to calculate and interpret, magnetic susceptibility is these days rarely used for quantifying aromaticity [171].

3.5 Bird's eye view of aromatic chemical space

3.5.1 Chemical space

We have now discussed the rules and the physicochemical properties that can be used to quantify aromaticity. Now it is time for a bird's-eye view of the chemical space of aromatic compounds.

The emergent nature of aromaticity is fascinating: due to delocalization, the properties of the whole system are more than a simple sum of its parts. Analog for aromaticity can be found in electric circuits, where the interplay of different components gives rise to its function, and the change or removal of any component most probably leads to the lack of it.

This is contrasted to cases where atomic fragments serve just a spatial and electrostatic role, such as in the problem of finding a drug that fits in a binding pocket of a protein. While the change of the compound's protonation or redox state will surely modulate this binding, such a change may completely kill the aromaticity of a compound, drastically changing its physicochemical properties. If one adopts the definition of chemistry as the science of understanding molecules and the art of designing new ones, the emergence arising from delocalization opens a conceptually new level, forcing one to think at the systems level.

Chemical space, defined as the set of all possible molecules, is a central concept in molecular design, and the territory explored by nature through evolution and by chemists with their intuition. The tools and language of chemoinformatics and mathematical chemistry are useful in making the practically infinite set amenable.

Here, we present some aromatic sections of the chemical space, with an attempt to highlight its vastness, different hierarchies, and the utility of simple aromaticity rules to make sense of it all.

3.5.2 Monocycles

In aromaticity, everything starts with monocycles. If one takes the archetypal benzene, and replaces CH with one or more isoelectronic fragments, such as N or O^+, one already obtains a dozen or so different structures. Guided by the Hückel rule, one can do similar substitutions to other aromatic carbon monocycles. For the pentagonal cyclopentadiene anion, $C_5H_5^-$, leads to pyrroles, imidazoles, thiazoles, oxazoles, and a plethora of other aromatic five-rings. Some of these are presented in Figure 3.12, showing what sort of richness can be obtained with a few atomic shuffles for single rings.

Figure 3.12: Some (a) six-membered and (b) five-membered heterocycles.

There is no need to limit the elements to main-group elements - one can throw in isoelectronic transition metal groups to obtain metalloaromatic compounds [172–178]. Metalloaromatic compounds have complicated bonding and can exhibit σ, π, δ, and ϕ delocalization. The aromaticities along these different conjugation channels may occur in combination - or, fascinatingly, may conflict with each other, being antiaromatic in one and aromatic in others.

Aesthetically and theoretically interesting monocycle is the carbomer, shown in Figure 3.13a. It is a hexagonal benzene-like molecule with an ethylene bridge between the hexagon nodes. First conceptualized by Chauvin [179, 180] and then synthesized by the group of Ueda [181, 182], they have also been made in naphthalene form, and have been investigated for electron capture properties. Another interesting large monocycle is C_{18}, shown in Figure 3.13b which was synthesized mechanically on a surface by Kaiser et al. in 2019, and extensively studied theoretically by Baryshnikov et al. [183]. The all-carbon rings have been previously observed by spectroscopic signatures, and their aromaticities and properties have been studied at varying ring sizes [184–186].
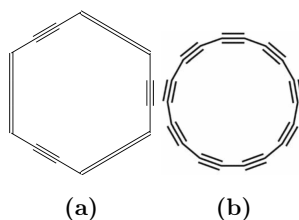
Figure 3.13: (a) Carbomer and (b) C_{18}

Under certain conditions, substituent ring of a monocycle can also be aromatic, as we will discuss in Section 4.2 presenting the findings of Article II.

3.5.3 Polycycles

The set of monocycles is a small drop in the sea of the aromatic space chemical space. When one fuses these rings, the number of possible unique molecules explodes. As some examples of works dealing with their enumeration in the field of drug discovery, Pitt et al. formed a dataset of one and two ring aromatic structures with C, N, O, and S, yielding 25,000 compounds [187], Ertl et al. generated 600,000 structures combining one to three five- and six-membered heterocycles [188], and Visini et al. enumerated a large set of carbon ring structures, generating for a subset of ring structures their aromatized counterparts, yielding 900,000 aromatic structures with up to four rings [189].

While these projects do good work in enumerating usable scaffolds for new drugs, they are still a slightly less small drop in the space of polycyclic compounds. The vastness is exemplified by the study of polycyclic benzenoid compounds, like those shown in Figure 3.14, with graph theoretical methods [190–192]. One can consider a graphene lattice and think of the number of different ways to color adjacent hexagons. With 21 hexagons, the amount of unique compounds is in the range of 10^{14} [193–195] - and this is just for the all-carbon structures. Chakrabotry et al. took a subset of some dozen of these PAHs and enumerated all the permutations doing isoelectronic replacements with B and N atoms, resulting in the order of 10^{13} molecules [196].

A beautiful member of the polycyclic compounds are the superbenzenes, in which a benzene-like structure is obtained from fused monocycles. Smallest superbenzene is the coronene, shown in Figure 3.15a, which one can view either as a benzene with a
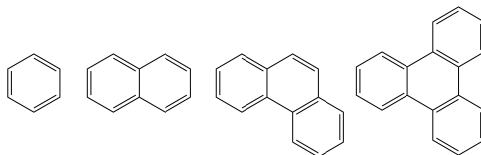
Figure 3.14: Some small polycyclic benzenoid compounds

benzene fused at each edge, or as a cyclic arrangement of benzenes with a hexagonal hole. Kekulene, shown in Figure 3.15b synthesized by Staab and co-workers in 1978 [197], is a larger superbenzene with a coronene sized hole in its center.
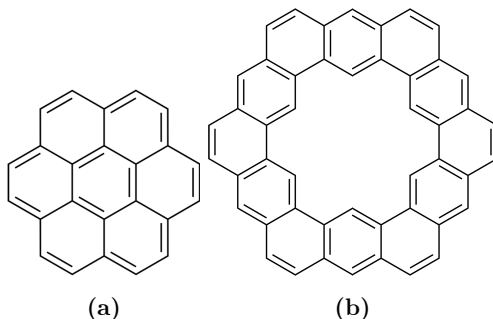

Figure 3.15: (a) Coronene and (b) kekulene

3.5.4 Macrocycles

The mono/polycyclic fragments can be joined to each other via linker groups, leading structures that are called in this thesis macrocycles[2]. The linker can be as simple as having a single bond between two rings, or it may consist of several atoms. Similar to coronene, there is some freedom in choosing how to look at these compounds: is the phenanthrene shown in Figure 3.16a a polycyclic compound, or a macrocycle made of two benzenes with a single bond and an ethene bridge?

Porphyrinoids are ubiquitous macrocycles in the context of aromaticity, with their archetype, porphyrin, shown in Figure 3.16b. It has four pyrroles linked with sp^2 carbon bridges. The pyrroles could also be other monocycles, such as thiophenes, and

---

[2]Macrocycle can also refer to e.g. cyclic polypeptides - we are interested in conjugated ones
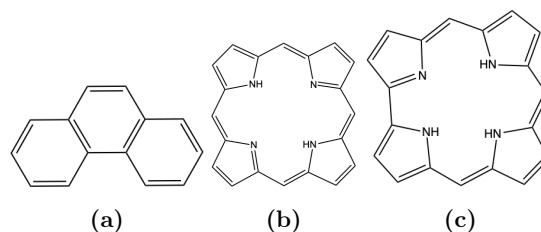
Figure 3.16: (a) Phenanthrene and two porphyrinoids, (b) porphyrin, and (c) corrole

pyridines. They can also be polycycles, such as naphthalenes. The bridges can be just a bond between two rings, as in corrole shown in Figure 3.16c, or they can one, two, or more atoms, which could be carbon, nitrogen, or sulfur. The bridges may attach to different parts of the ring, and new rings can be formed by connecting the bridging atom to the pyrrole ring. Porphyrins also have a rich coordination chemistry and can bind many metals, which again can bind axial ligands. Nothing of course limits the number of rings in porphyrin to just four - subporphyrins with three rings, hexaphyrins with six rings, and so on have been made. The modular structure of porphyrins nicely elucidates the utility of viewing molecules from the point of view of building blocks - if they would be forgotten, the zinc porphyrin could be seen as a polycyclic compound with five and six-membered rings consisting of carbons, nitrogens, and a zinc atom.

The combinatorial explosion arising from different possibilities was exemplified in work by Nandy et al. [198], in which the chemical space of tetrapyrrolic coordination compounds spanned by 15 rings and 9 bridges yielded 16,986 molecules were generated in the process of exploring methane oxidation catalysts. Porphyrins can be fused in several different ways from the edges to yield porphyrin tapes [199]. They can be extended in one dimension, branched in L and T shape [200], and constructed in two dimensions to yield porphyrin sheets [201]. Porphyrins can be connected with bridging groups, commonly attached to the meso-carbons. An impressive feat of this is a synthesis of directly meso-meso singly linked porphyrin tapes with 1024 porphyrin units with an 850 nm length [202]. The three-dimensional arrangements of these are discussed in the next section.

The richness of the heterocyclic polycyclic compounds and macrocycles was recently collected in two seminal reviews by Stępień and co-workers [203, 204], amassing over 2400 references.

3.5.5 Nanobelts and Möbius-aromatic molecules

Aromaticity is not constrained to two dimensions. One interesting class of compounds are the helicenes [205]. Phenanthrene in Figure 3.16a loses its planarity owing to the steric repulsion of hydrogens in the bay area. Adding benzenes leads to the formation of a helical corkscrew structure, as shown in Figure 3.17a, with a strong diatropic ring current circulating along the edge of the whole structure [206]. The diatropic ring current is affected only a little by the size of the helix. Recently the synthesis of infinitine was reported [207], shown in Figure 3.17b, a molecule with an infinity loop structure consisting of two fused helicenes with different chiralities. Current density calculations found that the molecule non-crossing diatropic currents around the scaffold [208, 209].
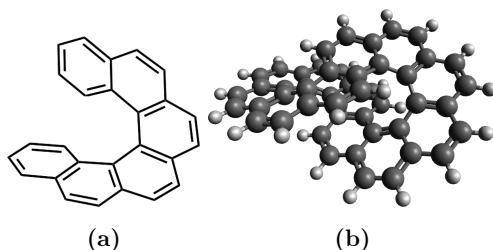

(a)   **(b)**

Figure 3.17: (a) Helicene and (b) infinitene

Linking benzenes from para positions via single bonds, as shown on the upper left part of Figure 3.18, leads to the formation of cycloparaphenylenes (CPP), first synthesized in 2008 with 9, 12 and 18 benzenes [210]. A beautiful example of chemical ingenuity is the recent synthesis of an interlocked CPP [211]. The direct fusion of benzenes leads to carbon nanobelts, with the para-fused one shown on the upper right of Figure3.18. These nanobelts and nanohoops can be seen as arising from the stacking of cis or trans ethene fragments to rings, as depicted in the upper row of Figure 3.18, which lead to an armchair or zigzag nanotubes, respectively. In an armchair nanotube, the continuous line of benzenes is vertical along the tubular axis, while in zigzag nanobelts it is horizontal. A third type is the chiral nanotubes, in which the continuous line is diagonal. Similar to the coloring of a hexagonal lattice, different nanobelt structures can be formed by coloring adjacent hexagons. A recent review by Itami et al. [212] describes the process of synthesizing various nanobelts, and their unique geometric and optoelectronic properties open many possibilities in supramolecular and optoelectronic
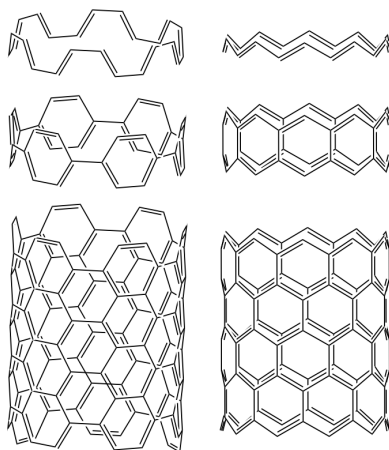
applications [213].

Figure 3.18: Stacking of cycloparaphenylenes (left) and nanobelts (right) to form nanotubes

The building blocks of these belt-like structures are not limited to monocycles. Porphyrin nanohoops with varying ring sizes have been built by a template-induced assembly approach by the group of Anderson [214–216], a six-member porphyrin nanoring is shown in Figure 3.19a. These have also been stacked to form nanotubes and spherical structures [217, 218], shown in Figures 3.19b and 3.19c. The largest nanoring contains 40 porphyrin rings [219], starting to bridge the gap between molecular chemistry and mesoscale physics [220, 221].

These systems are analogous to CPPs. There has also been recent work in synthesizing porphyrin nanobelts, built from directly fused porphyrins. The group of Sessler has synthesized carbaporphyrinic belts [222, 223] and the group of Yamada has synthesized one with all the inner ring atoms being pyrrolic, allowing one to utilize porphyrin coordination chemistry [224].

The first synthesis of Möbius aromatic carbon molecule was done by Herges et al. [225, 226], shown in Figure 3.20a. It consists of two anthracenes, joined at the central benzene ring via a single bond, and a cyclo-octatetraene. Expanded porphyrins distort into three-dimensional structures and often exhibit Möbius aromaticity [227–229]. Hexaphyrin is the smallest of these, shown in Figure 3.20b. The Möbius conduction pathway in these compounds is single-stranded - the π pathway occurs in one strand of
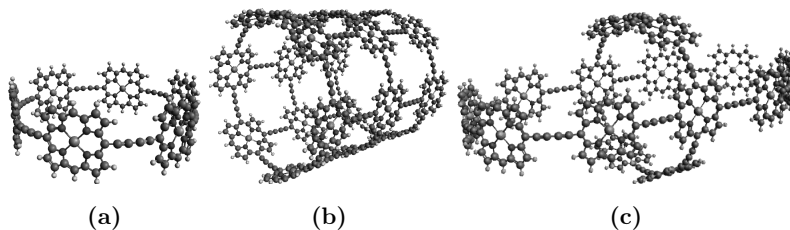
Figure 3.19: Porphyrin (a) nanoring (b) nanotube (c) nanoball

atoms, although the current splits in pyrrolic rings of heteroporphyrins [230, 231]. A double-stranded Möbius nanobelt with a single twist was synthesized by Itami's group in 2022, shown in Figure 3.20c [232], with twist moiety was found to move quickly around the ring in solution.
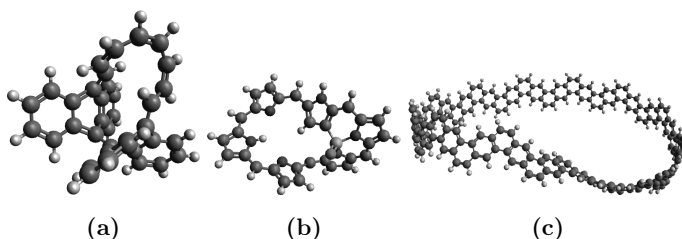

Figure 3.20: (a) [16] Möbius annulene (b) Hexaphyrin (c) Möbius nanobelt

3.5.6   Spherical compounds

When smaller or larger rings are included in polycyclic benzenoid compounds, the molecules become curved, gaining either negative or positive curvature [233]. Two examples of negative curvature are the corannulene [234, 235] and sumanene [236], shown in Figures 3.21a and 3.21b.

These bowl-shaped molecules are fragments of buckminsterfullerene C_{60}, the most famous of the fullerenes, shown in Figure 3.21c. It was first observed spectroscopically in 1985 [237] and synthesized in 1990 [238]. Fullerenes are pseudo-spherical compounds consisting of sp^2 carbon atoms and can be considered polyhedral analogs to the 2D graphene sheets [239]. The smallest fullerene is C_{20}, shown in Figure 3.21d, which is formed of pentagonal carbon rings. It is highly reactive but has been shown to
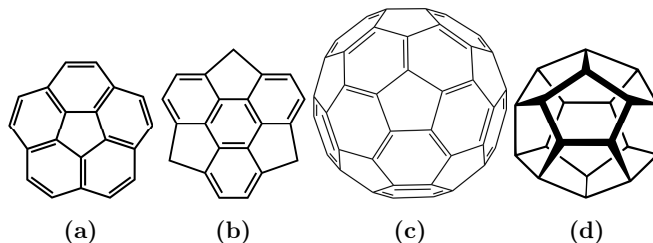
Figure 3.21: (a) Corannulene, (b) sumanene, (c) C_{60}, (d) C_{20}

exist in the gas phase [240]. Fullerenes with isolated pentagons are thermodynamically most stable, and C_{60} is the smallest of such fullerenes [241]. The amount of possible fullerene isomers for ones consisting of N carbon atoms grows as $\mathcal{O}\left(N^9\right)$ [239]. When one considers again the ways one can color adjacent rings in these to generate fullerenes with holes, and then the different ways one can shuffle the carbons to other elements, the space of fullerenes becomes practically infinite.

Spherical inorganic compounds have rich chemistry, and aromaticity has an important role in understanding their properties [242]. These compounds often take beautiful forms of Platonic solids. Two prime examples are the dodecaborate $[B_{12}H_{12}]^-$ [243] and the thiolate-protected nanoclusters, such as the $Au_{25}(SR)_{18}^-$ [244, 245], both having icosahedral structures. The inorganic spherical compounds are often studied within the framework of superatomic theory - their electrons are delocalized along the nuclear scaffold, and those molecules following Hirsch's rule of aromaticity are typically obtained experimentally [246].

Chapter 4

Results

In Article I, we studied the aromaticity and the orientation dependence of ring currents of gaudiene, a spherical carbon molecule. In Article II, we studied the phenomena of double aromaticity in persubstituted benzenes, using an implementation of the Gauge-Including Magnetically Induced Current method extended for the use of effective core potentials. In Article III, we used ring current calculations to help our collaborators understand the aromaticity of organometallic $[Cu_6(dmPz)_6(OH)_6]$compound. In Article IV, ring current calculations were used to elucidate the aromaticity of naphtalene-fused heteroporphyrinoids and correct the incorrect deductions given by other methods.

4.1   Article I: Gaudiene

4.1.1   Setting

Gaudiene (C_{72}), denoted **1**, is a hypothetical spherical molecule envisioned Sundholm in 2013 [247], inspired and named after the Spanish architect Antoni Gaudi. The molecule can be seen consisting of triangular hexahydro[12]annulenes **2**, fused at the edges. Alternatively, one can see it being built of rectangular tetrahydro[12]annulenes **3**. The molecular structure of gaudiene and these fragments are shown in Figure 4.1.

Spherically aromatic systems, as described by Hirsch's rule [248], sustain sphere currents with a uniform shell-like distribution around atom scaffold [249, 250]. While gaudiene fulfills Hirsch's rule for spherical aromaticity, the size of cavities does not allow the current to take a uniform spherical distribution.
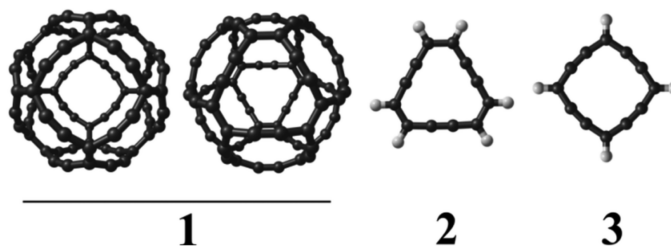
Figure 4.1: Gaudiene **1** viewed through the four-fold and three-fold symmetry axes, hexahydro[12]annulene **2** and tetrahydro[12]annulene **3**.

Sundholm confirmed both that gaudiene is aromatic, with net diatropic RCs of roughly 40nA/T, and that it is not spherically aromatic by deducing that the current flows along the bonds via analysis of the current profile at varying radial distances. Gaudiene thus is an interesting compound: while not spherically aromatic, it is spherical and aromatic.

One of the hallmark properties of spherically aromatic compounds is the isotropicity of their magnetic response properties, a manifestation of the uniform sphere current. We wanted to better understand the chameleon nature of gaudiene, and we continued the original study of gaudiene by examining the orientation dependence of its magnetic response, at both the current density and at the magnetic shielding level.

4.1.2 Results

We first calculated the ring currents of the fragments. The fragments follow Hückel's rule: the neutral triangular **2** is antiaromatic with a paratropic RC of -34.0 nA/T, while its dication is aromatic with a diatropic RC of 18.4 nA/T. The dicationic **3** is aromatic with diatropic RC of 18.7 nA/T, similar to the dicationic **2** with both having 10 π electrons. The dianionic **3** is aromatic as well, with a larger diatropic RC of 22.3 nA/T. The findings were also reflected in the NICS calculations, showing characteristic shielding/deshielding patterns of aromatic and antiaromatic molecules.

To study the orientation dependency of gaudiene's magnetic response properties, we did calculations with the magnetic field aligned through the three-fold symmetry axis (through ring **2**) and through the four-fold symmetry axis (ring **3**). The orientations along with the current pathways and strengths are shown in Figures 4.2a-b.

The current density for the four-fold orientation is shown in Figure 4.2c. It shows that the flow of current happens exclusively along the carbon framework, confirming the earlier conclusion that gaudiene is not a spherically aromatic compound.
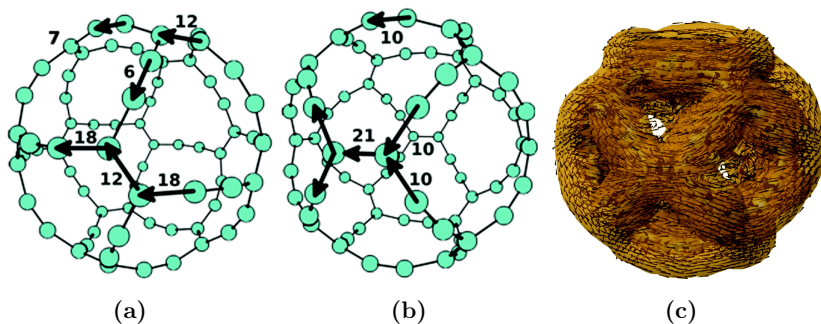

Figure 4.2: The bond current strengths (in nA/T) for gaudiene with magnetic field aligned along the (a) three-fold and (b) four-fold symmetry axis, and (c) the current density field

Gaudiene sustains a relatively constant net diatropic current of around 40 nA/T in both configurations, consisting of currents at the poles and at the equator of gaudiene. The current pathways are orientation-dependent: in the three-fold orientation, the polar and equatorial flows are connected, whereas in the four-fold orientation they are decoupled.

In the three-fold orientation, shown in Figure 4.2a, the net current of gaudiene is 36.3 nA/T. In this orientation, gaudiene can be seen as consisting of alternatively arranged three- and four-membered fragments **2** and **3**, fused at their C4 edge. The branching pattern of this repeating unit is shown in Figure 4.3. The direction and strength of the current are shown with arrows, each arrow corresponding to a current of 6 nA/T. In this orientation, gaudiene sustains currents at the equator and poles. Starting from the center of the illustration and going left, at the C4 edge fusing the rings **2** and **3**, there is a current of 18 nA/T. At the junction, 12 nA/T of it takes the equatorial branch, while 6 nA/T goes to the lower pole. The 12 nA/T at the equatorial branch is combined with a 6 nA/T coming from the upper pole to yield the same 18 nA/T current. The poles consist of three-membered rings **2**, with bond current strengths alternating from 7 to 12 nA/T.
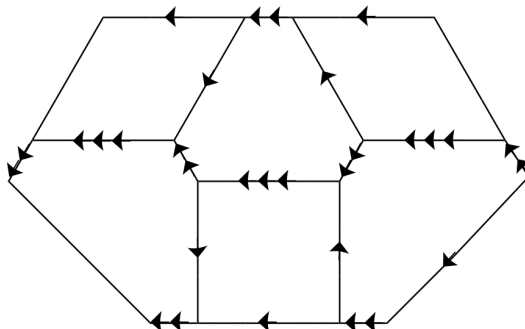
Figure 4.3: Current branching pattern of gaudiene in three-fold orientation

When the magnetic field is applied along the four-fold axis, the total ring current is 40.5 nA/T. The current pathways are distributed to decoupled equatorial and polar circulations, shown in Figure 4.2b. The equatorial current has a strength of 21 nA/T, split equally in a diamond-like manner at the sp^2 junctions, while the poles have their own circulation of 10 nA/T each.

Finally, we studied how the orientation dependency of current pathways manifests in the magnetic shielding of gaudiene. The isotropic contributions and components of the four- and three-fold orientations of the magnetic shielding tensor of gaudiene are shown in Figure 4.4. The upper row shows its isosurface with a ± 5 ppm cutoff, and the lower row shows the corresponding slices at a plane dissecting the sphere.

The magnetic shielding in the interior of gaudiene is highly isotropic. The tighter horizontal distribution of the equatorial current in the three-fold orientation compared to the diamond-like branching in the four-fold orientation manifests as orientation dependency of the magnetic shielding outside of the ring, with deshielding regions reflecting the shape of the equatorial branching patterns.

4.1.3 Conclusions

Our results show that the magnetic response of gaudiene is to some extent isotropic: it has a nearly constant net diatropic current strength and interior shielding. However, more detailed calculations reveal that this net diatropic current consists of distinct current pathways, which is also manifested in the change of the shielding function at the outside of the gaudiene.
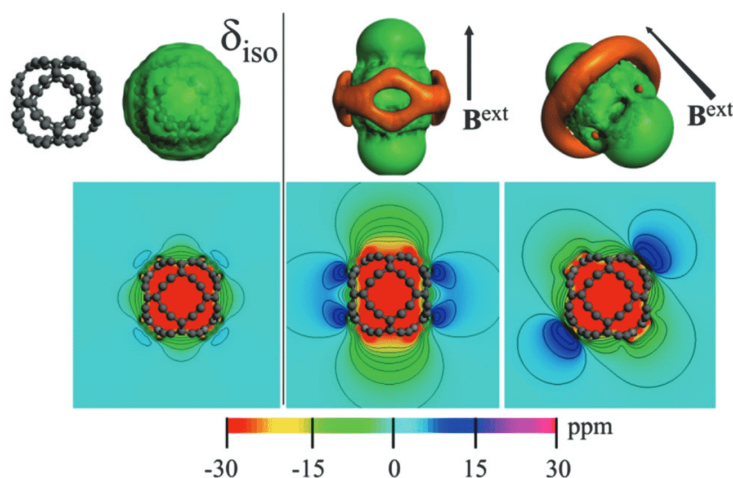
Figure 4.4: The magnetic shielding function of gaudiene

Based on these findings, one could describe gaudiene as a pseudo-spherically aromatic compound. While gaudiene is not a spherically aromatic compound, it is a spherical aromatic compound with a relatively isotropic magnetic response. An interesting future direction would be to continue the exploration of this border region by envisioning new hypothetical molecules, with the aim to find the limit at which the molecule becomes purely spherically aromatic.

4.2 Article II: Double aromaticity in persubstituted benzenes

4.2.1 Setting

In 1988, Sagl and Martin presented their findings of double aromaticity of $C_6I_6^{2+}$ [251]. The carbon NMR spectra of oxidized species showed a 42.6 ppm upfield shift with respect to the neutral one, indicative of a diatropic ring current at the substituent ring. Based on extended Hückel calculations, they arrived at an intuitive explanation for the new aromatic pathway opened at the substituent ring. When the atoms in the peripheral substituent ring increase in size, the repulsion between the electrons in the in-

plane p-orbitals increase, increasing the energy of the associated σ MO. For the halogen series, the energy of this MO increases going down the rows, until for C_6I_6 it becomes the highest-occupied molecular orbital (HOMO). As each iodine atom contributes two electrons, the double oxidation leads to the fulfillment of Hückel's $4n + 2$ rule.

The aromaticity of $C_6I_6{}^{2+}$ was studied by Ciofini et al. [252] using nuclear-independent chemical shift (NICS) calculations, and by Havenith et al. [253] using ring-current maps and multi-center bond indices (MCI). In the former study, double aromaticity showed as an increase of isotropic NICS $C_6I_6{}^{2+}$ increased with comparison to the neutral species, and the scanned NICS values had a maximum at the molecular plane, indicating a σ shape distribution of the ring current. In the latter study, ring current maps showed the existence of ring current circulating in the iodine perimeter. The authors provided selection rule arguments for the existence of the ring current: the transition from the e_{1u} HOMO to the a_{2g} LUMO is translationally allowed and thus leads to a diatropic ring current. The MCI results show that there the neutral molecule has no delocalization on the substituent ring, while the dication had MCI values showing a delocalization roughly half of that of benzene.

In 2014, Hatanaka and co-workers extended studied substituents from halogens [254]. In their computational study, they looked at benzene with group 14 (Ge, Sn), 15 (P, As, Sb), and group 16 (S, Se, Te) substituents, assessing the aromaticity with NICS calculations.

The substituent ring elements had different functional groups attached, and the substituent ring aromaticity was found to be modulated by their conformation. The singlet state of $C_6(SH)_6{}^{2+}$ was doubly aromatic when all the axis of S−H bond was perpendicular to the molecular plane, having a HOMO and LUMO patterns and NICS$(1)_{zz}$ value similar to that of $C_6I_6{}^{2+}$. The non-aromatic triplet state was however lower in energy for this conformer, and it had no double aromaticity. The low energy conformer with four of the SH groups parallel to the molecular plane was antiaromatic in its singlet ground state, with the triplet state having similar NICS values as the one with perpendicular SH groups. Similarly to the halogen series, the benzenes with heavier substituents had their HOMO on the substituent ring, and the dications had singlet ground states exhibiting double aromaticity.

In further work, one of the doubly aromatic compounds from their study, $C_6(SePh)_6$, was synthesized [255]. Experimental data supported the predictions of double aromatic-

ity. The authors performed bonding analysis and found a weak bonding interaction between the selenium ring in the dication that was absent in neutral species.

After the publication of Article II, Havenith and Fowler extended the study of doubly aromatic compounds to different ring sizes [256]. In their computational work, they studied C_8I_8 in different charge states. The substituent perimeter of the octagonal carbon scaffold is more crowded, leading to non-planar geometries. The molecules were constrained to be planar during the geometry optimization, which lead to the fragmentation of the studied systems. They found that the neutral C_8I_8, constrained to have a planar D_{4h} symmetry, is doubly antiaromatic as predicted by Hückel's rule.

4.2.2   Results

The earlier studies assessed the double aromaticity with NICS values, qualitative ring current maps, and MCI delocalization indices. We extended these by calculating current strengths with the GIMIC method, which was extended to use effective core potentials (ECP) for the heavier elements.

4.2.2.1   Benchmarking the methods

We tested the effect of using different functionals on the calculated current strengths, and found that increasing the amount of HF exchange leads to an increase in the net current strength J of benzene and $C_6I_6^{2+}$, as shown in Table 4.1. The difference is due to the increase of the diatropic component J_{dia}, while paratropic component J_{para} was insensitive to the amount of HF exchange.

The effect of representing core electrons with Stuttgart family ECPs on the RCS tested for $C_6I_6^{2+}$, C_6At_6, and $C_6At_6^{2+}$, shown in 4.2. We tested ECPs representing a different number of core electrons, parametrized with non-relativistic (NR), quasi-relativistic (QR), and fully relativistic (FR) calculations, and used different basis sets for the rest of the electrons.

In the current density calculations, ECPs are able to approximate the core electrons, as shown by the very small difference between RCS calculated with an all-electron basis set and using a non-relativistic ECP. This allows one to reduce the computational cost: by using ECPs, only 7 electrons of its 85 are included for astatine. This is also a great example of how the ring current is a valence-level phenomenon.

Table 4.1: Effect of different functionals with a varying amount of HF exchange E_{HF}^X on the ring current strength J and its dia- and paratropic components (in nA/T)

Molecule	Functional	E_{HF}^X %	J	J_{dia}	J_{para}
C_6H_6	PBE	0	11.67	16.67	−5.00
	BP86	0	11.72	16.70	−4.99
	BLYP	0	11.65	16.58	−4.93
	B3LYP	20	11.97	16.94	−4.96
	PBE0	25	12.07	17.10	−5.03
	BHLYP	50	12.41	17.38	−4.97
	HF	100	13.08	18.05	−4.97
$C_6I_6^{2+}$	PBE	0	26.12	29.73	−3.61
	BP86	0	27.21	30.87	−3.66
	BLYP	0	25.91	29.49	−3.58
	B3LYP	20	27.21	30.87	−3.66
	PBE0	25	27.75	31.45	−3.70
	BHLYP	50	29.03	32.79	−3.76
	HF	100	31.84	35.77	−3.93

Scalar relativistic effects can be estimated by the use of ECPs. The effect of spin-orbit coupling is however not included, and it is known to lead to differences in the current densities [257]. The difference between using a relativistic and non-relativistic ECP was quite found to be quite small, on the order of 1 nA/T.

4.2.2.2 Halogen series

Next, we studied the halogen series. In Figure 4.5a, the current density of $C_6I_6^{2+}$ is visualized, diatropic circulations colored in blue and paratropic circulations in red. The current profile for C_6I_6 and $C_6I_6^{2+}$ is shown in Figure 4.5b, calculated by computing the ring current on slices starting from the center of the ring and extending out through the center of C−C bond.

4.5b,

The RCS and NICS values for perhalogenated benzenes are shown in Table 4.3 for the neutral molecules and in Table 4 for the cationic molecules. We dissected the total RCS J to the carbon and substituent ring components C_6 and X_6 and to dia-

Table 4.2: RCS J (in nA/T) for $C_6I_6{}^{2+}$, C_6At_6, and $C_6At_6{}^{2+}$, calculated at the B3LYP functional using the def2-TZVP basis set for C and the Stuttgart ECP basis sets for I and At. Abbreviations NR, QR, or FR stand for non-relativistic, quasi-relativistic, and fully relativistic ECPs.

Molecule	Rel	ECP	Valence	J
$C_6I_6{}^{2+}$	NR	AE	TZ	26.5
$C_6I_6{}^{2+}$	FR	ECP28MDF	TZ	27.2
$C_6I_6{}^{2+}$	FR	ECP28MDF	QZ	27.2
$C_6I_6{}^{2+}$	QR	ECP46MWF	TZ	29.9
$C_6I_6{}^{2+}$	QR	ECP46MWF	QZ	29.5
$C_6At_6{}^{2+}$	NR	AE	DZ	29.2
$C_6At_6{}^{2+}$	NR	ECP78MHF	DZ	29.7
$C_6At_6{}^{2+}$	FR	ECP78MDF	DZ	28.5
C_6At_6	NR	AE	DZ	7.2
C_6At_6	NR	ECP78MHF	DZ	7.6
C_6At_6	FR	ECP78MDF	DZ	9.1
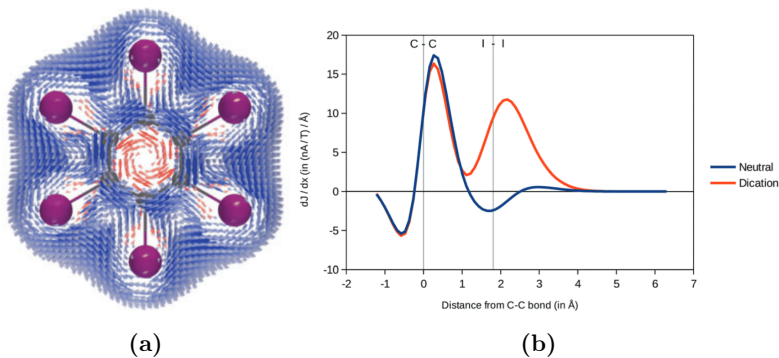
Figure 4.5: (a) Magnetically induced current density of $C_6I_6{}^{2+}$ and (b) current profile of neutral and dicationic C_6I_6

and paratropic contributions J_{dia} and J_{para}, and calculated both isotropic NICS(0) and NICS(1)$_{zz}$ values .

The perhalogenated compounds have 2-3 nA/T weaker ring currents than benzene. Interestingly, a weak circulation was found at the substituent ring even for the neutral

compounds. The dications of F, Cl, and Br substituted benzenes were calculated in their singlet and triplet states. This can be seen in the current profile of 4.5b as the negative dip near the marked I-I bond.

Table 4.3: Total RCS J, its carbon and substituent ring components C_6 and X_6, dia- and paratropic contributions (in nA/T), isotropic NICS(0) and NICS(1)$_{zz}$ values (in ppm) for neutral perhalogenated benzenes

Molecule	J	C_6	X_6	J_{dia}	J_{Para}	NICS(0)	NICS(1)$_{zz}$
C_6F_6	9.7	9.4	0.3	12.6	−2.9	−17.6	−23.2
C_6Cl_6	9.0	8.1	0.9	13.5	−4.5	−9.2	−19.2
C_6Br_6	9.2	8.6	0.6	13.8	−4.7	−8.5	−18.6
C_6I_6	8.5	10.0	−1.5	14.2	−5.6	−7.8	−17.5
C_6At_6	7.8	11.1	−3.3	14.7	−6.9	−8.7	−17.1

The RCS and NICS values for cationic species are shown in Table 4.4. For $C_6C_6^{2+}$ with X=F, Cl, Br, and I, both the singlet and triplet states were considered, with their difference $\Delta E_{\text{S−T}}$ given in eV. Both $C_6I_6^{2+}$ and $C_6At_6^{2+}$ are double aromatic with diatropic ring currents of 27.4 nA/T and 30.0 nA/T, respectively. The radical $C_6I_6^+$ is also doubly aromatic, with a net ring current 50% larger than benzene.

The singlet $C_6C_6^{2+}$ with X=F, Cl, Br had large current strengths, as reflected also in the NICS values. $C_6F_6^{2+}$ had a large paratropic current circulating in the carbon framework, while $C_6Cl_6^{2+}$, this large current was diatropic. In $C_6Br_6^{2+}$ the current was circulating in the substituent ring. In their triplet ground states, all these had net diatropic RCSs of roughly half of benzenes. Similar extreme results were reported by Palusiak and co-workers in their study of dicationic substituted benzenes [258], where they wrote *"Nevertheless, NICS values estimated for charged systems escape any rational interpretation, which may suggest that the NICS index is perhaps not a suitable measure of p-electron delocalization in dicationic systems."*. These large currents can be understood with the inverse relationship of the magnetic response to the energy difference of the unoccupied and occupied energy levels, presented in Equation 2.85 of Section 2.7.2. It may also be that the used level of theory and methods do not properly describe these states.

Table 4.4: Total RCS J (in nA/T), spin multiplicity $(2S + 1)$, isotropic NICS(0) and NICS(1)$_{zz}$ values (in ppm), singlet–triplet energy difference $\Delta E_{\text{S}-\text{T}}$ (in eV) for the cationic perhalogenated benzenes.

Molecule	$2S + 1$	J	NICS(0)	NICS(1)$_{zz}$	$\Delta E_{\text{S}-\text{T}}$
$C_6F_6^{2+}$	1	-40.7	46.0	124.2	0.39
$C_6F_6^{2+}$	3	6.1			
$C_6Cl_6^{2+}$	1	128.3	-138.3	-370.1	0.45
$C_6Cl_6^{2+}$	3	5.3			
$C_6Br_6^{2+}$	1	20.4	-18.6	-38.1	0.68
$C_6Br_6^{2+}$	3	5.6			
$C_6I_6^{2+}$	1	27.4	-16.4	-46.9	-0.30
$C_6I_6^{+}$	2	18.2			
$C_6At_6^{2+}$	1	30.0	-19.2	-49.3	-0.45

4.2.2.3 Group 15/16 substituted benzenes

Next, we studied benzenes with group 15 and 16 substituents (G15/16). From the molecules studied by [254], we focused on a subset of compounds, C_6X_6 with X= SeH, SeMe, TeH, TeMe and SbH$_2$, which we studied in their neutral and dicationic states.

The average torsional angles are shown in Table 4.5. The neutral molecules have small out-of-plane in the carbon ring and larger ones in the perimeter rings. Upon oxidation, the molecules became nearly planar.

Table 4.5: Average torsion angles for the carbon ring C_6 and Se, Te, and Sb atoms in the substituent ring, X_6.

Molecule	Neutral, C_6	Neutral, X_6	Dication, C_6	Dication, X_6
$C_6(SeH)_6$	3.6	9.2	1.2	0.4
$C_6(SeMe)_6$	4.5	22.3	2.2	3.4
$C_6(TeH)_6$	4.9	33.3	0.9	6.4
$C_6(TeMe)_6$	4.8	30.9	1.2	4.4
$C_6 (SbH_2)_6$	2.4	28.7	1.5	2.8

The net currents strengths and NICS values of the neutral and dicationic G15/16 substituted benzenes are shown in Table 4.6. The results are similar to the findings

for the halogen series and those made earlier by Hatanaka: neutral compounds have weakened aromaticity compared to that of benzene, and the dicationic compounds exhibit aromaticity on the substituent ring.

Table 4.6: RCS J (in nA/T), and isotropic NICS(0) and NICS(1)$_{zz}$ values (in ppm) for neutral G15/16 substituted benzenes.

Molecule	J	NICS (0)	NICS (1)$_{zz}$
$C_6(SeH)_6$	8.5	−6.2	−17.4
$C_6(SeH)_6{}^{2+}$	16.6	−9.3	−26.8
$C_6(SeMe)_6$	10.4	−7.8	−21.4
$C_6(SeMe)_6{}^{2+}$	24.5	−16.1	−44.5
$C_6(TeH)_6$	10.6	−7.3	−23.2
$C_6(TeH)_6{}^{2+}$	33.2	−21.0	−56.9
$C_6(TeMe_6)_6$	11.2	−7.9	−22.0
$C_6(TeMe)_6{}^{2+}$	32.0	−20.6	−55.2
$C_6(SbH_2)_6$	9.9	−5.5	−20.4
$C_6(SbH_2)_6{}^{2+}$	29.4	−18.7	−49.1

Of the doubly aromatic compounds in this series, $C_6(SeH)_6{}^{2+}$ showed a weaker net RCS. The modulus plot of its current density is shown in Figure 4.6, showing how the conformation of the substituents leads to a bottleneck in the conduction pathways. This is an interesting example of conformation-dependent aromaticity switching, and the GIMIC calculations show the picture of what was previously deduced from NICS values.

4.2.3 Conclusions

With our ring current calculations, we were able to quantify the ring current strengths of these doubly aromatic substituted benzenes. Owing to the delocalization at the substituent ring, the total ring current strengths of these molecules were 1.5-2.5 times larger than benzenes.

These molecules also acted as test-set for doing ring current calculations with ECPs. The error from approximating core electrons with ECPs was found to be negligible, allowing the reduction of computational cost and studying molecules with heavier atoms.
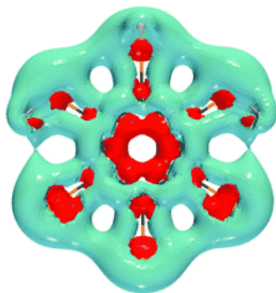
Figure 4.6: Current density $C_6(SeH)_6{}^{2+}$

The effect of relativity on ring currents, as captured by ECPs, was found to be small as well.

One of the most interesting results was the double aromaticity of $C_6Br_6{}^{2+}$ in its singlet state. While the ground state of the dication is a triplet, in which the molecule has diminished aromaticity compared to benzene, the opening of the conjugation pathway at the singlet state is perhaps indicative of bromine being at the limit of becoming double aromatic.

As already done by Fowler et al. [256] with C_8I_8, the chemical space of double aromatic molecules can be expanded. The limit highlighted by $C_6Br_6{}^{2+}$ can help to guide the discovery of such molecules, a task for which the solutions arise from a delicate balance of electronic structure, geometry, and electron counts. Combining this with the shown ability to switch conjugation channels on and off by conformational change, which can be induced by an external stimulus, could make these compounds useful for some interesting applications.

4.3 Article III: $[Cu_6(dmPz)_6(OH)_6]$

4.3.1 Setting

In Article III, we studied the current pathways of $[Cu_6(dmPz)_6(OH)_6]$, further denoted as Cu6. Cu6 is a polynuclear coordination compound, with a cyclic structure consisting of six Cu(II) atoms coordinated by 3,5-dimethylpyrazoles and hydroxyl groups in trans-arrangement, as shown in Figure 4.7 [259]. This class of compounds has structural

richness, variations existing with a different number of repeating units, and types and cis/trans arrangements of the ligands [260, 261], and the modifiability allows their tailoring to different purposes.
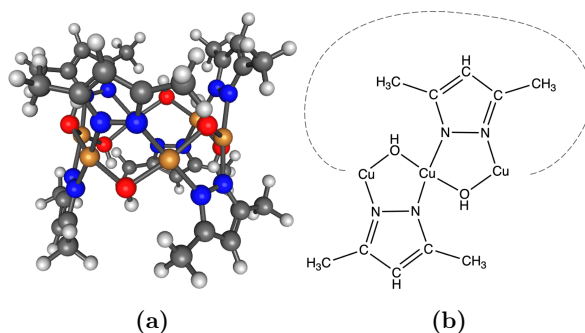

(a) **(b)**

Figure 4.7: (a) Molecular structure of Cu6 and (b) the pattern of its repeating unit

Our collaborators in Chile, led by Dr. Muñoz-Castro, were interested to understand better the magnetic properties Cu6. While the Cu(II) atoms are formally paramagnetic, the Cu6 molecule is diamagnetic with a singlet ground state. As the Cu(II) atoms are far away (3.2Å), they are coupled with superexchange interactions, i.e., the ligands mediate their interaction.

Our collaborators did extensive computational studies of the metal-ligand interactions of Cu6. The copper 3d orbitals were shown to be delocalized along both pyrazole and hydroxide ligands. Their NICS calculations showed that the inner part of Cu6 is shielded, indicating that it sustains a diatropic ring current. However, as NICS calculations can lead to unreliable results for molecules with transition metal atoms, and they were unable to deduce the finer details of aromaticity with it, questions remained: is Cu6 truly aromatic, and what delocalization pathways play a role in it?

4.3.2 Results

To answer these questions, we did ring current calculations with GIMIC. The results for the current pathways and strengths are shown in Figure 4.8a, and the modulus of the current density on a plane bisecting two Cu atoms is shown in Figure 4.8b.

The ring current calculations supported the NICS calculations: Cu6 is aromatic according to the magnetic criteria. The molecule sustains a diatropic ring current of
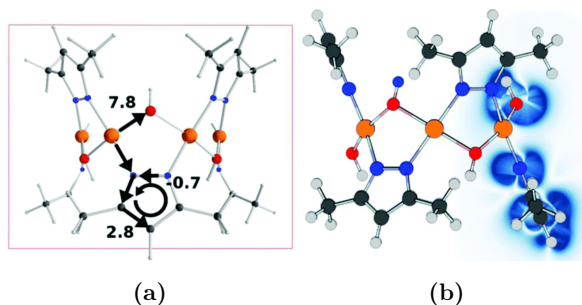
Figure 4.8: (a) The current pathways and strengths of Cu6 and the (b) modulus of the current density on a plane bisecting two Cu atoms.

9.9 nA/T, similar to that of benzene. The hydroxyl ligand joining two copper atoms is the predominant conduction pathway, with 80% (7.8 nA/T) of the total current flowing through it. The rest of the current (2.1 nA/T) goes through the pyrazole. Interestingly, instead of taking the geometrically shortest pathway through the $-$N$-$N$-$ moiety, the current flows through the outer perimeter of the pyrazole. Pyrazole sustains a weak local circulation of 0.7 nA/T. No current passes directly between the copper atoms, as shown in Figure 4.8b.

4.3.3 Conclusions

The results answer the original research questions and give rise to many new ones. Can Cu6's aromaticity or its pathways be switched with redox reactions? These compounds are known to bind anions - how is the binding related to, and how does it affect the electronic structure of Cu6? How about different ring sizes - what iss the largest ring one can build from the repeating unit, how does the aromaticity behave asymptotically when nearing the meso-scale limit? The modularity of the structures opens a door to enumerative studies: what properties exist in the chemical space that can be obtained by varying the ligands and the metal centers? Computational modeling and ring current calculations could answer these relatively easily, and the findings could open some interesting new possibilities.

4.4 Article IV: Naphtalene-fused heteroporphyrinoids

4.4.1 Setting

As discussed earlier in Section 3.5.3, porphyrinoids are an important family of macro-cycles, existing naturally in many forms and with many functions. In this work, we studied porphyrinoids synthesized and studied by Hong et al. [262], shown in Figure 4.9. The molecules **1** and **2** were synthesized by Hong et al. The Molecule **1** is a porphyrin derivative with one pyrrole replaced with thiophene, and one with a naphtalene moiety connected to the mesa carbon. The Molecule **2** is its Pd-coordination complex. The Molecule **3** has a quinoline instead of naphtalene - the inner CH group is replaced by nitrogen. This was not included in the original study, but I thought that it would be interesting to see how the global and local currents are affected by the annealation of two related polycycles.
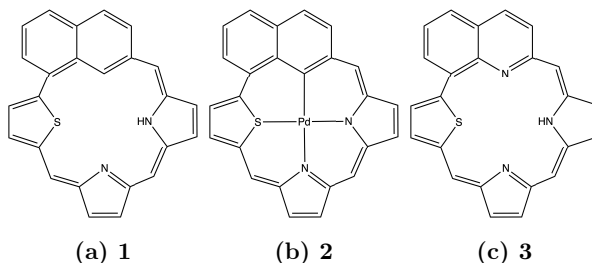

(a) **1**   (b) **2**   (c) **3**

Figure 4.9: Molecular structures of **1** − **3**.

In the original study, the experimental NMR spectra showed that the molecules were aromatic. The authors deduced that there are two 22 π electron pathways, shown in Figure 4.10a. The pathways differ on the naphtalene-moiety, with the dominant one taking the inner path at the central ring. In other parts, current takes the outer pathway at thiophene and protonated pyrrole, and the inner path at the unprotonated pyrrole. The conclusion is supported by NICS, HOSE, and ACID calculations, with ACID results for **1** is shown in Figure 4.10b

While this conclusion is supported by the methods used by the authors, they are not in line with the current understanding given by the ring current calculations for porphyrins [263]. At pyrrole rings, the global current is typically split, and more complicated cases typically exhibit an intricate balance of local and global circulations.
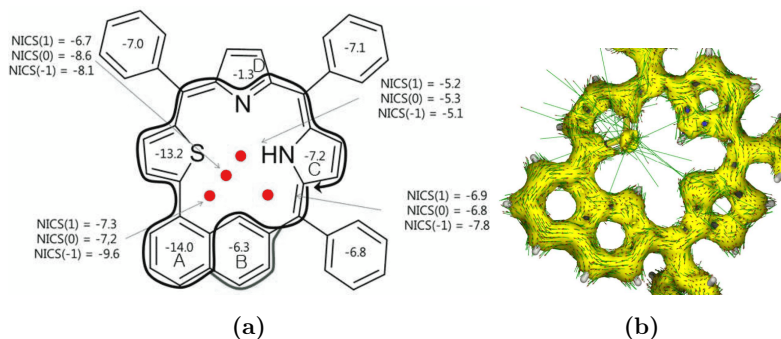
Figure 4.10: (a) Predicted current pathways in the original work, and (b) ACID plot of the **1**. Reprinted with permission from Reference [262]. Copyright 2022 American Chemical Society.

4.4.2 Results

Once again, to understand the aromaticity of this molecule, we did ring current calculations with the GIMIC program. The current pathways and strengths (in nA/T) are shown in Figure 4.11. The branch points of the current are highlighted with diamonds in Figure 4.11a.

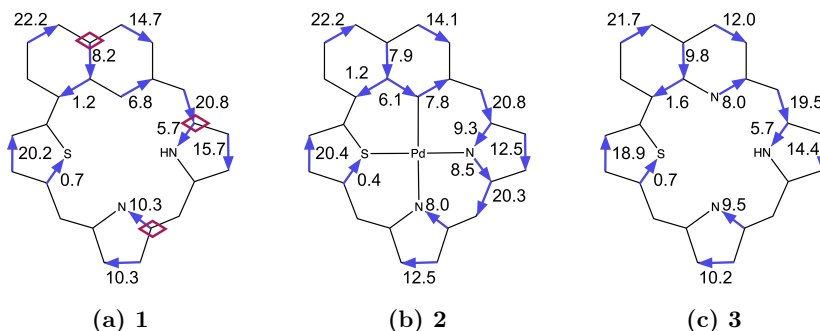**Figure 4.11:** Current pathways and strengths of **1 − 3**

The molecules are all aromatic, with a global diatropic current strength of the order of 20 nA/T. Starting from the annealed quinone and continuing clockwise, the global current takes the outer pathway of the meso-annealed benzene ring, which sustains a weak local circulation of 1-2 nA/T. The current then branches, over half taking the

outer pathway. At the protonated pyrrole ring of **1** and **2**, roughly 75% of the current takes the outer pathway. In **2** the split is more equal, and it additionally has a small local circulation in the 6-element cycle consisting of Pd, pyrrole, and the naphtalene ring. At the next pyrrole ring, the current branches equally, and at the thiophene ring, practically all current takes the outer pathway.

4.4.3   Conclusions

The calculation of the current pathways highlights the importance of choosing a proper method in assessing the aromaticity of complex compounds. It also shows a beautiful example of emergent phenomena in more complicated aromatic compounds. While thiophene and naphtalene are both aromatic compounds, they lose their original aromaticity when embedded in a macrocyclic framework.

The complexities in the aromaticity that the results show motivate a wider study of porphyrinoids. Porphyrinoids are important compounds with a wide set of applications, and new designs are constantly being reported in the literature. Aromaticity is an important determinant of the molecular properties of porphyrinoids, but its intricacies and emergence can be hard to understand. Computational exploration of their chemical space can accelerate the discovery process of new porphyrinoids, and as the aromaticity of these is a weird and intricate emergent phenomenon, the quantitative results that ring current calculations give could play an important role in this process.

Chapter 5

Conclusions and future directions of research

The results of Articles I-IV showcase the use of ring current calculations in the study of aromaticity. With these calculations, we were able to understand the intricacies of the current pathways for a diverse set of aromatic molecules. The results highlight the utility of studying the current density directly, instead of relying on its manifestation as magnetic shielding with NICS, for understanding the aromaticity of a molecule. This is especially important for more complex molecules, such as those with nonplanar geometries, transition metal atoms, and polycyclic compounds.

In Chapter 4, I discussed some future research directions for each of the articles presented. The articles studied the emergent phenomena of aromaticity - how the right building blocks of the circuit make the magic happen. The design of such molecules requires thinking at the systems level. Each of the studied systems is the result of human imagination, creativity, and hard work - beautiful arrangements of nuclei and electrons, some of which have been made in the laboratory, others waiting for a curious chemist to stir them up to existence. Theory and computation, described in Chapter 2, allow us to calculate the properties of molecules relatively accurately and efficiently. These methods were used in this work to study individual molecules, and the years spent with excessive browsing of Google Scholar allowed pattern-matching facilities to synthesize the results to come up with some new molecules that could be interesting.

In addition to using the computer as a calculator - "Hey Linux machine, what is the ring current of this molecule" - one can use it to aid in solving the inverse problem.

In chemistry, the inverse problem is most typically equal to the very fundamental task of molecular design. Quantum chemical methods give us "good enough" properties, and the fields of chemoinformatics and deep learning have developed a wide variety of ways to represent molecules. Combining these two and formulating the task of molecular design as an optimization problem makes it amenable to a wide variety of computational tools [264–268].

The computational molecular design has a long history in drug discovery [269–272]. This thesis was written during the era of rapid advances in deep learning, catalyzed by the progress in machine vision with convolutional neural networks around the time I started doing research. This has brought huge interest in applying these to all areas of chemistry and materials science [273–276]. Aromatic chemistry is one of the remaining fields practically untouched in this gold rush. I hypothesize that this is due to two reasons: its emergent nature and ambiguities in its determination.

Whether the task is to find a futuristic molecular transistor for a nanocircuit [277], a ligand for an organometallic catalyst that withstands harsh oxidative conditions and stabilizes the metal center in various oxidation states [278], or an organic anode for next-generation batteries [279], the aromaticity fundamental to these processes is hard to obtain and easy to break. This makes the task of finding these needles in the haystack of practically infinite chemical space much harder. However, we are quite good at finding them [280], and the methods for this task develop rapidly.

The other hindrance of ambiguity reflects the fuzziness of aromaticity. To the extent that magnetic criteria are meaningful, the ring current calculations could be used to answer this problem. The central object we used to answer the problems in Articles I-IV was the bond current strength I_{AB} between selected atoms A and B, and this process can be automated. As the two indices in the subscript indicate, one can collect these to represent the aromaticity of the molecule of n atoms as a bond current matrix $\mathbf{I}_{n \times n}$, and further present it as a directed graph. Both are data structures readily crunched by algorithms.

A problem arises from the orientation dependence of magnetic response: to some extent, this can be overcome by collating the results with the used magnetic field orientation, and an orientation defined e.g. as the principal axis of rotation. The automation of bond current calculations and collecting the results as bond current matrix could facilitate the automated exploration of the aromatic chemical space, perhaps by applying

combining them with the tools of computational circuit design [281–283].

Such a method would be very useful for the humane chemistry as well. In computational biology, the tools are often delivered in the form of a web server [284, 285]. The current paradigm of computational quantum chemistry still relies on use of complex HPC environments and a myriad of different software with their own input and output formats, stitched together with scripts. An ideal tool would take in a molecule via a web interface and spit out the ring current strengths and visualizations. Such a tool would facilitate the evaluation of aromaticity by ring currents, instead of its easier-to-calculate proxy measure of NICS.

While it is still a bit too early to treat quantum chemical methods as an answer-delivering black box, the results obtained with the current black box of B3LYP/def2-SVP are often good enough. The choice of the method also can also be supported by e.g. recommendation engines [286], and the results could be coupled with an uncertainty metric of some sort [287].

I hope that this thesis highlights the power of quantum chemical methods in understanding chemistry and the complexities of both the debated topic of aromaticity and the aromatic chemical space. Many future possibilities can be imagined, and it is an interesting time to be a computational chemist.

Humanity needs better molecules, and aromatic molecules are often that.

Bibliography

(1)   Shankar, R., *Principles of Quantum Mechanics*; Springer Science & Business Media: 1994.

(2)   Jensen, F., *Introduction to Computational Chemistry*; John Wiley & Sons: 2017.

(3)   Koopmans, T. *Physica* **1934**, *1*, 104–113.

(4)   Truhlar, D. G. *Chem. Phys. Lett.* **1998**, *294*, 45–48.

(5)   Bartlett, R. J.; Purvis, G. D. *Int. J. Quantum Chem.* **1978**, *14*, 561–581.

(6)   Pople, J. A.; Binkley, J. S.; Seeger, R. *Int. J. Quantum Chem.* **1976**, *10*, 1–19.

(7)   Čížek, J. *J. Chem. Phys.* **1966**, *45*, 4256–4266.

(8)   Møller, C.; Plesset, M. S. *Phys. Rev.* **1934**, *46*, 618–622.

(9)   Hohenberg, P.; Kohn, W. *Phys. Rev.* **1964**, *136*, B864–B871.

(10) Kohn, W.; Sham, L. J. *Phys. Rev.* **1965**, *140*, A1133–A1138.

(11) Bootsma, A. N.; Wheeler, S. *ChemRxiv preprint, 10.26434/chemrxiv.8864204.v5* **2019**.

(12) Lehtola, S.; Marques, M. A. *arXiv preprint arXiv:2206.14062* **2022**.

(13) Perdew, J. P.; Schmidt, K. *AIP Conf. Proc.* **2001**, *577*, 1–20.

(14) Cohen, A. J.; Mori-Sánchez, P.; Yang, W. *Chem. Rev.* **2012**, *112*, 289–320.

(15) Bao, J. L.; Gagliardi, L.; Truhlar, D. G. *J. Phys. Chem. Lett.* **2018**, *9*, 2353–2358.

(16) Tsuneda, T.; Hirao, K. *J. Chem. Phys.* **2014**, *140*, 18A513.

(17) Grimme, S.; Antony, J.; Ehrlich, S.; Krieg, H. *J. Chem. Phys.* **2010**, *132*, 154104.

(18) Caldeweyher, E.; Ehlert, S.; Hansen, A.; Neugebauer, H.; Spicher, S.; Bannwarth, C.; Grimme, S. *J. Chem. Phys.* **2019**, *150*, 154122.

(19) Lehtola, S.; Steigemann, C.; Oliveira, M. J. T.; Marques, M. A. L. *SoftwareX* **2018**, *7*, 1–5.

(20) Bursch, M.; Mewes, J.-M.; Hansen, A.; Grimme, S. *Angew. Chem. Int. Ed.* **2022**, *61*, e2022057.

(21) Goerigk, L.; Grimme, S. *Phys. Chem. Chem. Phys.* **2011**, *13*, 6670–6688.

(22) Goerigk, L.; Hansen, A.; Bauer, C.; Ehrlich, S.; Najibi, A.; Grimme, S. *Phys. Chem. Chem. Phys.* **2017**, *19*, 32184–32215.

(23) Norman, P.; Ruud, K.; Saue, T., *Principles and Practices of Molecular Properties: Theory, Modeling, and Simulations*; John Wiley & Sons: 2018.

(24) Sundholm, D.; Dimitrova, M.; Berger, R. *Chem. Commun.* **2021**, *57*, 12362–12378.

(25) Epstein, S. T. *Isr. J. Chem.* **1980**, *19*, 154–158.

(26) London, F. *J. Phys. Radium* **1937**, *8*, 397–409.

(27) Epstein, S. *J. Chem. Phys.* **1973**, *58*, 1592–1595.

(28) Epstein, S. T. *J. Chem. Phys.* **1965**, *42*, 2897–2898.

(29) Keith, T. A.; Bader, R. F. W. *Chem. Phys. Lett.* **1993**, *210*, 223–231.

(30) Lazzeretti, P.; Malagoli, M.; Zanasi, R. *Chem. Phys. Lett.* **1994**, *220*, 299–304.

(31) Coriani, S.; Lazzeretti, P.; Malagoli, M.; Zanasi, R. *Theor. Chim. Acta* **1994**, *89*, 181–192.

(32) Lazzeretti, P. *Prog. Nucl. Magn. Reson. Spectrosc.* **2000**, *36*, 1–88.

(33) Jusélius, J.; Sundholm, D.; Gauss, J. *J. Chem. Phys.* **2004**, *121*, 3952–3963.

(34) Fliegl, H.; Taubert, S.; Lehtonen, O.; Sundholm, D. *Phys. Chem. Chem. Phys.* **2011**, *13*, 20500–20518.

(35) Sundholm, D.; Fliegl, H.; Berger, R. J. F. *Wiley Interdiscip. Rev. Comput. Mol. Sci.* **2016**, *6*, 639–678.

(36) Taubert, S.; Sundholm, D.; Jusélius, J. *J. Chem. Phys.* **2011**, *134*, 054123.

(37) Rauhalahti, M.; Taubert, S.; Sundholm, D.; Liégeois, V. *Phys. Chem. Chem. Phys.* **2017**, *19*, 7124–7131.

(38) Gauss, J.; Stanton, J. F. *Adv. Chem. Phys* **2003**, *123*, 355–422.

(39) Keith, T. A., TK Gristmill Software AIMAll, 2019.

(40) Irons, T. J. P.; Spence, L.; David, G.; Speake, B. T.; Helgaker, T.; Teale, A. M. *J. Phys. Chem. A* **2020**, *124*, 1321–1333.

(41) Monaco, G.; Summa, F. F.; Zanasi, R. *J. Chem. Inf. Model.* **2021**, *61*, 270–283.

(42) Brock, W. H., *The History of Chemistry: A Very Short Introduction*; Oxford University Press: 2016.

(43) Faraday, M. *Philos. Trans. R. Soc. A* **1825**, 440–466.

(44) Kekulé, A. *Bull. Soc. Chim. Paris* **1865**, *3*, 98.

(45) Kekulé, A. *Liebigs Ann.* **1872**, *162*, 77–124.

(46) Pauling, L.; Wheland, G. W. *J. Chem. Phys.* **1933**, *1*, 362–374.

(47) Hückel, E. *Z. Phys. Chem* **1931**, *70*, 104–186.

(48) Hückel, E. *Z. Phys. Chem* **1931**, *72*, 310–337.

(49) Hückel, E. *Z. Phys. Chem* **1931**, *76*, 628–648.

(50) Gonthier, J. F.; Steinmann, S. N.; Wodrich, M. D.; Corminboeuf, C. *Chem. Soc. Rev.* **2012**, *41*, 4671–4687.

(51) Grunenberg, J. *Int. J. Quantum Chem.* **2017**, *117*, e25359.

(52) Chen, Z.; Wannere, C. S.; Corminboeuf, C.; Puchta, R.; Schleyer, P. v. R. *Chem. Rev.* **2005**, *105*, 3842–3888.

(53) Solà, M. *Front. Chem.* **2017**, *5*, 22.

(54) Solà, M. *Wiley Interdiscip. Rev. Comput. Mol. Sci.* **2019**, *9*, e1404.

(55) Solà, M. *Nat. Chem.* **2022**, *14*, 585–590.

(56) Solà, M.; Bickelhaupt, F. M. *J. Chem. Ed.* **2022**, *99*, 3497–3501.

(57) Hirsch, A.; Chen, Z.; Jiao, H. *Angew. Chem. Int. Ed Engl.* **2000**, *39*, 3915–3917.

(58) Baird, N. C. *J. Am. Chem. Soc.* **1972**, *94*, 4941–4948.

(59) Soncini, A.; Fowler, P. W. *Chem. Phys. Lett.* **2008**, *450*, 431–436.

(60) Mandado, M.; Graña, A. M.; Pérez-Juste, I. *J. Chem. Phys.* **2008**, *129*, 164114.

(61) Valiev, R. R.; Kurten, T.; Valiulina, L. I.; Ketkov, S. Y.; Cherepanov, V. N.; Dimitrova, M.; Sundholm, D. *Phys. Chem. Chem. Phys.* **2022**, *24*, 1666–1674.

(62) Poater, J.; Solà, M. *Chem. Commun.* **2011**, *47*, 11647–11649.

(63) Heilbronner, E. *Tetrahedron Lett.* **1964**, *5*, 1923–1928.

(64) Rappaport, S. M.; Rzepa, H. S. *J. Am. Chem. Soc.* **2008**.

(65) Rosenberg, M.; Dahlstrand, C.; Kilså, K.; Ottosson, H. *Chem. Rev.* **2014**, *114*, 5379–5425.

(66) Clar, E., *Aromatic Sextet*; Wiley: 1972.

(67) Solà, M. *Front. Chem.* **2013**, *1*, 1–8.

(68) Glidewell, C.; Lloyd, D. *Tetrahedron* **1984**, *40*, 4455–4472.

(69) Katritzky, A. R.; Karelson, M.; Sild, S.; Krygowski, T. M.; Jug, K. *J. Org. Chem.* **1998**, *63*, 5228–5231.

(70) Cyrañski, M. K.; Krygowski, T. M.; Katritzky, A. R.; Schleyer, P. v. R. *J. Org. Chem.* **2002**, *67*, 1333–1338.

(71) Stanger, A. *Chem. Commun.* **2009**, *15*, 1939–1947.

(72) Bultinck, P. *Faraday Discuss.* **2007**, *135*, 347–65, discussion 367–401, 503–6.

(73) Alonso, M.; Fernández, I. In *Aromaticity*; Elsevier: 2021, pp 195–235.

(74) Mo, Y.; Peyerimhoff, S. D. *J. Chem. Phys.* **1998**, *109*, 1687–1697.

(75) Mo, Y.; Schleyer, P. v. R. *Eur. J. Chem* **2006**, *12*, 2009–2020.

(76) Schleyer, P. V. R.; Pühlhofer, F. *Org. Lett.* **2002**, *4*, 2873–2876.

(77) Cyrański, M. K. *Chem. Rev.* **2005**, *105*, 3773–3811.

(78) Ziegler, T.; Rauk, A. *Theor. Chim. Acta* **1977**, *46*, 1–10.

(79) Morokuma, K. *J. Chem. Phys.* **1971**, *55*, 1236–1244.

(80) Fernández, I.; Frenking, G. *Faraday Discuss.* **2007**, *135*, 403–421.

(81) Krygowski, T. M.; Szatylowicz, H.; Stasyuk, O. A.; Dominikowska, J.; Palusiak, M. *Chem. Rev.* **2014**, *114*, 6383–6422.

(82) Julg, A.; Francois, P. *Theor. Chim. Acta* **1967**, *7*, 249–261.

(83) Krygowski, T. M. *J. Chem. Inf. Comput. Sci.* **1993**, *33*, 70–78.

(84) Kruszewski, J.; Krygowski, T. M. *Tetrahedron Lett.* **1972**, *13*, 3839–3842.

(85) Krygowski, T. M.; Wieckowski, T. *Croat. Chem. Acta* **1981**, *54*, 193–202.

(86) Shaik, S.; Shurki, A.; Danovich, D.; Hiberty, P. C. *Chem. Rev.* **2001**, *101*, 1501–1539.

(87) Pierrefixe, S. C.; Bickelhaupt, F. M. *Chem.–Eur. J.* **2007**, *13*, 6321–6328.

(88) Pierrefixe, S. C.; Bickelhaupt, F. M. *J. Phys. Chem. A* **2008**, *112*, 12816–12822.

(89) Pierrefixe, S. C. A.; Matthias Bickelhaupt, F. *Aust. J. Chem.* **2008**, *61*, 209–215.

(90) Poater, J.; Feixas, F.; Bickelhaupt, F. M.; Solà, M. *Phys.Chem. Chem. Phys* **2011**, *13*, 20673–20681.

(91) Feixas, F.; Matito, E.; Poater, J.; Solà, M. *Chem. Soc. Rev.* **2015**, *44*, 6434–6451.

(92) Bader, R. F. W.; Stephens, M. E. *J. Am. Chem. Soc.* **1975**, *97*, 7391–7399.

(93) Bader, R. F. *Acc. Chem. Res.* **1985**, *18*, 9–15.

(94) Matito, E.; Duran, M.; Sola, M. *J. Chem. Phys.* **2005**, *122*, 014109.

(95) Giambiagi, M.; de Giambiagi, M. S.; Mundim, K. C. *Struct. Chem.* **1990**, *1*, 423–427.

(96) Giambiagi, M.; de Giambiagi, M. S.; dos Santos Silva, C. D.; de Figueiredo, A. P. *Phys. Chem. Chem. Phys.* **2000**, *2*, 3381–3392.

(97) Bultinck, P.; Ponec, R.; Van Damme, S. *J. Phys. Org. Chem.* **2005**, *18*, 706–718.

(98) Cioslowski, J.; Matito, E.; Solà, M. *J. Phys. Chem. A* **2007**, *111*, 6521–6525.

(99) Becke, A. D.; Edgecombe, K. E. *J. Chem. Phys.* **1990**, *92*, 5397–5403.

(100) Savin, A.; Silvi, B.; Colonna, F. *Can. J. Chem.* **1996**, *74*, 1088–1096.

(101) Silvi, B.; Savin, A. *Nature* **1994**, *371*, 683–686.

(102) Santos, J. C.; Tiznado, W.; Contreras, R.; Fuentealba, P. *J. Chem. Phys.* **2004**, *120*, 1670–1673.

(103) Fernandez, A.; Rincon, L.; Almeida, R. *J. Mol. Struct* **2009**, *911*, 118–123.

(104) Fuentealba, P.; C. Santos, J. *Curr. Org. Chem.* **2011**, *15*, 3619–3626.

(105) Szczepanik, D. W. *Comput. Theor. Chem.* **2016**, *1080*, 33–37.

(106) Szczepanik, D. W.; Andrzejak, M.; Dominikowska, J.; Pawełek, B.; Krygowski, T. M.; Szatylowicz, H.; Solà, M. *Phys. Chem. Chem. Phys.* **2017**, *19*, 28970–28981.

(107) Foster, J. P.; Weinhold, F. *J. Am. Chem. Soc.* **1980**, *102*, 7211–7218.

(108) Zubarev, D. Y.; Boldyrev, A. I. *Phys. Chem. Chem. Phys* **2008**, *10*, 5207–5217.

(109) Zubarev, D. Y.; Boldyrev, A. I. *J. Org. Chem.* **2008**, *73*, 9251–9258.

(110) Zubarev, D. Y.; Averkiev, B. B.; Zhai, H.-J.; Wang, L.-S.; Boldyrev, A. I. *Phys. Chem. Chem. Phys.* **2008**, *10*, 257–267.

(111) Mandado, M.; González-Moa, M. J.; Mosquera, R. A. *J. Comput. Chem.* **2007**, *28*, 127–136.

(112) Poater, J.; Fradera, X.; Duran, M.; Solà, M. *Chemistry* **2003**, *9*, 400–406.

(113) Liu, S. *J. Chem. Phys.* **2007**, *126*, 191107.

(114) Yu, D.; Rong, C.; Lu, T.; Chattaraj, P. K.; De Proft, F.; Liu, S. *Phys. Chem. Chem. Phys.* **2017**, *19*, 18635–18645.

(115) Oh, J.; Sung, Y. M.; Hong, Y.; Kim, D. *Acc. Chem. Res.* **2018**, *51*, 1349–1358.

(116) Woller, T.; Geerlings, P.; De Proft, F.; Champagne, B.; Alonso, M. *Molecules* **2018**, *23*, 1333.

(117) Setiawan, D.; Kraka, E.; Cremer, D. *J. Org. Chem.* **2016**, *81*, 9669–9686.

(118) Woodward, R. B.; Hoffmann, R. *J. Am. Chem. Soc.* **1965**, *87*, 395–397.

(119) Zimmerman, H. E. *J. Am. Chem. Soc.* **1966**, *88*, 1564–1565.

(120) Woodward, R. B.; Hoffmann, R. *Angew. Chem. Int. Ed Engl.* **1969**, *8*, 781–853.

(121) Zimmerman, H. E. *Acc. Chem. Res.* **1971**, *4*, 272–280.

(122) Krygowski, T.; Cyranski, M.; Czarnocki, Z.; Häfelinger, G.; Katritzky, A. R. *Tetrahedron* **2000**, *13*, 1783–1796.

(123) Mucsi, Z.; Viskolcz, B.; Csizmadia, I. G. *J. Phys. Chem. A* **2007**, *111*, 1123–1132.

(124) Kumar, C.; Fliegl, H.; Sundholm, D. *J. Phys. Chem. A* **2017**, *121*, 7282–7289.

(125) Fliegl, H.; Sundholm, D.; Taubert, S.; Jusélius, J.; Klopper, W. *J. Phys. Chem. A* **2009**, *113*, 8668–8676.

(126) Soncini, A.; Fowler, P. W. *Chem. Phys. Lett.* **2004**, *396*, 174–181.

(127) Monaco, G.; Zanasi, R.; Pelloni, S.; Lazzeretti, P. *J. Chem. Theory Comput.* **2010**, *6*, 3343–3351.

(128) Steiner, E.; Fowler, P. W. *J. Phys. Chem. A* **2001**, *105*, 9553–9562.

(129) Steiner, E.; Fowler, P. W. *Chem. Commun.* **2001**, 2220–2221.

(130) Fowler, P. W.; Gibson, C. M.; Bean, D. E. *Proc. Math. Phys. Eng. Sci.* **2014**, *470*, 20130617.

(131) Herges, R.; Geuenich, D. *J. Phys. Chem. A* **2001**, *105*, 3214–3220.

(132) Fliegl, H.; Juselius, J.; Sundholm, D. *The Journal of Physical* **2016**.

(133) Monaco, G.; Zanasi, R. *J. Phys. Chem. A* **2018**, *122*, 4681–4686.

(134) Monaco, G.; Zanasi, R. *Phys. Chem. Chem. Phys.* **2019**, *21*, 11564–11568.

(135) Keith, T. A.; Bader, R. F. *J. Chem. Phys.* **1993**, *99*, 3669–3682.

(136) Lazzeretti, P. *J. Chem. Phys.* **2018**, *149*, 154106.

(137) Barquera-Lozada, J. E. *Int. J. Quantum Chem.* **2018**, *44*, e25848.

(138) Barquera-Lozada, J. E. *J. Comput. Chem.* **2019**, *40*, 2602–2610.

(139) Pelloni, S.; Lazzeretti, P. *Phys. Chem. Chem. Phys.* **2020**, *22*, 1299–1305.

(140) Merino, G.; Heine, T.; Seifert, G. *Chemistry* **2004**, *10*, 4367–4371.

(141) Vaara, J. *Phys. Chem. Chem. Phys.* **2007**, *9*, 5399–5418.

(142) Jinger, R. K.; Fliegl, H.; Bast, R.; Dimitrova, M.; Lehtola, S.; Sundholm, D. *J. Phys. Chem. A* **2021**, *125*, 1778–1786.

(143) Fliegl, H.; Dimitrova, M.; Berger, R. J. F.; Sundholm, D. *Chemistry* **2021**, *3*, 1005–1021.

(144) Schleyer, P. v. R.; Maerker, C.; Dransfeld, A.; Jiao, H.; van Eikema Hommes, N. J. R. *J. Am. Chem. Soc.* **1996**, *118*, 6317–6318.

(145) Schleyer, P. v. R.; Jiao, H.; Hommes, N. J. R. v. E.; Malkin, V. G.; Malkina, O. L. *J. Am. Chem. Soc.* **1997**, *119*, 12669–12670.

(146) Fowler, P. W.; Steiner, E.; Zanasi, R.; Cadioli, B. *Mol. Phys.* **1999**, *96*, 1099–1108.

(147) Cernusak, I.; Fowler, P. W.; Steiner, E. *Mol. Phys.* **2000**, *98*, 945–953.

(148) Kutzelnigg, W. *Isr. J. Chem.* **1980**, *19*, 193–200.

(149) Heine, T.; Schleyer, P. v. R.; Corminboeuf, C.; Seifert, G.; Reviakine, R.; Weber, J. *J. Phys. Chem. A* **2003**, *107*, 6470–6475.

(150) Ramirez-Tagle, R.; Alvarado-Soto, L.; Arratia-Perez, R.; Bast, R.; Alvarez-Thon, L. *J. Chem. Phys.* **2011**, *135*, 104506.

(151) Badri, Z.; Pathak, S.; Fliegl, H.; Rashidi-Ranjbar, P.; Bast, R.; Marek, R.; Foroutan-Nejad, C.; Ruud, K. *J. Chem. Theory Comput.* **2013**, *9*, 4789–4796.

(152) Torres-Vega, J. J.; Vásquez-Espinal, A.; Caballero, J.; Valenzuela, M. L.; Alvarez-Thon, L.; Osorio, E.; Tiznado, W. *Inorg. Chem.* **2014**, *53*, 3579–3585.

(153) Foroutan-Nejad, C. *Theor. Chem. Acc.* **2015**, *134*, 8.

(154) Boronski, J. T.; Seed, J. A.; Hunger, D.; Woodward, A. W.; van Slageren, J.; Wooles, A. J.; Natrajan, L. S.; Kaltsoyannis, N.; Liddle, S. T. *Nature* **2021**, *598*, 72–75.

(155) Cuyacot, B. J. R.; Foroutan-Nejad, C. *Nature* **2022**, *603*, E18–E20.

(156) Szczepanik, D. W. *Angew. Chem. Int. Ed Engl.* **2022**, e202204337.

(157) Klod, S.; Kleinpeter, E. *J. Chem. Soc. Perkin Trans. 2* **2001**, 1893–1898.

(158) Stanger, A. *J. Org. Chem.* **2006**, *71*, 883–893.

(159) Jimenez-Halla, J. O. C.; Matito, E.; Robles, J.; Solà, M. *J. Organomet. Chem.* **2006**, *691*, 4359–4366.

(160) Gershoni-Poranne, R.; Stanger, A. *Eur. J. Chem.* **2014**, *20*, 5673–5688.

(161) Juselius, J.; Sundholm, D. *Phys. Chem. Chem. Phys.* **1999**, *1*, 3429–3435.

(162) Pelloni, S.; Lazzeretti, P. *J. Phys. Chem. A* **2011**, *115*, 4553–4557.

(163) Pelloni, S.; Monaco, G.; Lazzeretti, P.; Zanasi, R. *Phys. Chem. Chem. Phys.* **2011**, *13*, 20666–20672.

(164) Monaco, G.; Zanasi, R. *J. Phys. Chem. A* **2014**, *118*, 1673–1683.

(165) Berger, R. J. F.; Dimitrova, M.; Nasibullin, R. T.; Valiev, R. R.; Sundholm, D. *Phys. Chem. Chem. Phys.* **2022**, *24*, 624–628.

(166) Van Damme, S.; Acke, G.; Havenith, R. W. A.; Bultinck, P. *Phys. Chem. Chem. Phys.* **2016**, *18*, 11746–11755.

(167) Paenurk, E.; Gershoni-Poranne, R. *Phys. Chem. Chem. Phys.* **2022**, *24*, 8631–8644.

(168) Lehtola, S.; Dimitrova, M.; Fliegl, H.; Sundholm, D. *J. Chem. Theory Comput.* **2021**, *17*, 1457–1468.

(169) Gomes, J. A.; Mallion, R. B. *Chem. Rev.* **2001**, *101*, 1349–1383.

(170) Flygare, W. H.; Benson, R. C. *J. Am. Chem. Soc.* **1970**, *92*, 7523–7529.

(171) Gershoni-Poranne, R.; Stanger, A. *Chem. Soc. Rev.* **2015**, *44*, 6597–6615.

(172) Feixas, F.; Matito, E.; Poater, J.; Sola, M. *Wiley Interdiscip. Rev. Comput. Mol. Sci.* **2013**, *3*, 105–122.

(173) Mercero, J. M.; Boldyrev, A. I.; Merino, G.; Ugalde, J. M. *Chem. Soc. Rev.* **2015**, *44*, 6519–6534.

(174) Fernández, I.; Frenking, G.; Merino, G. *Chem. Soc. Rev.* **2015**, *44*, 6452–6463.

(175) Mahmoudi, G.; Afkhami, F. A.; Castiñeiras, A.; Garcia-Santos, I.; Gurbanov, A.; Zubkov, F. I.; Mitoraj, M. P.; Kukułka, M.; Sagan, F.; Szczepanik, D. W.; Konyaeva, I. A.; Safin, D. A. *Inorg. Chem.* **2018**, *57*, 4395–4408.

(176) Szczepanik, D. W.; Solà, M. *ChemistryOpen* **2019**, *8*, 219–227.

(177) Cheung, L. F.; Kocheril, G. S.; Czekner, J.; Wang, L.-S. *J. Am. Chem. Soc.* **2020**, *142*, 3356–3360.

(178) Zhang, Y.; Yu, C.; Huang, Z.; Zhang, W.-X.; Ye, S.; Wei, J.; Xi, Z. *Acc. Chem. Res.* **2021**.

(179) Chauvin, R. *Tetrahedron Lett.* **1995**, *36*, 397–400.

(180) Chauvin, R. *Tetrahedron Lett.* **1995**, *36*, 401–404.

(181) Kuwatani, Y.; Watanabe, N.; Ueda, I. *Tetrahedron Lett.* **1995**, *36*, 119–122.

(182) Suzuki, R.; Tsukuda, H.; Watanabe, N.; Kuwatani, Y.; Ueda, I. *Tetrahedron* **1998**, *54*, 2477–2496.

(183) Baryshnikov, G. V.; Valiev, R. R.; Kuklin, A. V.; Sundholm, D.; Ågren, H. *J. Phys. Chem. Lett.* **2019**, *10*, 6701–6705.

(184) Fowler, P. W.; Mizoguchi, N.; Bean, D. E.; Havenith, R. W. A. *Chemistry* **2009**, *15*, 6964–6972.

(185) Baryshnikov, G. V.; Valiev, R. R.; Nasibullin, R. T.; Sundholm, D.; Kurten, T.; Ågren, H. *J. Phys. Chem. A* **2020**, *124*, 10849–10855.

(186) Baryshnikov, G. V.; Valiev, R. R.; Valiulina, L. I.; Kurtsevich, A. E.; Kurtén, T.; Sundholm, D.; Pittelkow, M.; Zhang, J.; Ågren, H. *J. Phys. Chem. A* **2022**, *126*, 2445–2452.

(187) Pitt, W. R.; Parry, D. M.; Perry, B. G.; Groom, C. R. *J. Med. Chem.* **2009**, *52*, 2952–2963.

(188) Ertl, P.; Jelfs, S.; Mühlbacher, J.; Schuffenhauer, A.; Selzer, P. *J. Med. Chem.* **2006**, *49*, 4568–4573.

(189) Visini, R.; Arús-Pous, J.; Awale, M.; Reymond, J.-L. *J. Chem. Inf. Model.* **2017**, *57*, 2707–2718.

(190) Balaban, A. T.; Harary, F. *Tetrahedron* **1968**, *24*, 2505–2516.

(191) Balaban, A. T.; Brunvoll, J.; Cioslowski, J.; Cyvin, B. N.; Cyvin, S. J.; Gutman, I.; Wenchen, H.; Wenjie, H.; Knop, J. V.; Kovačević, M.; Müller, W. R.; Szymanski, K.; Tošić, R.; Trinajstić, N. *Z. Naturforsch. A.* **1987**, *42*, 863–870.

(192) Gutman, I.; Cyvin, S. J., *Introduction to the Theory of Benzenoid Hydrocarbons*; Springer Science & Business Media: 1989.

(193) Dias, J. R. *Acc. Chem. Res.* **1985**, *18*, 241–248.

(194) Vöge, M.; Guttmann, A. J.; Jensen, I. *J. Chem. Inf. Comput. Sci.* **2002**, *42*, 456–466.

(195) Dias, J. R. *J. Chem. Inf. Model.* **2007**, *47*, 707–715.

(196) Chakraborty, S.; Kayastha, P.; Ramakrishnan, R. *J. Chem. Phys.* **2019**, *150*, 114106.

(197) Krieger, C.; Diederich, F.; Schweitzer, D.; Staab, H. A. *Angew. Chem. Int. Ed Engl.* **1979**, *18*, 699–701.

(198) Nandy, A.; Duan, C.; Goffinet, C.; Kulik, H. J. *JACS Au* **2022**, *2*, 1200–1213.

(199) Kim, D.; Osuka, A. *Acc. Chem. Res.* **2004**, *37*, 735–745.

(200) Nakamura, Y.; Jang, S. Y.; Tanaka, T.; Aratani, N.; Lim, J. M.; Kim, K. S.; Kim, D.; Osuka, A. *Eur. J. Chem.* **2008**, *14*, 8279–8289.

(201) Nakamura, Y.; Aratani, N.; Shinokubo, H.; Takagi, A.; Kawai, T.; Matsumoto, T.; Yoon, Z. S.; Kim, D. Y.; Ahn, T. K.; Kim, D.; Muranaka, A.; Kobayashi, N.; Osuka, A. *J. Am. Chem. Soc.* **2006**, *128*, 4119–4127.

(202) Aratani, N.; Takagi, A.; Yanagawa, Y.; Matsumoto, T.; Kawai, T.; Yoon, Z. S.; Kim, D.; Osuka, A. *Chemistry* **2005**, *11*, 3389–3404.

(203) Borissov, A.; Maurya, Y. K.; Moshniaha, L.; Wong, W.-S.; Żyła-Karwowska, M.; Stępień, M. *Chem. Rev.* **2022**, *122*, 565–788.

(204) Stępień, M.; Gońka, E.; Żyła, M.; Sprutta, N. *Chem. Rev.* **2017**, *117*, 3479–3716.

(205) Shen, Y.; Chen, C.-F. *Chem. Rev.* **2012**, *112*, 1463–1535.

(206) Cherni, E.; Champagne, B.; Ayadi, S.; Liégeois, V. *Phys. Chem. Chem. Phys.* **2019**, *21*, 14678–14691.

(207) Krzeszewski, M.; Ito, H.; Itami, K. *J. Am. Chem. Soc.* **2022**, *144*, 862–871.

(208) Orozco-Ic, M.; Valiev, R. R.; Sundholm, D. *Phys. Chem. Chem. Phys.* **2022**, *24*, 6404–6409.

(209) Monaco, G.; Zanasi, R.; Summa, F. F. *J. Phys. Chem. A* **2022**, *126*, 3717–3723.

(210) Jasti, R.; Bhattacharjee, J.; Neaton, J. B.; Bertozzi, C. R. *J. Am. Chem. Soc.* **2008**, *130*, 17646–17647.

(211) Segawa, Y.; Kuwayama, M.; Itami, K. *Org. Lett.* **2020**, *22*, 1067–1070.

(212) Cheung, K. Y.; Segawa, Y.; Itami, K. *Eur. J. Chem.* **2020**, *26*, 14791–14801.

(213) Kawase, T.; Kurata, H. *Chem. Rev.* **2006**, *106*, 5250–5273.

(214) Hoffmann, M.; Kärnbratt, J.; Chang, M.-H.; Herz, L. M.; Albinsson, B.; Anderson, H. L. *Angew. Chem. Int. Ed Engl.* **2008**, *47*, 4993–4996.

(215) Hoffmann, M.; Wilson, C. J.; Odell, B.; Anderson, H. L. *Angew. Chem. Int. Ed Engl.* **2007**, *46*, 3122–3125.

(216) O'Sullivan, M. C.; Sprafke, J. K.; Kondratuk, D. V.; Rinfray, C.; Claridge, T. D. W.; Saywell, A.; Blunt, M. O.; O'Shea, J. N.; Beton, P. H.; Malfois, M.; Anderson, H. L. *Nature* **2011**, *469*, 72–75.

(217) Neuhaus, P.; Cnossen, A.; Gong, J. Q.; Herz, L. M.; Anderson, H. L. *Angew. Chem. Int. Ed Engl.* **2015**, *54*, 7344–7348.

(218) Cremers, J.; Haver, R.; Rickhaus, M.; Gong, J. Q.; Favereau, L.; Peeks, M. D.; Claridge, T. D. W.; Herz, L. M.; Anderson, H. L. *J. Am. Chem. Soc.* **2018**, *140*, 5352–5355.

(219) Judd, C. J.; Nizovtsev, A. S.; Plougmann, R.; Kondratuk, D. V.; Anderson, H. L.; Besley, E.; Saywell, A. *Phys. Rev. Lett.* **2020**, *125*, 206803.

(220) Rickhaus, M.; Jirasek, M.; Tejerina, L.; Gotfredsen, H.; Peeks, M. D.; Haver, R.; Jiang, H.-W.; Claridge, T. D. W.; Anderson, H. L. *Nat. Chem.* **2020**, *12*, 236–241.

(221) Jirásek, M.; Anderson, H. L.; Peeks, M. D. *Acc. Chem. Res.* **2021**, *54*, 3241–3251.

(222) Ke, X.-S.; Kim, T.; He, Q.; Lynch, V. M.; Kim, D.; Sessler, J. L. *J. Am. Chem. Soc.* **2018**.

(223) Wang, Y.; Ke, X.-S.; Lee, S.; Kang, S.; Lynch, V. M.; Kim, D.; Sessler, J. L. *J. Am. Chem. Soc.* **2022**.

(224) Xue, S.; Kuzuhara, D.; Aratani, N.; Yamada, H. *Org. Lett.* **2019**, *21*, 2069–2072.

(225) Ajami, D.; Oeckler, O.; Simon, A.; Herges, R. *Nature* **2003**, *426*, 819–821.

(226) Herges, R. *Chem. Rev.* **2006**, *106*, 4820–4842.

(227) Yoon, Z. S.; Osuka, A.; Kim, D. *Nat. Chem.* **2009**, *1*, 113–122.

(228) Saito, S.; Osuka, A. *Angew. Chem. Int. Ed.* **2011**, *50*, 4342–4373.

(229) Osuka, A.; Saito, S. *Chem. Commun.* **2011**, *47*, 4330–4339.

(230) Fliegl, H.; Sundholm, D.; Taubert, S.; Pichierri, F. *J. Phys. Chem. A* **2010**, *114*, 7153–7161.

(231) Fliegl, H.; Sundholm, D.; Pichierri, F. *Phys. Chem. Chem. Phys.* **2011**, *13*, 20659–20665.

(232) Segawa, Y.; Watanabe, T.; Yamanoue, K.; Kuwayama, M.; Watanabe, K.; Pirillo, J.; Hijikata, Y.; Itami, K. *Nat. Synth.* **2022**, 1–7.

(233) Rickhaus, M.; Mayor, M.; Juríček, M. *Chem. Soc. Rev.* **2017**, *46*, 1643–1660.

(234) Lawton, R. G.; Barth, W. E. *J. Am. Chem. Soc.* **1971**, *93*, 1730–1745.

(235) Nestoros, E.; Stuparu, M. C. *Chem. Commun.* **2018**, *54*, 6503–6519.

(236) Sakurai, H.; Daiko, T.; Hirao, T. *Science* **2003**, *301*, 1878.

(237) Kroto, H. W.; Heath, J. R.; O'Brien, S. C.; Curl, R. F.; Smalley, R. E. *Nature* **1985**, *318*, 162–163.

(238) Krätschmer, W.; Lamb, L. D.; Fostiropoulos, K.; Huffman, D. R. *Nature* **1990**, *347*, 354–358.

(239) Schwerdtfeger, P.; Wirz, L. N.; Avery, J. *Wiley Interdiscip. Rev. Comput. Mol. Sci.* **2015**, *5*, 96–145.

(240) Prinzbach, H.; Weiler, A.; Landenberger, P.; Wahl, F.; Worth, J.; Scott, L. T.; Gelmont, M.; Olevano, D.; v. Issendorff B *Nature* **2000**, *407*, 60–63.

(241) Kroto, H. *Nature* **1987**, *329*, 529–531.

(242) Kulichenko, M.; Fedik, N.; Tkachenko, N. V.; Muñoz-Castro, Á.; Sun, Z.-M.; Boldyrev, A. I. In *Aromaticity*; Elsevier: 2021, pp 447–489.

(243) Pitochelli, A. R.; Hawthorne, F. M. *J. Am. Chem. Soc.* **1960**, *82*, 3228–3229.

(244) Heaven, M. W.; Dass, A.; White, P. S.; Holt, K. M.; Murray, R. W. *J. Am. Chem. Soc.* **2008**, *130*, 3754–3755.

(245) Kang, X.; Chong, H.; Zhu, M. *Nanoscale* **2018**, *10*, 10758–10834.

(246) Jena, P.; Sun, Q. *Chem. Rev.* **2018**, *118*, 5755–5870.

(247) Sundholm, D. *Phys. Chem. Chem. Phys.* **2013**, *15*, 9025–9028.

(248) Bühl, M.; Hirsch, A. *Chem. Rev.* **2001**, *101*, 1153–1183.

(249) Zanasi, R.; Fowler, P. *Chem. Phys. Lett* **1995**, *238*, 270–280.

(250) Johansson, M. P.; Jusélius, J.; Sundholm, D. *Angew. Chem. Int. Ed Engl.* **2005**, *44*, 1843–1846.

(251) Sagl, D. J.; Martin, J. C. *J. Am. Chem. Soc.* **1988**, *110*, 5827–5833.

(252) Ciofini, I.; Lainé, P. P.; Adamo, C. *Chem. Phys. Lett.* **2007**, *435*, 171–175.

(253) Havenith, R. W. A.; Fowler, P. W.; Fias, S.; Bultinck, P. *Tetrahedron Lett.* **2008**, *49*, 1421–1424.

(254) Hatanaka, M.; Saito, M.; Fujita, M.; Morokuma, K. *J. Org. Chem.* **2014**, *79*, 2640–2646.

(255) Furukawa, S.; Fujita, M.; Kanatomi, Y.; Minoura, M.; Hatanaka, M.; Morokuma, K.; Ishimura, K.; Saito, M. *Commun. Chem.* **2018**, *1*, 60.

(256) Fowler, P. W.; Havenith, R. W. A. **2021**, *125*, 6374–6383.

(257) Berger, R. J.; Repisky, M.; Komorovsky, S. *Chem. Commun.* **2015**, *51*, 13961–13963.

(258) Palusiak, M.; Domagała, M.; Dominikowska, J.; Bickelhaupt, F. M. *Phys. Chem. Chem. Phys.* **2014**, *16*, 4752–4763.

(259) Canon-Mancisidor, W.; Gómez-Garcıa, C. J.; Espallargas, G. M.; Vega, A.; Spodine, E.; Venegas-Yazigi, D.; Coronado, E. *Chem. Sci.* **2014**, *5*, 324–332.

(260) Ardizzoia, G. A.; Angaroni, M. A.; La Monica, G.; Cariati, F.; Cenini, S.; Moret, M.; Masciocchi, N. *Inorg. Chem.* **1991**, *30*, 4347–4353.

(261) Mezei, G.; Baran, P.; Raptis, R. G. *Angew. Chem. Int. Ed.* **2004**, *43*, 574–577.

(262) Hong, J.-H.; Aslam, A. S.; Ishida, M.; Mori, S.; Furuta, H.; Cho, D.-G. *J. Am. Chem. Soc.* **2016**, *138*, 4992–4995.

(263) Fliegl, H.; Valiev, R.; Pichierri, F.; Sundholm, D. In *Chemical Modelling*, Springborg, M., Joswig, J.-O., Eds.; Royal Society of Chemistry: United Kingdom, 2018, pp 1–42.

(264) Virshup, A. M.; Contreras-Garcia, J.; Wipf, P.; Yang, W.; Beratan, D. N. *J. Am. Chem. Soc.* **2013**, *135*, 7296–7303.

(265) Brown, N.; McKay, B.; Gilardoni, F.; Gasteiger, J. *J. Chem. Inf. Comput. Sci.* **2004**, *44*, 1079–1087.

(266) Jensen, J. H. *Chem. Sci.* **2019**, *10*, 3567–3572.

(267) Sanchez-Lengeling, B.; Aspuru-Guzik, A. *Science* **2018**, *361*, 360–365.

(268) Schwalbe-Koda, D.; Gómez-Bombarelli, R. In *Machine Learning Meets Quantum Physics*, Schütt, K. T., Chmiela, S., von Lilienfeld, O. A., Tkatchenko, A., Tsuda, K., Müller, K.-R., Eds.; Springer International Publishing: Cham, 2020, pp 445–467.

(269) Schneider, G.; Fechner, U. *Nat. Rev. Drug Discov.* **2005**, *4*, 649–663.

(270) Schneider, G., *De Novo Molecular Design*; John Wiley & Sons: 2013.

(271) Gawehn, E.; Hiss, J. A.; Schneider, G. *Mol. Inform.* **2016**, *35*, 3–14.

(272) Schneider, G. *Nat. Rev. Drug Discov.* **2018**, *17*, 97–113.

(273) Freeze, J. G.; Kelly, H. R.; Batista, V. S. *Chem. Rev.* **2019**, *119*, 6595–6612.

(274) Yao, Z.; Sánchez-Lengeling, B.; Bobbitt, N. S.; Bucior, B. J.; Kumar, S. G. H.; Collins, S. P.; Burns, T.; Woo, T. K.; Farha, O. K.; Snurr, R. Q.; Aspuru-Guzik, A. *Nat. Mach. Intell.* **2021**, *3*, 76–86.

(275) Pollice, R.; Dos Passos Gomes, G.; Aldeghi, M.; Hickman, R. J.; Krenn, M.; Lavigne, C.; Lindner-D'Addario, M.; Nigam, A.; Ser, C. T.; Yao, Z.; Aspuru-Guzik, A. *Acc. Chem. Res.* **2021**, *54*, 849–860.

(276) Yao, Z.; Sánchez-Lengeling, B.; Bobbitt, N. S.; Bucior, B. J.; Kumar, S. G. H.; Collins, S. P.; Burns, T.; Woo, T. K.; Farha, O. K.; Snurr, R. Q., et al. *Nat. Mach. Intell.* **2021**, *3*, 76–86.

(277) Mol, J. A.; Lau, C. S.; Lewis, W. J. M.; Sadeghi, H.; Roche, C.; Cnossen, A.; Warner, J. H.; Lambert, C. J.; Anderson, H. L.; Briggs, G. A. D. *Nanoscale* **2015**, *7*, 13181–13185.

(278) Skara, G.; Pinter, B.; Geerlings, P.; De Proft, F. *Chem. Sci.* **2015**, *6*, 4109–4117.

(279) Eder, S.; Yoo, D.-J.; Nogala, W.; Pletzer, M.; Santana Bonilla, A.; White, A. J. P.; Jelfs, K. E.; Heeney, M.; Choi, J. W.; Glöcklhofer, F. *Angew. Chem. Int. Ed Engl.* **2020**, *59*, 12958–12964.

(280) Henault, E. S.; Rasmussen, M. H.; Jensen, J. H. *PeerJ Phys. Chem.* **2020**, *2*, e11.

(281) Gielen, G. G. E.; Walscharts, H. C. C.; Sansen, W. M. C. *IEEE J. Solid-State Circuits* **1990**, *25*, 707–713.

(282) Fakhfakh, M.; Cooren, Y.; Sallem, A.; Loulou, M.; Siarry, P. *Analog Integr. Circuits Signal Process.* **2010**, *63*, 71–82.

(283) Gielen, G. G. E.; Rutenbar, R. A. *Proc. IEEE Inst. Electr. Electron. Eng.* **2000**, *88*, 1825–1854.

(284) Zheng, H.; Zhang, G.; Zhang, L.; Wang, Q.; Li, H.; Han, Y.; Xie, L.; Yan, Z.; Li, Y.; An, Y.; Dong, H.; Zhu, W.; Guo, X. *Front. Oncol.* **2020**, *10*, 68.

(285) Singh, N.; Chaput, L.; Villoutreix, B. O. *Brief. Bioinform.* **2021**, *22*, 1790–1818.

(286) Duan, C.; Nandy, A.; Meyer, R.; Arunachalam, N.; Kulik, H. J. *arXiv preprint arXiv:2207.10747* **2022**.

(287) Reiher, M. *Isr. J. Chem.* **2022**, *62*, e202100101.